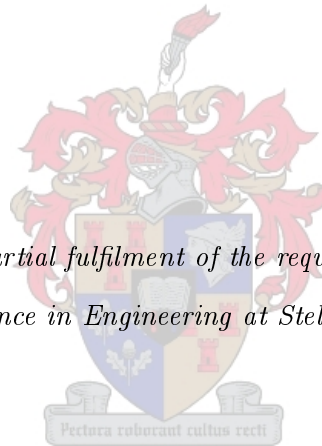


# TUNE-ALL WIDEBAND PLANAR FILTERS FOR KAT-7

by

Theunis Steyn Beukman

*Thesis presented in partial fulfilment of the requirements for the degree  
of Master of Science in Engineering at Stellenbosch University*



Supervisor: Dr. R.H. Geschke

Department of Electrical and Electronic Engineering

December 2011

# Declaration

By submitting this thesis electronically, I declare that the entirety of the work contained therein is my own, original work, that I am the sole author thereof (save to the extent explicitly otherwise stated), that reproduction and publication thereof by Stellenbosch University will not infringe any third party rights and that I have not previously in its entirety or in part submitted it for obtaining any qualification.

Date: December 2011

Copyright © 2011 Stellenbosch University

All rights reserved

# Abstract

A new type of wideband filters, with tunability in both the centre frequency and bandwidth, is presented in this thesis. These filters are based on perturbed ring-resonators in cascade, while varactor diodes are used for electronic tuning.

The Karoo Array Telescope (KAT-7) requires a front-end filter that has the ability for fine-tuning the response after fabrication, in order to obtain the designed filtering response. Not only are tune-all characteristics required, but also wide bandwidth, flat passband, high selectivity and implementation in microstrip technology.

In this thesis an extensive investigation of both tunable and wideband filters is done, in order to find a possible solution for the KAT-7 specifications. Following this investigation, it is concluded that no suitable design approach for tune-all wideband filters, implemented in microstrip, exists in current literature.

Therefore, this thesis proposes a new type of filter along with the development of a complete design procedure. Two filters are designed with this procedure to achieve the required passband from 1.2 to 1.95 GHz (i.e. a fractional bandwidth of 49%). In the first filter design, with a network consisting of 4 cascaded filtering-sections, the centre frequency is 5% tunable and the bandwidth 17.5%. With the second filter consisting of 6 cascaded filtering-sections, higher selectivity is achieved but with lower return loss. Here the centre frequency is 8.5% tunable and the bandwidth 18.8%. The theoretical results are validated with the fabrication of both filters.

This design is very unique in that it achieves wide bandwidth, is realisable in microstrip and most importantly is tunable in both the centre frequency and bandwidth. An advantage of this design procedure is that full wave simulations are minimal, due to the complete circuit models used for optimisation.

# Opsomming

'n Nuwe soort van wye-band filters, met verstelbaarheid in beide senter frekwensie en bandwydte, word voorgelê in hierdie tesis. Hierdie filters is gebaseer op versteurde ring-resoneerders in kaskade, terwyl varaktordiodes gebruik word vir elektroniese verstelling.

Die *Karoo Array Telescope* (KAT-7) vereis 'n voorkant filter wat die vermoë het vir die instemming van die respons na fabrikasie, sodat die geontwerpde filter respons behaal kan word. Nie net word verstel-als eienskappe vereis nie, maar ook wye bandwydte, plat deurlaatband, hoë selektiwiteit en implimentering in mikrostrook tegnologie.

In hierdie tesis is 'n veelomvattende ondersoek gedoen van beide verstelbare en wye-band filters, sodat 'n moontlike oplossing vir die KAT-7 spesifikasies gevind kan word. Na aanleiding van hierdie ondersoek, is die gevolgtrekking dat daar geen gepaste ontwerp benadering vir verstel-als wye-band filters, wat geïmplimenter is in mikrostrook, in huidige literatuur bestaan nie.

Daarom stel hierdie tesis, saam met die ontwikkeling van 'n volledige ontwerp prosedure, 'n nuwe tipe filter voor. Twee filters is ontwerp met hierdie prosedure om die vereiste deurlaatband vanaf 1.2 tot 1.95 GHz (dit is 'n fraksionele bandwydte van 49%) te behaal. In die eerste filter ontwerp, met 'n netwerk wat uit 4 kaskade filter-seksies bestaan, is die senter frekwensie 5% verstelbaar en die bandwydte 17.5%. Met die tweede filter bestaande uit 6 kaskade filter-seksies, word hoër selektiwiteit behaal maar met laer eggoerswakking. Hier is die senter frekwensie 8.5% verstelbaar en die bandwydte 18.8%. Die teoretiese resultate is geldig bewys deur die fabrikasie van albei filters.

Hierdie ontwerp is baie uniek in dat dit wye bandwydte behaal, is realiseerbaar in mikrostrook en mees belangrikste dat dit verstelbaar is in beide senter frekwensie en bandwydte. 'n Voordeel van hierdie prosedure is dat heelgolf simulاسies minimaal is, a.g.v. die volledige stroombaan modelle wat gebruik word vir optimering.

# Acknowledgements

The following people and organisations are acknowledged for their special contribution to this successful project:

- God the Father, for His endless favour and support. Jesus my Lord and Saviour, for the hope and comfort that He is. All the glory be given to Him!
- My wife, Coba, for her sacrifices, selfless support and understanding. She has always believed in me and for that I am very grateful.
- My supervisor, Dr. Riana Geschke, for her advice, guidance and believe in my determination to succeed.
- The SKA project for the scholarship. Without their financial support this would not have been possible.
- The FP7-IRSES MultiWaveS project for the opportunity and financial support to visit Heriot-Watt University.
- Wessel Crouwkamp and Wynand van Eeden, for their help with all the fabrications.
- CPUUT for the use of their facilities.
- Sonnet Software for the academic license.
- Applied Wave Research for the academic license.

*Trust in the LORD with all your heart, and lean not on your own understanding.  
In all your ways acknowledge Him, and He shall direct your paths.*  
Proverbs 3:5-6

*Matlab* is a registered trademark of *The Mathworks, Inc.* ©1984-2011.

*Microwave Office* is a registered trademark of *Applied Wave Research, Inc.* ©1999-2011.

*Sonnet* is a registered trademark of *Sonnet Software Inc.* ©1986-2011.

Typeset by the author in 12 pt. Roman using LyX version 2.0.0.

# Contents

<b>List of Figures</b>	<b>ix</b>
<b>List of Tables</b>	<b>xviii</b>
<b>List of Abbreviations</b>	<b>xix</b>
<b>List of Symbols</b>	<b>xx</b>
<b>1 Introduction</b>	<b>1</b>
1.1 Motivation for research . . . . .	1
1.2 Objectives . . . . .	2
1.3 Contributions . . . . .	3
1.4 Overview . . . . .	3
<b>2 Narrowband Filters with Tunability</b>	<b>5</b>
2.1 Introduction . . . . .	5
2.2 Transfer functions . . . . .	5
2.3 Lumped element prototype . . . . .	7
2.4 Distributed element prototype . . . . .	9
2.5 Techniques for tuning narrowband filters . . . . .	15
2.5.1 Frequency tuning . . . . .	16
2.5.2 Frequency and bandwidth tuning . . . . .	20
2.5.3 Filter reconfigurability . . . . .	23
2.6 Quality factor and filter losses . . . . .	24
2.7 Conclusion . . . . .	26
<b>3 Implementation of Tunable Narrowband Filters</b>	<b>28</b>
3.1 Introduction . . . . .	28
3.2 Formulation and extraction of design parameters . . . . .	28
3.2.1 Coupling coefficient . . . . .	29
3.2.2 External quality factor . . . . .	30
3.3 Design of tunable combline filter . . . . .	32

3.3.1	Resonator design . . . . .	34
3.3.2	Coupling design . . . . .	39
3.3.3	Optimisation of complete microwave structure . . . . .	41
3.4	Results of tunable combline filter . . . . .	42
3.5	Conclusion . . . . .	45
<b>4</b>	<b>Wideband Filters</b>	<b>47</b>
4.1	Introduction . . . . .	47
4.2	Coupled resonator filters . . . . .	47
4.2.1	Wideband implementation . . . . .	47
4.2.2	Improved equations for coupled-lines . . . . .	49
4.3	Exact synthesis based on Richards' transformation . . . . .	52
4.4	Signal-interference techniques . . . . .	54
4.5	Conclusion . . . . .	60
<b>5</b>	<b>Prototype Filters for KAT-7</b>	<b>63</b>
5.1	Introduction . . . . .	63
5.2	Tunable transversal-sections based on perturbation . . . . .	63
5.2.1	Premise for the investigation of tune-all filtering-sections . . . . .	64
5.2.2	First proposed filtering-section . . . . .	65
5.2.3	Second proposed filtering-section . . . . .	68
5.3	Prototype development . . . . .	70
5.3.1	Development of the tune-all filtering-section . . . . .	70
5.3.2	Network analysis of filtering-section . . . . .	75
5.3.3	Proposition for a filter prototype for KAT-7 . . . . .	77
5.4	First prototype: 4 cascaded filtering-sections . . . . .	78
5.4.1	Cascaded filtering-sections . . . . .	79
5.4.2	Design of prototype circuit . . . . .	83
5.4.3	Biasing network . . . . .	87
5.4.4	Components for filter network . . . . .	89
5.4.5	Implementation of filter network . . . . .	90
5.4.6	Fabricated filter . . . . .	94
5.5	Second prototype: 6 cascaded filtering-sections . . . . .	96
5.5.1	Design of prototype circuit . . . . .	96
5.5.2	Components for filter network . . . . .	101
5.5.3	Implementation of filter network . . . . .	102
5.5.4	Fabricated filter . . . . .	104
5.6	Compare prototype filters . . . . .	107
5.7	Conclusion . . . . .	108



<i>CONTENTS</i>	viii
<b>6 Conclusion</b>	<b>111</b>
6.1 Conclusion of reviewed literature . . . . .	111
6.2 Achievement of initial goals . . . . .	111
6.3 Recommendations for future work . . . . .	113
<b>Bibliography</b>	<b>114</b>
<b>A Derivation of Coupling Coefficient</b>	<b>118</b>

# List of Figures

2.1	The lowpass 4 <sup>th</sup> order prototype filter responses with cut-off frequency at $ S_{21}  = -3$ dB. (a) The transmission coefficient against the normalised frequency and (b) the normalised group delay against the normalised frequency.	6
2.2	The circuit for a lowpass lumped element prototype in (a) with its dual circuit in (b).	7
2.3	A $n^{\text{th}}$ order bandpass lumped element prototype that is transformed from the lowpass prototype shown in Fig. 2.2a.	9
2.4	The impedance inverter in (a) with its dual circuit the admittance inverter in (b). Note that an ideal inverter is frequency independent with a $\pm 90^\circ$ phase shift.	10
2.5	Practical realisations of the impedance inverter using either (a) inductors or (b) capacitors and the admittance inverter using either (c) inductors or (d) capacitors.	11
2.6	The lowpass distributed prototype with (a) series inductors or (b) shunt capacitors. Note that the circuit in (b) is a dual circuit of (a).	12
2.7	The general form of the distributed bandpass prototype filter, where (b) is the dual circuit of (a).	13
2.8	Frequency spectrum windows for different EM wave applications. Illustration taken from [1].	16
2.9	The schematics of (a) a varactor-loaded transmission line resonator and (b) a combline filter consisting of a coupled-array of these resonators.	17
2.10	The extraction of an embedded admittance inverter from a section of the equivalent combline filter circuit. (a) The circuit represents two inductive coupled combline resonators, where the susceptance of the distributed inductance of the first resonator is $\frac{-Y_r}{\tan\theta}$ . (b) The adapted lumped circuit. (c) The distributed circuit of the combline filter.	18
2.11	The normalised bandwidth ( $BW/BW_0$ ) of a combline filter for different resonator electrical lengths ( $\theta_0$ ), calculated with equation (2.32).	19
2.12	Schematic of an interdigital filter with frequency tuning ability.	20

2.13	BW control subnetwork between two adjacent parallel resonators. In principle this configuration is a $2^{nd}$ order BPF. Illustration taken from [2]. . . . .	21
2.14	Schematic of $2^{nd}$ order combline filter with detuned resonator for continuous BW and $f_0$ tuning. Illustration taken from [2]. . . . .	22
2.15	Constructed $3^{rd}$ order combline filter with continuous BW and $f_0$ tuning capabilities. Illustration taken from [2]. . . . .	23
2.16	The affect of resonator dissipation on a $4^{th}$ order Chebyshev filter with 20% FBW at 1 GHz. . . . .	25
3.1	Equivalent circuit for the inductive coupling between two synchronously tuned series resonators. . . . .	29
3.2	The method of extracting the coupling coefficient from two coupled resonators using an EM solver. (a) The microstrip layout of two lightly coupled resonators. The two centre strips are the capacitive-loaded resonators with the perpendicular two terminal strips on either sides known as feeds. The feeds are connected to port 1 and 2 as indicated by the labels. (b) The EM simulated results of the structure's transmission coefficient. Note that the two peaks are the eigenmode frequencies. . . . .	30
3.3	Equivalent circuit for the coupling between a terminal load and I/O resonator.	31
3.4	Common I/O coupling structures used for realising microstrip filters. Both structures consists of a feed between the labelled port 1 and a capacitive-loaded resonator. (a) Coupled-line feed and (b) tapped-line feed. . . . .	32
3.5	A typical response of the normalised group delay of the reflection coefficient of a type of coupling structure as shown in Fig. 3.4. . . . .	33
3.6	The total capacitance ( $C_T$ ) of the BBY52 varactor diode against the reversed biasing voltage ( $V_R$ ). This graph is taken from the datasheet provided by Infineon. . . . .	35
3.7	The schematics of two possible biasing networks for a varactor diode in a capacitive-loaded transmission line resonator. . . . .	36
3.8	The typical schematic of the parasitic components of a varactor diode package.	37
3.9	The values of the capacitance at the design frequency ( $C_{r0}$ ) corresponding to the lower ( $f_1$ ) and upper ( $f_2$ ) tuning frequency limits. For the filter response to be tuned symmetrically around the design frequency of 1.53 GHz (dashed line), the capacitance value should be 1.8 pF. . . . .	38
3.10	Microstrip layout of the complete resonator with dimension parameters. Note that the bottom strip is grounded with five vias and the strip connected to the left of $R_c$ is a DC line. . . . .	39
3.11	(a) Two coupled resonators with lightly coupled feeds. (b) The coupling coefficient of the resonators as a function of the gap ( $s$ ) between them. . .	40

3.12	(a) The resonator with a tapped-line feed. (b) The $Q_e$ as a function of the feed offset ( $l_{offset}$ ). . . . .	40
3.13	The 3 <sup>rd</sup> order coupled resonator prototype circuit. Note that the three indicated “stages” are the different optimisation stages. . . . .	41
3.14	The simulation layout of the tunable combline filter. The grey boxes represent the component packages. . . . .	42
3.15	The tuned responses of the Sonnet simulations (a) - (b) and measurements (c) - (d) of the fabricated filter. Note that $V_b$ represents the biasing voltage. . . . .	43
3.16	Photo of the fabricated tunable combline filter. . . . .	44
3.17	Investigation of symmetry in fabricated filter. (a) The reflections at port 1 and port 2 for $V_b = 1.5V$ , seem to be unsymmetrical due to a detuned resonator. (b) The measured response where resonator 1 and 2 are both set to $V_b = 2.4V$ and resonator 3 is set to $V_b = 3V$ . The dashed lines are the simulated response with all resonators tuned at $V_b = 1.5V$ . . . . .	45
4.1	The microstrip layout of a $n^{th}$ order end-coupled half-wavelength resonator filter. . . . .	48
4.2	The microstrip layout of a $n^{th}$ order stepped-impedance half-wavelength resonator filter. . . . .	49
4.3	(a) The equivalent circuit, containing an ideal admittance inverter, of (b) the coupled-line section. . . . .	50
4.4	The microstrip layout of a $n^{th}$ order parallel-coupled half-wavelength resonator filter. . . . .	51
4.5	The equivalent circuit for a combline filter proposed by Wenzel [3]. Note these elements are distributed lumped elements in the S-domain. . . . .	53
4.6	A transversal signal-interference filtering-section consisting of two parallel transmission lines. . . . .	54
4.7	The transmission responses of the transversal-section with (a) $k=1$ and (b) $k=2$ , while the equations (4.9), (4.10) and (4.11) are met with $2Z_0 = Z_1 = 100\Omega$ . . . . .	55
4.8	(a) The schematic of a transversal-section consisting of short-circuited coupled-lines in parallel with another transmission line, as proposed in [4]. (b) An example of the calculated s-parameters of such a filtering-section. Here the coupled-line section has a length of $\theta_1 = 90^\circ$ and even- and odd-mode characteristic impedances of $Z_{1e} = 41\Omega$ and $Z_{1o} = 96\Omega$ , respectively. The lower line has a length of $\theta_2 = 270^\circ$ and characteristic impedance of $Z_2 = 66\Omega$ . Note that the coupling coefficient for the coupled-lines is approximately $M \approx 0.49$ . . . . .	57

4.9 The microstrip layout of a transversal-type filter proposed in [5]. The filter consists of terminals coupling in an interdigital configuration into a transversal-section. The feeds are asymmetrically loaded with  $\lambda_g/2$  open-circuited stubs to produce transmission zeros in the stopband. The illustration is taken from [5]. . . . . 58

4.10 (a) The microstrip layout of a ring-resonator with tapped-feed lines and a circumference of  $\lambda_g$ . (b) The ring-resonator of (a) are loaded with two open-circuit stubs and one square stub, as proposed in [6]. . . . . 58

4.11 The transmission coefficient for the stub-loaded ring-resonator in Fig. 4.10b, with  $Z_0 = 50\Omega$  and  $Z_{stub1} = Z_{stub2} = 64\Omega$ . (a) The length of  $\theta_{stub1}$  is varied while  $\theta_{stub2} = 0^\circ$ . The degenerate modes marked with 'X' and 'O', which are initially positioned at  $f_0$  and  $3f_0$  respectively, are moved to lower frequencies as  $\theta_{stub1}$  increases. (b) Here  $\theta_{stub1} = 90^\circ$  while  $\theta_{stub2}$  is varied. The remaining degenerate modes, also marked with 'X' and 'O', are now moved to lower frequencies as  $\theta_{stub2}$  increases. . . . . 59

5.1 The two possible field distributions of the ring-resonator that may propagate at resonance, when the circumference of the ring is  $\lambda_g$ . The X's and arrows indicate the voltage and current absolute maxima, respectively. . . 64

5.2 (a) The first proposed tunable filtering-section, consisting of a stub-loaded ring-resonator with tuning capacitors. (b) An optimised response for the filtering-section in (a) to meet the passband specifications of KAT-7. The parameter values are  $\theta_1 = 90^\circ$ ,  $\theta_2 = 270^\circ$ ,  $Z_1 = 43\Omega$ ,  $Z_2 = 47\Omega$ ,  $\theta_{s1} = \theta_{s2} = 60^\circ$ ,  $Z_{s1} = Z_{s2} = 80\Omega$  and  $C_{s1} = C_{s2} = 0.73$  pF. . . . . 66

5.3 The (a) transmission coefficient and (b) reflection coefficient of the proposed tunable filtering-section in Fig. 5.2a, for different capacitor values. The parameter values of the filtering-section are  $\theta_1 = 90^\circ$ ,  $\theta_2 = 270^\circ$ ,  $Z_1 = Z_2 = 50\Omega$ ,  $\theta_{s1} = \theta_{s2} = 60^\circ$  and  $Z_{s1} = Z_{s2} = 90\Omega$ . . . . . 67

5.4 (a) A ring-resonator loaded with a single open-circuit stub. (b) The transmission coefficient of this filtering-section for different stub lengths, with the terminals lightly coupled. The parameter values are  $\theta_1 = 90^\circ$ ,  $\theta_2 = 270^\circ$ ,  $Z_1 = Z_2 = 50\Omega$  and  $Z_{s2} = 50\Omega$ , except for the dashed line where  $Z_2 = 100\Omega$ . The X's indicate the transmission zeros of the excited degenerate modes, while the O's indicate the transmission poles found between them. . . . . 68

- 5.5 (a) A ring-resonator loaded with a single open-circuit stub on the lower path and a shunt capacitor on the upper path. (b) The transmission coefficient of this filtering-section for different capacitor values, with the terminals lightly coupled. The parameter values are  $\theta_1 = 90^\circ$ ,  $\theta_2 = 270^\circ$ ,  $Z_1 = 50\Omega$ ,  $Z_2 = 100\Omega$ ,  $Z_{s2} = 50\Omega$  and  $\theta_{s2} = 60^\circ$ . The O's indicate the lower transmission poles that are tuned with  $C_1$ . . . . . 70
- 5.6 (a) A ring-resonator loaded with a single open-circuit stub on the lower path and a series capacitor on the upper path. (b) The transmission coefficient of this filtering-section for different capacitor values, with the terminals lightly coupled. The parameter values are  $\theta_1 = 90^\circ$ ,  $\theta_2 = 270^\circ$ ,  $Z_1 = 50\Omega$ ,  $Z_2 = 100\Omega$ ,  $Z_{s2} = 50\Omega$  and  $\theta_{s2} = 60^\circ$ . The O's indicate the upper transmission poles that are tuned with  $C_1$ . . . . . 71
- 5.7 (a) Proposed filtering-section with tune-all capabilities. (b) The filter response of this TEM-circuit in MWO, with optimised parameter values given in Table 5.1. . . . . 71
- 5.8 The FBW at  $|s_{21}| = -0.043$  dB ( $FBW_{ripple}$ ) and at  $|s_{21}| = -20$  dB ( $FBW_{20dB}$ ) are plotted respectively against the impedance ratio  $Z_2/Z_1$ , for different values of  $Z_1$ . Note that the terminal impedance are also changed according to  $Z_1$ , in order to maintain a minimum  $L_R$  of 20 dB in the passband. 73
- 5.9 The tunability of the bandwidth and centre frequency with the (a) series capacitor and the (b) shunt capacitor. The design parameter values of the filtering-section (Fig. 5.7a) are  $\theta_1 = 81^\circ$ ,  $\theta_2 = 212^\circ$ ,  $Z_1 = 48.4\Omega$ ,  $Z_2 = 94.4\Omega$ ,  $C_1 = 7$  pF and  $C_2 = 4.9$  pF. . . . . 74
- 5.10 The (a) transmission coefficient and (b) reflection coefficient for different tuned passband states, given in Table 5.2. . . . . 75
- 5.11 (a) The schematic of a TEM-circuit of filtering-sections cascaded with lines of  $Z_0 = 50\Omega$  and  $\theta_0 = 90^\circ$ . (b) The filter responses of the networks consisting of 2 and 3 cascaded sections with parameter values given in Table 5.4. The gray regions indicate the areas not adhering to the filter specifications. Note that  $s_{11}$  (dashed line) is only plotted in the passband. . . . . 79
- 5.12 (a) The schematic of a TEM-circuit of direct cascaded filtering-sections. (b) The filter responses of the networks consisting of 2 and 4 cascaded sections with parameter values given in Table 5.5. The gray regions indicate the areas not adhering to the filter specifications. Note that  $s_{11}$  (dashed line) is only plotted at the passband frequencies. . . . . 81

5.13	The tuned wideband responses of the networks consisting respectively of 4 direct cascaded sections (Fig. 5.12a) and 2 sections cascaded with a $\lambda_g/4$ line (Fig. 5.11a). The former network is tuned here with $C_1 = 5.5$ pF and $C_2 = 5.7$ pF, while the latter is tuned with $C_1 = 4.6$ pF and $C_2 = 5.85$ pF. The gray region indicate the return loss specification. . . . .	83
5.14	The design graphs of different capacitor values for a filter network consisting of 4 cascaded sections. The TEM-network is optimised in each case for the correct passband specifications. The gray regions indicate the areas not adhering to the filter specifications. . . . .	84
5.15	The filter response of the 4 section prototype circuit with the optimised parameter values given in Table 5.7. . . . .	86
5.16	The (a) transmission coefficient and (b) reflection coefficient for different tuned passband states, given in Table 5.8. . . . .	87
5.17	Possible implementations of biasing networks in the prototype circuit. . . .	88
5.18	The insertion loss of the 4 section TEM-circuit for different resistors, denoted by $R_{s1}$ and $R_{s2}$ , that are connected in series with the capacitors $C_1$ and $C_2$ , respectively. The dashed lines indicate the two cut-off frequencies. . . . .	89
5.19	The complete circuit layout of the first prototype filter with microstrip elements in MWO. The parameters in the first section, closest to the input terminal, are repeated in each of the three sections to the right. The microstrip elements are specified in the table at the bottom right. . . . .	91
5.20	The layout of the 4 section microstrip structure with all the dimension parameters. . . . .	93
5.21	The centred filter responses of the 4 section microstrip model in MWO and EM simulation in Sonnet. . . . .	94
5.22	The results of the EM simulation of the 4 section filter for (a) BW tuning and (b) $f_0$ tuning. . . . .	95
5.23	A picture of the fabricated first prototype filter. . . . .	96
5.24	The measurements of the 4 section fabricated filter for (a) BW tuning and (b) $f_0$ tuning. . . . .	97
5.25	The passband of the 4 section fabrication that is tuned closest to the specifications for the centred response, plotted against the passband of the simulation. Due to a shift in frequency the fabrication's return loss deteriorates significantly. . . . .	97
5.26	The filter responses of the first prototype for a 100% deviation in the value of the series inductance ( $0.7 \pm 0.7$ nH) of the varactor (a) $C_1$ and (b) $C_2$ , respectively. These results are obtained with the microstrip circuit in MWO. . . . .	98

5.27	The filter responses of the networks consisting of 5 and 6 cascaded sections. These results are obtained with the simplified TEM-circuit in MWO shown in Fig. 5.12a. The gray regions indicate the areas not adhering to the filter specifications. Note that $s_{11}$ (dashed line) is only plotted at the passband frequencies. . . . .	99
5.28	The design graphs of different capacitor values for a filter network consisting of 6 cascaded sections. The TEM-network is optimised in each case for the correct passband specifications. The gray regions indicate the areas not adhering to the filter specifications. . . . .	100
5.29	The filter response of the optimised 6 section prototype circuit in MWO. The parameter values are given in Table 5.11. . . . .	101
5.30	The (a) transmission coefficient and (b) reflection coefficient for different tuned passband states, summarised in Table 5.12. . . . .	102
5.31	The microstrip node between $C_2$ (at 1), $C_{b2}$ (at 2) and $R_c$ (at 3). . . . .	103
5.32	The layout of the 6 section microstrip structure with all the dimension parameters. Note that only the first 3 sections of the filter are shown here. The remaining 3 sections are symmetrical to the first 3. The polygon indicated as “node” is shown more clearly in Fig. 5.31. . . . .	103
5.33	The centred filter responses of the 6 section microstrip model in MWO and EM simulation in Sonnet. . . . .	104
5.34	The results of the EM simulation of the 6 section filter for (a) BW tuning and (b) $f_0$ tuning. . . . .	105
5.35	A picture of the fabricated second prototype filter. . . . .	105
5.36	The measurements of the fabricated 6 section filter for (a) BW tuning and (b) $f_0$ tuning. . . . .	106
5.37	The passband of the 6 section fabrication that is fine-tuned to the specifications for the centred response, plotted against (a) the designed passband of the simulation and (b) the adapted microstrip circuit in MWO. Due to a shift in frequency the fabrication’s return loss deteriorates significantly. . . . .	106
5.38	The filter responses of the second prototype for a 100% deviation in the value of the series inductance ( $0.7 \pm 0.7$ nH) of the varactor (a) $C_1$ and (b) $C_2$ , respectively. These results are obtained with the microstrip circuit in MWO. . . . .	107
5.39	A picture of the fabricated fixed passband filter consisting of 6 cascaded sections. . . . .	109
5.40	The simulated and measured results of the fixed passband filter consisting of 6 cascaded sections. . . . .	109



6.1 (a) The 6 section TEM-circuit, with filter response shown in Fig. 5.29, in cascade with the coupled-line transversal-section in Fig. 4.8a. (b) The response of the complete filter network against the response of the coupled-line transversal-section indicated by the dashed lines. . . . . 113

# List of Tables

1.1	The required filter specifications for the front-end filter of KAT-7. . . . .	2
3.1	Specifications for tunable combline filter. . . . .	33
3.2	The physical dimensions of microstrip resonator shown in Fig. 3.10, with resonant frequency at 1.53 GHz. . . . .	39
3.3	The final dimensions of the tunable combline filter shown in Fig. 3.14. (Refer to Fig. 3.10, Fig. 3.11a and Fig. 3.12a for clear reference of the dimension parameters.) . . . . .	42
4.1	The results obtained in [7] for $3^{rd}$ and $5^{th}$ order coupled-line filters. They are designed with the classical implementation method [8], as well as the new improved method [7]. The FBW of all the filters are designed for 50%. Note how small the measured BWs are for the filters designed with the classical method. . . . .	51
5.1	The optimised parameter values of the TEM-circuit in Fig. 5.7a with filter response shown in Fig. 5.7b. The terminal impedance is $Z_A = 50\Omega$ . . . . .	72
5.2	The tune-all results of the proposed filtering-section, for the design values given in Table 5.1. . . . .	75
5.3	The behaviour of a filtering-section with regard to its parameter values. This table serves as guidelines for the optimisation of the filtering response. Note that the numbering of the transmission poles and zeros, respectively increases from the lower to higher frequency positions. Refer to the schematic and filter response in Fig. 5.7. . . . .	76
5.4	The optimised parameter values for the networks consisting respectively of 2 and 3 cascaded sections (Fig. 5.11a), with corresponding responses shown in Fig. 5.11b. . . . .	80
5.5	The optimised parameter values for the networks consisting respectively of 2 and 4 cascaded sections (Fig. 5.12a), with corresponding responses shown in Fig. 5.12b. . . . .	81
5.6	Characteristics of the RO4003C substrate from Rogers. . . . .	85

5.7	The optimised parameter values of the 4 section prototype circuit with filter response shown in Fig. 5.15. The terminal impedance is $Z_A = 50\Omega$ .	86
5.8	The tune-all results of the 4 section prototype circuit for the design values given in Table 5.7.	87
5.9	The corresponding microstrip dimensions of the parameters of the 4 section TEM-circuit given in Table 5.7. The terminal impedance of $Z_A = 50\Omega$ has a line width $w_A = 1.14$ mm. Note that these are calculated for the RO4003C substrate.	92
5.10	Dimensions of the microstrip structure in Fig. 5.20 as obtained with the full wave EM simulation in Sonnet.	94
5.11	The optimised parameter values of the 6 section prototype circuit with filter response shown in Fig. 5.29. The terminal impedance is $Z_A = 50\Omega$ .	101
5.12	The tune-all results of the 6 section prototype for the design values given in Table 5.11.	102
5.13	Dimensions of the microstrip structure in Fig. 5.32 as obtained with the full wave EM simulation in Sonnet.	104
5.14	The characteristics of both the simulated prototype filters, consisting of 4 and 6 cascaded sections respectively.	108
6.1	The characteristics of the simulated and measured results of both prototype filters, consisting respectively of 4 and 6 cascaded sections. Note that the red numbers indicate the specifications not met by the corresponding filter.	112

# List of Abbreviations

<i>BPF</i>	Bandpass Filter
<i>BW</i>	Bandwidth
<i>EM</i>	Electromagnetic
<i>FBW</i>	Fractional Bandwidth
<i>I/O</i>	Input or Output
<i>KAT-7</i>	Karoo Array Telescope
<i>LPF</i>	Lowpass Filter
<i>MEMS</i>	Microelectromechanical Systems
<i>MWO</i>	Microwave Office
<i>RF</i>	Radio Frequency
<i>SKA</i>	Square Kilometre Array
<i>SRF</i>	Self-Resonating Frequency
<i>TEM</i>	Transverse Electromagnetic
<i>UWB</i>	Ultra-wideband

# List of Symbols

$c$	Speed of light in vacuum ( $\approx 3 \cdot 10^8$ m/s)
$\Delta BW$	Bandwidth deviation
$\Delta f_0$	Centre frequency deviation
$\epsilon_r$	Relative permittivity or dielectric constant
$\epsilon_{eff}$	Effective permittivity
$f$	Frequency
$f_o$	Centre or design frequency
$f_{c1}$	Lower cut-off frequency ( $< f_0$ )
$f_{c2}$	Upper cut-off frequency ( $> f_0$ )
$g$	Lowpass prototype element value
$J$	Admittance inverter or J-inverter
$j$	Imaginary unit with value $\sqrt{-1}$
$K$	Impedance inverter or K-inverter
$k$	Normalised coupling coefficient
$L_A$	Passband insertion loss
$L_m$	Mutual inductance
$L_R$	Passband return loss
$LC$	Inductor and capacitor combination
$\lambda$	Wavelength
$\lambda_g$	Guided wavelength

$M$	Coupling coefficient
$n$	Order of filter
$\Omega$	Angular frequency variable used for a lowpass prototype filter
$\Omega_c$	Angular cut-off frequency variable used for a lowpass prototype filter
$\omega$	Angular frequency
$\phi_{s11}$	Phase of the reflection coefficient ( $s_{11}$ )
$Q$	Quality factor
$Q_e$	External quality factor
$q_e$	Normalised external quality factor
$Q_L$	Loaded quality factor
$Q_u$	Unloaded quality factor
$s_{11}$	Reflection coefficient at port 1. In all graphs, except if differently stated, it is represented in dB calculated as $20 \cdot \log s_{11} $ .
$s_{22}$	Reflection coefficient at port 2. In all graphs, except if differently stated, it is represented in dB calculated as $20 \cdot \log s_{22} $ .
$s_{21}$	Transmission coefficient from port 1 to 2. In all graphs, except if differently stated, it is represented in dB calculated as $20 \cdot \log s_{21} $ .
$\tau_{s11}$	Group delay of the reflection coefficient ( $s_{11}$ )
$\theta$	Electrical length
$\theta_0$	Electrical length at centre or design frequency
$Y$	Admittance
$Y_A$	Terminal admittance
$Y_0$	Characteristic admittance
$Z$	Impedance
$Z_A$	Terminal impedance
$Z_0$	Characteristic impedance

*LIST OF TABLES*

xxii

$Z_{0e}$  Even-mode characteristic impedance

$Z_{0o}$  Odd-mode characteristic impedance

# Chapter 1

## Introduction

### 1.1 Motivation for research

The Square Kilometre Array (SKA) project is an international initiative to build the largest radio telescope in the world. A path finder for this instrument in South Africa is the Karoo Array Telescope, also known as KAT-7.

The KAT-7 system consists of seven dishes with state of the art technology. Extremely low-power signals are received from the outer parts of space, which calls for very sensitive front-end devices such as filters. For example, after filtering in the front-end of the radio frequency (RF) chain, the signal has to remain the same in magnitude variation across the specific highly selective frequency band.

Fabricated filters usually have some frequency shift or bandwidth (BW) change from the designed specifications. This is caused by tolerances in the fabrication process, which are always present to some extent and are inversely proportional to the cost of fabrication.

For this reason waveguide technology is a popular implementation for front-end filters in radio telescopes. Not only are the losses in waveguide filters very low, but high precision frequency responses can be achieved by using tuning screws to fine-tune the response after fabrication. However, these filters are very large in size, heavy in weight and are expensive to produce. Therefore, planar filters are a great alternative because it is smaller, easy to integrate in printed circuit boards and are more cost effective.

The front-end filter for KAT-7 must also have a wide BW. Design procedures for narrowband filters that are tunable in centre frequency ( $f_0$ ) and BW, referred to as tune-all filters, are well established. However, in the case of tune-all wideband filters these methods are not directly applicable. Therefore much research is required in order to produce such a filter for KAT-7.



## 1.2 Objectives

The purpose of this thesis is to identify and develop a possible solution for the front-end filter of KAT-7. Therefore the work must consist of a thorough investigation of literature and existing work, followed by a design of such a filter. The main objectives for the filter design is:

- Wide passband
- Tunable in  $f_0$  and BW
- Implementation in microstrip technology

The specifications for the filter is given in Table 1.1. Here the extent of the tune-all capability is not specified, only that tunability is required in  $f_0$  and BW. The end goal of the tunability is that the fabricated device can be fine-tuned in order to obtain the centred (or designed) passband. Thus for any tuned passband state the return loss ( $L_R$ ) should be higher than 15 dB.

**Table 1.1:** The required filter specifications for the front-end filter of KAT-7.

Characteristic	Requirement
Tunability in filter response	$f_0$ and BW
Centre or design frequency	$f_0 = 1.53$ GHz
Fractional bandwidth measured at the ripple	$FBW_{ripple} = 49\%$ (1.2 to 1.95 GHz)
Insertion loss deviation across passband	$\Delta L_A \leq 1$ dB
Insertion loss in passband	$L_A \leq 3$ dB
Return loss in passband	$L_R \geq 15$ dB
Lower frequency suppression with $ s_{21}  \leq -20$ dB	$0.89 \leq f \leq 1.1$ GHz
Upper frequency suppression with $ s_{21}  \leq -20$ dB	$2.1 \leq f \leq 2.5$ GHz

The centre frequency ( $f_0$ ) of the passband is specified as 1.53 GHz with a 49% fractional bandwidth (FBW). Note that the BW is defined from the lowest frequency (1.2 GHz) where the ripple starts, to the highest frequency (1.95 GHz) where the ripple ends. However, if there exists no passband ripple the insertion loss ( $L_A$ ) may not deviate with more than 1 dB in the passband, referred to with the parameter  $\Delta L_A$ .

There exists numerous impulsive signals outside this band which has to be rejected by 20 dB. I.e. the transmission coefficient ( $s_{21}$ ) must be smaller than -20 dB in magnitude. The concerned frequency bands are from 0.89 to 1.1 GHz, where distance measuring equipment on aircraft and GSM base stations operate and from 2.1 to 2.5 GHz, where fixed wireless networks operate.

## 1.3 Contributions

This thesis gives an extensive overview of tunability in microstrip filters. Applicable wideband filter syntheses are investigated and no suitable tune-all wideband filter design procedure is found in current literature. However, potential is found with perturbed ring-resonators and are investigated in the light of signal-interference techniques.

Following this, a new filtering-section with tune-all capabilities is proposed (Fig. 5.7a). This network is developed into filters consisting of 4 and 6 cascaded filtering-sections, respectively. These two prototype filters both demonstrate tunability in  $f_0$  and BW. The filters are fabricated and reasonably good results are obtained. Most of the specifications in Table 1.1 are achieved with this new design approach.

The proposed filter synthesis is unique in that it is tunable in  $f_0$  and BW, has a wide BW and is realisable in microstrip. An advantage of this design is that complete circuit models are used for optimisation, therefore avoiding time-consuming full wave simulations.

## 1.4 Overview

This thesis commences with a detailed review of tunability of narrowband filters in Chapter 2. The classic synthesis of lumped element prototypes are given, followed by an introduction to coupled resonator filters. Techniques for  $f_0$  and BW tuning in narrowband filters are discussed and various filter results found in literature are summarised. The reason for considering tunability in narrowband filters, is that this is a well developed field of research that enables insight for tunability in wideband applications. This chapter ends with a discussion of the affect of filter losses, due to tunable elements.

Techniques found in Chapter 2 are implemented in the design of a tunable combline filter in Chapter 3. The purpose of the design is to investigate the implementation of tunability with varactor diodes. Therefore this filter does not adhere to all the specifications given in Table 1.1. The formulation and extraction techniques for the design parameters of coupled resonator filters are also presented.

Wideband filter syntheses are reviewed in Chapter 4, along with discussions of the possibilities for implementation of tunability. The most applicable synthesis for tunable filters found in Chapter 2, is reviewed with regard to wideband application. This chapter ends with a premise for tunability in transversal-sections.

The conclusions and recommendations made in Chapter 4 are used in Chapter 5 to develop a new type of tunable wideband filter. A filtering-section (Fig. 5.7a) is developed and characterised, followed by the proposal of a new prototype filter, consisting of a cascade of these filtering-sections, for KAT-7. A design by optimisation synthesis is developed and two prototype filters are designed and fabricated according to the specifications in Table 1.1. Very good results are obtained (Table 5.14) and recommendations are given

for further improvements.

In Chapter 6 the thesis ends with a conclusion of the work. Recommendations are also made for future development.

# Chapter 2

## Narrowband Filters with Tunability

### 2.1 Introduction

This chapter consists of two main parts. The first part briefly discusses common transfer functions followed by the introduction of classic filter theory to implement the transfer functions. This is necessary in order to address the problem of tunability in filters.

The second part examines various tuning techniques for microwave planar filters. The discussion includes frequency as well as bandwidth tuning through varactor diodes. Electronic tuning components introduce significant losses in filters. For this reason the quality factor ( $Q$ -factor) along with its effects on filter characteristics are reviewed at the end of the chapter.

The tuning techniques that are reviewed in this chapter are mainly applied to narrowband filters. This is because classic filter theory, applicable for implementing tunability, is based on narrowband approximations. In Chapter 4 the need for synthesis of tunable wideband filters will become evident.

### 2.2 Transfer functions

A transfer function is the mathematical description of the characteristics of a network. In filter theory there are numerous types of transfer functions that has certain filtering properties. This section briefly discusses four common transfer functions namely Butterworth, Chebyshev, Elliptic and Gaussian.

In Fig. 2.1 the normalised lowpass responses of the transfer functions are given. Each is of the 4<sup>th</sup> order and normalised to a 3 dB angular cut-off frequency (i.e.  $|s_{21}| = -3$  dB at  $\Omega = \Omega_c$ ). The angular cut-off frequency ( $\Omega_c$ ) is not normalised to the ripple cut-off, as is practice for equal-ripple responses, in order to compare the responses against one another. Note that the angular frequency parameter for a lowpass response is represented by  $\Omega$  as opposed to  $\omega$ , in order to distinguish between lowpass and bandpass responses.

The passband of a lowpass filter response is defined for  $0 < \Omega < \Omega_c$  and for a bandpass filter between the lower and upper cut-off frequencies ( $\omega_{c1} < \omega < \omega_{c2}$ ).

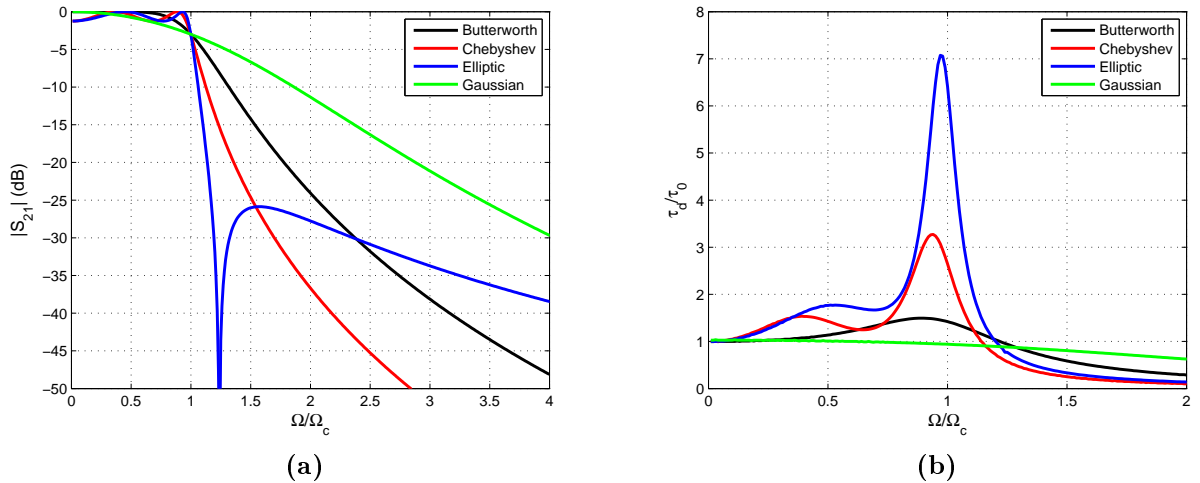


**Figure 2.1:** The lowpass 4<sup>th</sup> order prototype filter responses with cut-off frequency at  $|S_{21}| = -3$  dB. (a) The transmission coefficient against the normalised frequency and (b) the normalised group delay against the normalised frequency.

The Butterworth response, also known as the Maximally Flat response, has a maximum number of zero derivatives of the amplitude-squared transfer function at  $\Omega = 0$  rad/s [9]. As seen in Fig. 2.1a the passband gain deteriorates quite rapidly as  $\Omega$  approaches cut-off.

The Chebyshev response is probably the fundamental response most used in filter design. The response exhibits an equal-ripple passband and a maximally flat stopband. Note that the group delay in Fig. 2.1b peaks close to cut-off.

The Elliptic function gives much higher selectivity (i.e. a sharper attenuation slope) than the former two functions as seen in Fig. 2.1a. A trade-off for higher selectivity is that the stopband rejection level decreases. Note that there exists a ripple in the passband of the Elliptic function which can be altered to give an equal-ripple, such as that of the Chebyshev response, with a co-existing equal-ripple in the stopband [10].

The Gaussian response is designed to have a maximally flat group delay at  $\Omega = 0$  as seen in Fig. 2.1b. Here it is evident that flat group delay leads to very poor selectivity in the magnitude response seen in Fig. 2.1a.<sup>1</sup>

Comparing these responses it is noticed that the Elliptic response has the best selectivity and the Gaussian response the worst. On the contrary the Gaussian response has much better group delay distortion (or ratio of change in passband group delay) compared to the Elliptic. The selectivity and the group delay is always a trade-off in filters. This is why the Chebyshev response is often the preferred choice for design, with a good balance

<sup>1</sup>The 3 dB bandwidth of the Gaussian response is a function of the filter order.

between the two characteristics.

All microwave filters have some losses and this alters the passband response compared to the lossless case in Fig. 2.1a, especially the Chebyshev response [9]. This is discussed in more detail at the end of this chapter.

The Butterworth response is normally said to have less group delay distortion than the Chebyshev, as is observed from the instance in Fig. 2.1b. According to [9] this is not always the case. This depends on the size of the equal-ripple and the cut-off frequency reference.

### 2.3 Lumped element prototype

In classic filter synthesis, lumped element prototypes are used to realise transfer functions. Fig. 2.2 shows two forms of a  $n^{th}$  order lowpass prototype filter. Either of these circuits may be used to produce the Butterworth, Chebyshev or Gaussian filter responses, due to its dual properties. Prototype filters for the Elliptic response results in a circuit similar to this, but with resonators to produce transmission zeros in the stopband [10]. For the purpose of this thesis it will not be discussed here.

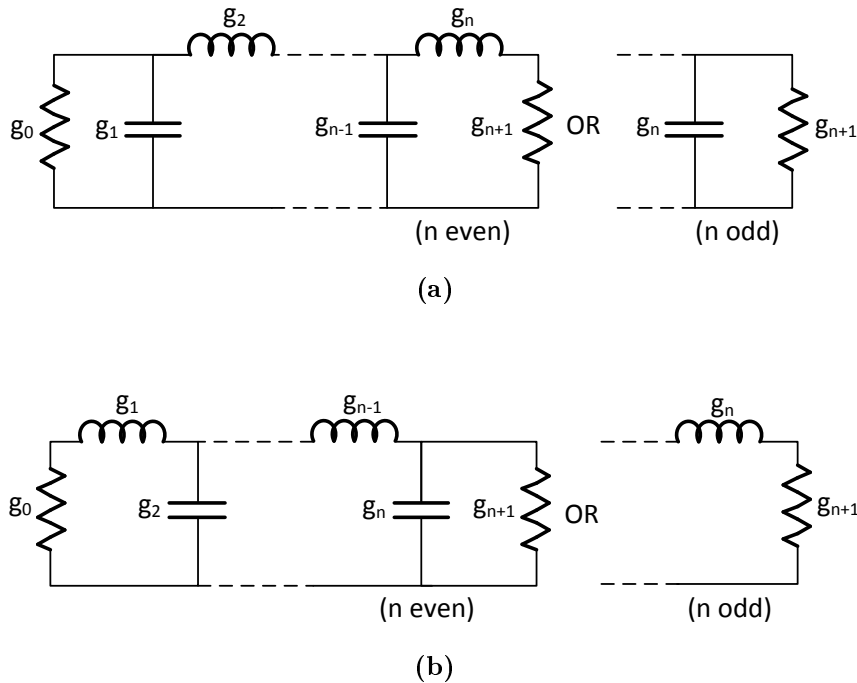


**Figure 2.2:** The circuit for a lowpass lumped element prototype in (a) with its dual circuit in (b).

The element  $g_i$ , for  $i = 1$  to  $n$ , is either the inductance of a series inductor or the capacitance of a shunt capacitor, depending on the circuit used or the order of the filter (see Fig. 2.2). The source and load resistances or conductances are given by  $g_0$  and

$g_{n+1}$ . The elements of the lowpass prototype circuit are normally scaled to give a source resistance of  $1\Omega$  and a cut-off angular frequency of 1 rad/s.

If  $g_1$  is a series inductor or shunt capacitor, then  $g_0$  is a source conductance or resistance respectively. The same applies to the load  $g_{n+1}$  when  $g_n$  is a series inductor or shunt capacitor.

These element values can be calculated for a specific transfer function [10] or may be obtained from element tables widely available in literature. An extensive book on element tables is [11].

In order to obtain a bandpass filter from these prototype circuits, the lowpass to bandpass transformation is considered. First the centre angular frequency and fractional bandwidth of the bandpass response are defined as

$$\omega_0 = \sqrt{\omega_{c1}\omega_{c2}} \quad (2.1)$$

and

$$FBW = \frac{\omega_{c2} - \omega_{c1}}{\omega_0}, \quad (2.2)$$

where  $\omega_{c1}$  is the lower and  $\omega_{c2}$  the upper cut-off frequencies of the bandpass response. The frequency transformation from lowpass to bandpass is given by

$$\Omega \rightarrow \frac{\Omega_c}{FBW} \left( \frac{\omega}{\omega_0} - \frac{\omega_0}{\omega} \right). \quad (2.3)$$

The impedance scaling factor is defined as

$$\gamma_0 = \frac{Z_0}{g_0} \quad (2.4)$$

where  $Z_0$  is the source (also referred to as terminal) resistance. The scaling factor not only scales the resistive components but also the reactive components of the lowpass filter (LPF) as

$$\begin{aligned} L &\rightarrow \gamma_0 L \\ C &\rightarrow C/\gamma_0 \end{aligned} \quad (2.5)$$

This step only normalises the source/load impedance and does not affect the filter response.

Applying the frequency transformation (2.3) to a reactive element  $g$  leads to

$$j\Omega g \rightarrow j\omega \left( \frac{\Omega_c}{FBW\omega_0} g \right) + \frac{1}{j\omega} \left( \frac{\omega_0\Omega_c}{FBW} g \right). \quad (2.6)$$

It is noticed that if  $g$  is an inductor in the LPF, the transformation gives a series LC resonator in the bandpass filter (BPF) resulting in

$$\begin{aligned} L_s &= \left( \frac{\Omega_c}{FBW\omega_0} \right) g\gamma_0 \\ C_s &= \left( \frac{FBW}{\omega_0\Omega_c} \right) \frac{1}{g\gamma_0}, \end{aligned} \quad (2.7)$$

with the impedance scaling factor (2.4) applied. In the same manner if  $g$  is a capacitor in the LPF, the transformation gives a parallel LC resonator in the BPF resulting in

$$\begin{aligned} L_p &= \left( \frac{FBW}{\omega_0\Omega_c} \right) \frac{\gamma_0}{g} \\ C_p &= \left( \frac{\Omega_c}{FBW\omega_0} \right) \frac{g}{\gamma_0}. \end{aligned} \quad (2.8)$$

The result of a transformed  $n^{\text{th}}$  order lowpass prototype of the form in Fig. 2.2a is shown in Fig. 2.3. This transformation holds for any other lowpass prototype circuit.

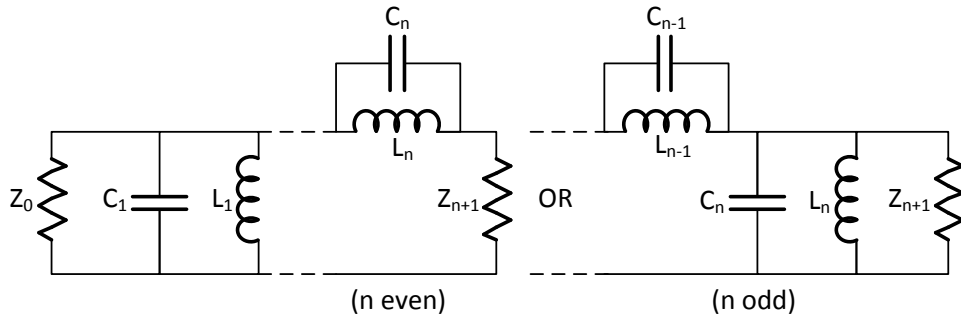


**Figure 2.3:** A  $n^{\text{th}}$  order bandpass lumped element prototype that is transformed from the lowpass prototype shown in Fig. 2.2a.

## 2.4 Distributed element prototype

The distributed element prototype is another way of realising filter functions. For bandpass filters this is also referred to the coupled resonator synthesis. The main idea of this synthesis is to transform the lumped element model into a distributed model that is easier to implement in microwave structures such as microstrip.

The derivation of the distributed model is based upon immittance inverters. An ideal inverter has the characteristic of scaling impedance or admittance levels independent of frequency. The impedance inverter shown in Fig. 2.4a, scale a load impedance to

$$Z_{in} = \frac{K^2}{Z_L}, \quad (2.9)$$

where  $K$  is the inverter parameter. Its dual circuit, the admittance inverter shown in Fig. 2.4b, scale a load admittance to



$$Y_{in} = \frac{J^2}{Y_L}, \quad (2.10)$$

with  $J$  the inverter parameter in the admittance case.

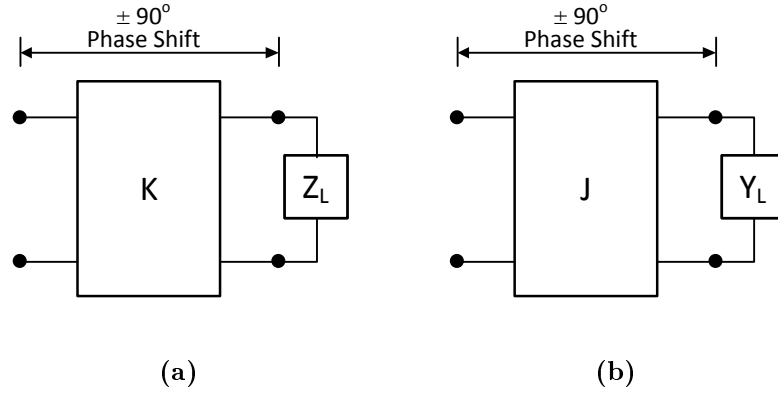


**Figure 2.4:** The impedance inverter in (a) with its dual circuit the admittance inverter in (b). Note that an ideal inverter is frequency independent with a  $\pm 90^\circ$  phase shift.

Two common ways of using lumped elements to realise inverters are shown in Fig. 2.5a and b, with its dual circuits in Fig. 2.5c and d. Note that negative inductors and capacitors are used in these circuits. This is not practically realisable and therefore the negative elements are generally absorbed into the rest of the network. Other practical ways of realising inverters can be found in [9].

A powerful characteristic of an inverter is that a series inductor between two inverters has the properties of a shunt capacitor from its exterior terminals. Similarly, a shunt capacitor between two inverters have the properties of a series inductor. Using these characteristics the lumped prototype circuits in Fig. 2.2 are converted to the new lowpass prototype circuits in Fig. 2.6.

The immittance inverters are derived in [9] using circuit theory and are given as

$$K_{01} = \sqrt{\frac{Z_0 L_{a1}}{g_0 g_1}}, \quad K_{i,i+1} = \sqrt{\frac{L_{ai} L_{a,i+1}}{g_i g_{i+1}}} \Big|_{i=1 \text{ to } n-1}, \quad K_{n,n+1} = \sqrt{\frac{L_{an} Z_{n+1}}{g_n g_{n+1}}} \quad (2.11)$$

and

$$J_{01} = \sqrt{\frac{Y_0 C_{a1}}{g_0 g_1}}, \quad J_{i,i+1} = \sqrt{\frac{C_{ai} C_{a,i+1}}{g_i g_{i+1}}} \Big|_{i=1 \text{ to } n-1}, \quad J_{n,n+1} = \sqrt{\frac{C_{an} Y_{n+1}}{g_n g_{n+1}}}. \quad (2.12)$$

Note that the original lumped prototype elements are still represented by  $g_i$  and the rest of these parameters are representative of the elements as shown in Fig. 2.6.

The significance of these circuits are not only that the reactive elements are now of

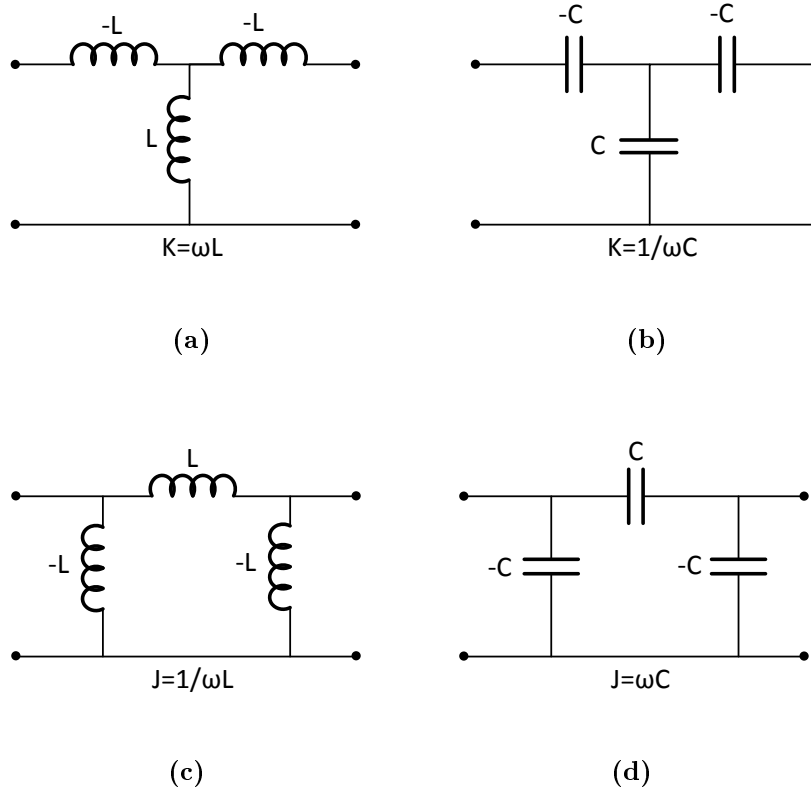


**Figure 2.5:** Practical realisations of the impedance inverter using either (a) inductors or (b) capacitors and the admittance inverter using either (c) inductors or (d) capacitors.

the same kind, but also that one can choose any value for  $Z_0$ ,  $Z_{n+1}$ ,  $L_{ai}$ ,  $Y_0$ ,  $Y_{n+1}$  and  $C_{ai}$ , and still have the same response as the original prototype, given that (2.11) or (2.12) holds.

Since the inverters are frequency independent, the frequency transformation (2.3) can also be applied to the new lowpass prototypes in Fig. 2.6 to obtain new bandpass prototypes. As shown in (2.7) and (2.8) all the reactive elements become LC resonators. The resulting bandpass circuits are shown in Fig. 2.7, where the reactance ( $X_i$ ) and susceptance ( $B_i$ ) elements represent these resonators. Note that the resonators are synchronously tuned, i.e. they have the same resonant frequency  $\omega_0$  but not necessarily the same  $L$  and  $C$  values.

As mentioned, it is not desirable to have lumped elements in the prototype model because of the difficulty to realise this in microwave structures. Therefore the LC resonators are replaced by distributed circuits [9], of where the name “distributed element form” originates. Generalising the model in Fig. 2.7 so that any type of resonator may be used with such a model, the new resonators must have reactances or susceptances equal to that of the LC resonators at all frequencies. In practise this is only true at the resonant frequency and thus the reactance and susceptance slopes are introduced.

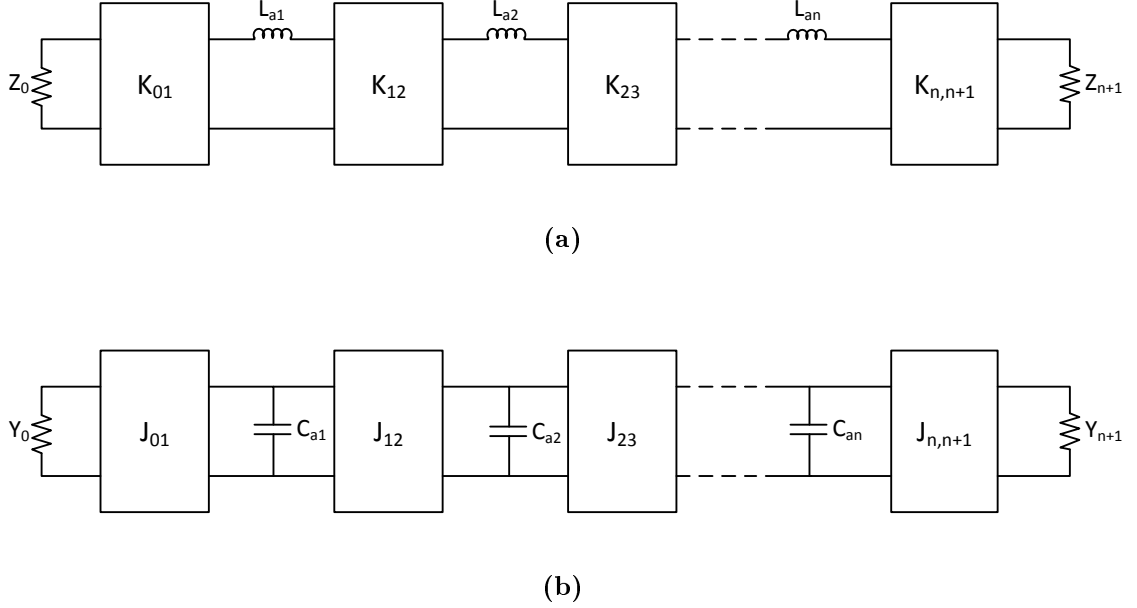


**Figure 2.6:** The lowpass distributed prototype with (a) series inductors or (b) shunt capacitors. Note that the circuit in (b) is a dual circuit of (a).

For any resonator with series-type resonance, the reactance slope is

$$x_i = \left. \frac{\omega_0}{2} \frac{dX_i}{d\omega} \right|_{\omega=\omega_0} \quad (2.13)$$

and with shunt-type resonance, the susceptance slope is

$$b_i = \left. \frac{\omega_0}{2} \frac{dB_i}{d\omega} \right|_{\omega=\omega_0}. \quad (2.14)$$

This means that any resonator can be used as long as one can approximate its slope parameter at resonance. For a series LC resonator the reactance slope is

$$x = \omega_0 L_s \quad (2.15)$$

and for a parallel LC resonator the susceptance slope is

$$b = \omega_0 C_p. \quad (2.16)$$

By applying the frequency transformation to (2.11) and (2.12), along with the slope parameters of the resulting LC resonators, the new inverter equations of Fig. 2.7 are given [9] as

$$K_{01} = \sqrt{\frac{Z_0 x_1 FBW}{g_0 g_1 \Omega_c}}, \quad K_{i,i+1} = \frac{FBW}{\Omega_c} \sqrt{\frac{x_i x_{i+1}}{g_i g_{i+1}}} \Big|_{i=1 \text{ to } n-1}, \quad K_{n,n+1} = \sqrt{\frac{x_n Z_{n+1} FBW}{g_n g_{n+1} \Omega_c}} \quad (2.17)$$

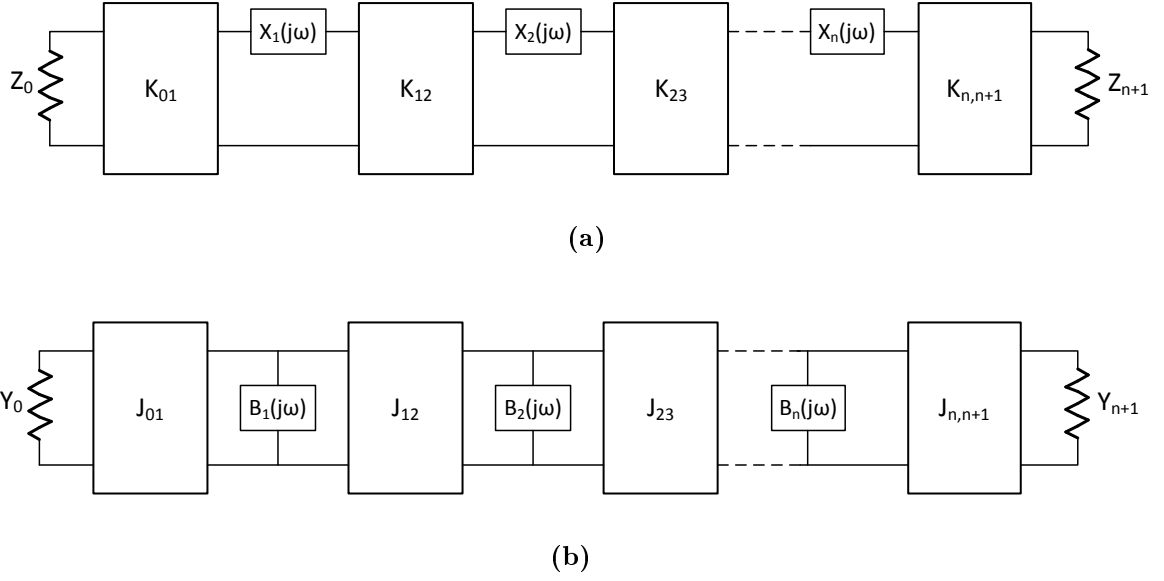


**Figure 2.7:** The general form of the distributed bandpass prototype filter, where (b) is the dual circuit of (a).

and

$$J_{01} = \sqrt{\frac{Y_0 b_1 FBW}{g_0 g_1 \Omega_c}}, \quad J_{i,i+1} = \frac{FBW}{\Omega_c} \sqrt{\frac{b_i b_{i+1}}{g_i g_{i+1}}} \Big|_{i=1 \text{ to } n-1}, \quad J_{n,n+1} = \sqrt{\frac{b_n Y_{n+1} FBW}{g_n g_{n+1} \Omega_c}}. \quad (2.18)$$

Note that all the parameters are the same as previously defined without any impedance scaling.

Since the inverters generally used for practical filters are frequency dependant and the resonators not purely series/parallel LC combinations, this approximation is best for narrowband filters. According to [9] bandwidths up to 20% can be achieved with half-wavelength resonators and in some cases approaching 40% with quarter-wavelength resonators.

In coupled resonator BPF design there are three main design parameters used for synthesis, namely the resonance frequency ( $f_0$ ), the coupling coefficient ( $M$ ) and the external quality factor ( $Q_e$ ). The resonance frequency is a well known parameter, but the latter two parameters need to be defined with respect to BPFs.

There are numerous interpretations of the coupling coefficient but the basic idea is that if two resonators (or any inclusions) are physically brought close enough, mutual coupling occurs. I.e. energy are exchanged between the resonators. For inductive coupling, the coupling coefficient is defined as

$$M_{i,i+1} = \frac{L_m}{\sqrt{L_i L_{i+1}}}, \quad (2.19)$$

where  $L_m$  is the mutual inductance between adjacent inductors  $L_i$  and  $L_{i+1}$ . The equivalent circuit for mutual coupling is exactly the same as the K-inverter circuit in Fig. 2.5a and therefore

$$K = \omega_0 L_m. \quad (2.20)$$

Substituting this equation along with (2.15) into (2.19) gives

$$M_{i,i+1} = \frac{K_{i,i+1}}{\sqrt{x_i x_{i+1}}}, \quad (2.21)$$

which makes the coupling coefficient the foundation for realising inverters between microwave resonators.

The  $Q_e$  is a measure of the coupling of a loaded external circuit into a lossless resonator [8].<sup>2</sup> The  $Q_e$  of the lossless series input/output (I/O) resonator of the prototype circuit in Fig. 2.7, is derived in [8] as

$$Q_e = \frac{\omega_0 L}{R}, \quad (2.22)$$

where  $L$  is the inductance of the resonator and  $R$  the source/load resistor as seen from the resonator. For a series resonator, (2.15) and (2.9) are substituted into (2.22) to give

$$Q_e = \frac{x}{(K^2/Z_0)}. \quad (2.23)$$

Rewriting (2.21) for the general inverters between adjacent resonators, as well as (2.23) for the inverters between the terminals and I/O resonators, the equations in (2.17) are replaced by these general equations for the series coupled resonator prototype (Fig. 2.7a)

$$K_{01} = \sqrt{\frac{Z_0 x_1 FBW}{q_{e0}}}, \quad K_{i,i+1} = FBW \cdot k_{i,i+1} \cdot \sqrt{x_i x_{i+1}} \Big|_{i=1 \text{ to } n-1}, \quad K_{n,n+1} = \sqrt{\frac{x_n Z_{n+1} FBW}{q_{en}}}. \quad (2.24)$$

The normalised parameters  $k$  and  $q_e$  are defined as

$$k_{i,i+1} = \frac{M_{i,i+1}}{FBW} \quad (2.25)$$

and

$$q_e = Q_e \cdot FBW. \quad (2.26)$$

In the same manner the derivation of the general equations for the parallel coupled resonators result in

---

<sup>2</sup>The quality factor of a resonant circuit is discussed in more detail later in this chapter.

$$J_{01} = \sqrt{\frac{Y_0 b_1 FBW}{q_{e0}}}, \quad J_{i,i+1} = FBW \cdot k_{i,i+1} \cdot \sqrt{b_i b_{i+1}} \Big|_{i=1 \text{ to } n-1}, \quad J_{n,n+1} = \sqrt{\frac{b_n Y_{n+1} FBW}{q_{en}}}. \quad (2.27)$$

Note that the  $q_e$ 's and  $k$ 's replace the classic  $g$  parameters and are referred to as the design parameters. These parameters can also be found in [11] according to the transfer function specifications.

The significance of this filter synthesis is that the prototype circuit can be realised with microwave resonators without much effort. The I/O inverter is realised using a feed structure<sup>3</sup> to couple between the I/O resonator and source/load terminal. This is done in accordance with the specified  $Q_e$ . The inverters between resonators are realised by mutually coupling the adjacent resonators according to the specific  $M_{i,i+1}$ .

Another great advantage of the coupled resonator synthesis over the lumped element synthesis, is that the BW and  $f_0$  can be extracted directly from the design equations.<sup>4</sup> This enables control of the filtering properties and give rise to the concept of tunable filters.

The Chebyshev, Butterworth and Gaussian functions can be realised with the general distributed prototype in Fig. 2.7, similar to the lumped element prototype. The Elliptic function, however, may be realised using more advanced coupling structures [10]. Here the concept is that non-adjacent resonators are coupled with one another according to  $M_{ij}$ , where  $j \neq i + 1$ . This introduces transmission zero's (i.e.  $|s_{21}| = 0$ ) at finite frequencies. Therefore the equations in (2.13) and (2.27) does not necessarily hold any longer.

A synthesis using such advanced coupling structures, called the coupling matrix synthesis, has been developed by Atia et al. [12] and Cameron [13]. This method allows much more freedom in the realisation of transfer functions, but yields more complex structures which in some cases are not physically feasible.

## 2.5 Techniques for tuning narrowband filters

Wireless systems use different frequency spectrum windows due to the electromagnetic (EM) wave characteristics at those frequencies shown in Fig. 2.8. Commercial and military institutions are placing high demands on efficient use of the frequency spectrum. Advances in efficiency have been made in technical areas such as modulation, access methods and fixed frequency band filters. New wireless applications require hardware to be adaptable for the use of multiple bands. This means that the hardware must be able to change to a specific frequency and bandwidth. One of the hardware subsystems that needs to be tunable or reconfigurable is the RF/microwave filter.

<sup>3</sup>Feeds are introduced in the next chapter.

<sup>4</sup> $BW \propto M$  and  $f_0 \propto \frac{1}{C}$ , where  $C$  is the capacitance of a resonator.

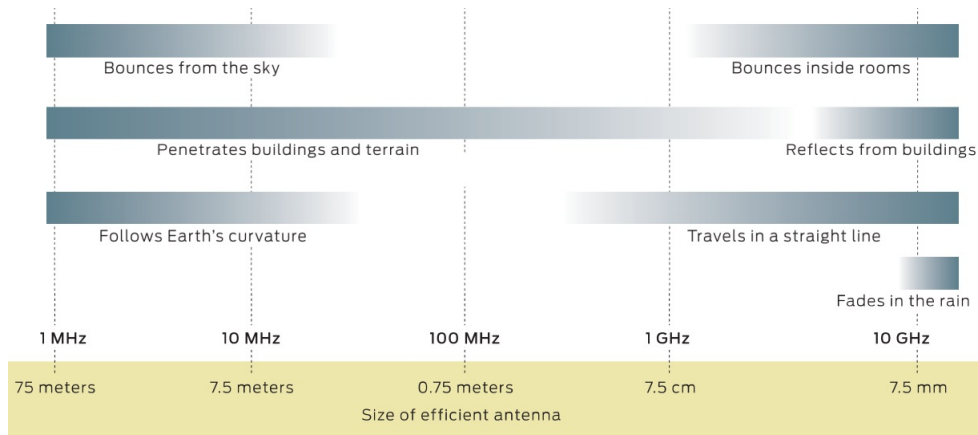


**Figure 2.8:** Frequency spectrum windows for different EM wave applications. Illustration taken from [1].

Tuning elements such as ferroelectric varactors and varactor diodes are used to enable electronic tunability in microstrip filters. Ferroelectric varactors have relatively high Q-factors, but has to be integrated in the substrate. This requires high temperatures for the fabrication process and therefore limits the substrates that may be used [14]. One of the reasons why varactor diodes are widely used in tunable filters, is because of its commercial availability in surface mount packaging, making it ideal for circuit integration. The downside is that it has very low Q-factors at microwave frequencies. Both the ferroelectric varactor and varactor diode acts as a tunable capacitor that is a function of the biased DC voltage. Therefore another aspect that is necessary to consider is the biasing network for a tuning element.<sup>5</sup>

In this section different techniques and existing methods for such tunable filters are discussed. Many of these tuning techniques are developed for wireless systems due to its popular demand, but in most instances are also relevant for radio astronomy applications.

### 2.5.1 Frequency tuning

The center frequency of a response is easily changed by tuning the resonators of a coupled resonator filter. For a simple LC resonator the resonant frequency is defined as

$$\omega_0 = \frac{1}{\sqrt{LC}}. \quad (2.28)$$

Fig. 2.9a shows an example of a varactor-loaded transmission line resonator that exhibits a shunt-type resonance. The transmission line must be shorter than a quarter wavelength in order to resonate with the capacitance of the varactor diode. Here the resonant frequency is approximated as

<sup>5</sup>This is discussed in the filter design of the next chapter.

$$\omega_0 = \frac{1}{C \cdot Z_0 \tan \theta_0}, \quad (2.29)$$

where  $C$  is the capacitance of the varactor,  $Z_0$  the characteristic impedance of the line and  $\theta_0$  the electrical length of the line at resonance.

This resonator is used in the well known linear coupled combline filter shown in Fig. 2.9b. When tuning all the resonators symmetrically, the center frequency of the filter response are changed. The problem with this tuning approach is that the bandwidth of the filter also changes because of the frequency dependence of the coupling network [15] and is not desirable in many systems.

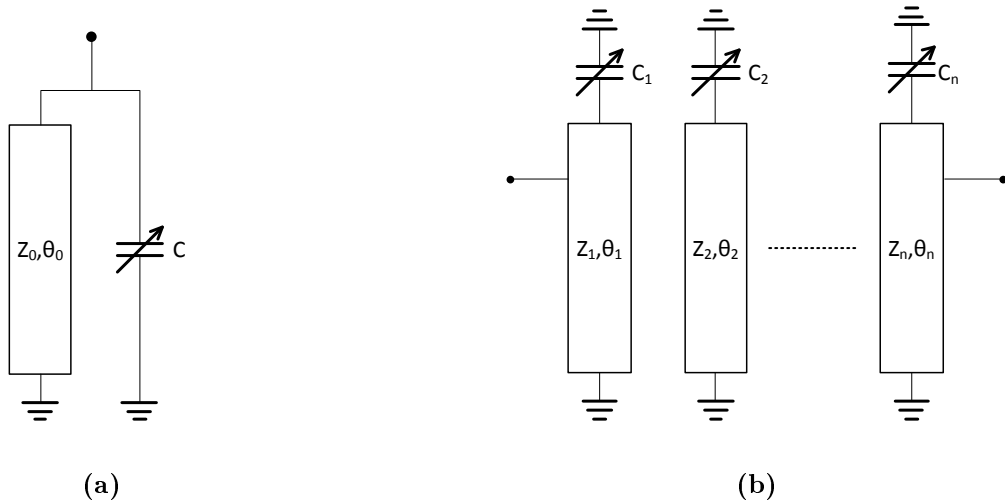


**Figure 2.9:** The schematics of (a) a varactor-loaded transmission line resonator and (b) a combline filter consisting of a coupled-array of these resonators.

In [16] this problem is minimised for a combline filter and design equations are presented for optimal frequency tuning. The equivalent circuit model of a combline filter is shown in Fig. 2.10a, with resonator admittance  $Y_{(r)} = j\omega C_r + \frac{Y_r}{j \tan(\theta)}$ . The coupling between adjacent resonators is inductive and therefore it is represented by distributed inductors with admittances  $Y_{r-1,r}$ ,  $Y_{r,r+1}$ , etc. By adapting the resonator admittances (Fig. 2.10b), admittance inverters may be extracted to give the distributed form as shown in Fig. 2.10c. The admittance inverters are calculated as

$$J_{r,r+1} = \frac{Y_{r,r+1}}{\tan(\theta)}. \quad (2.30)$$

Note that  $\theta$  is a variable parameter for the electrical length. For the lossless case of a purely transverse electromagnetic (TEM) line,  $\theta$  is proportional to the frequency and therefore



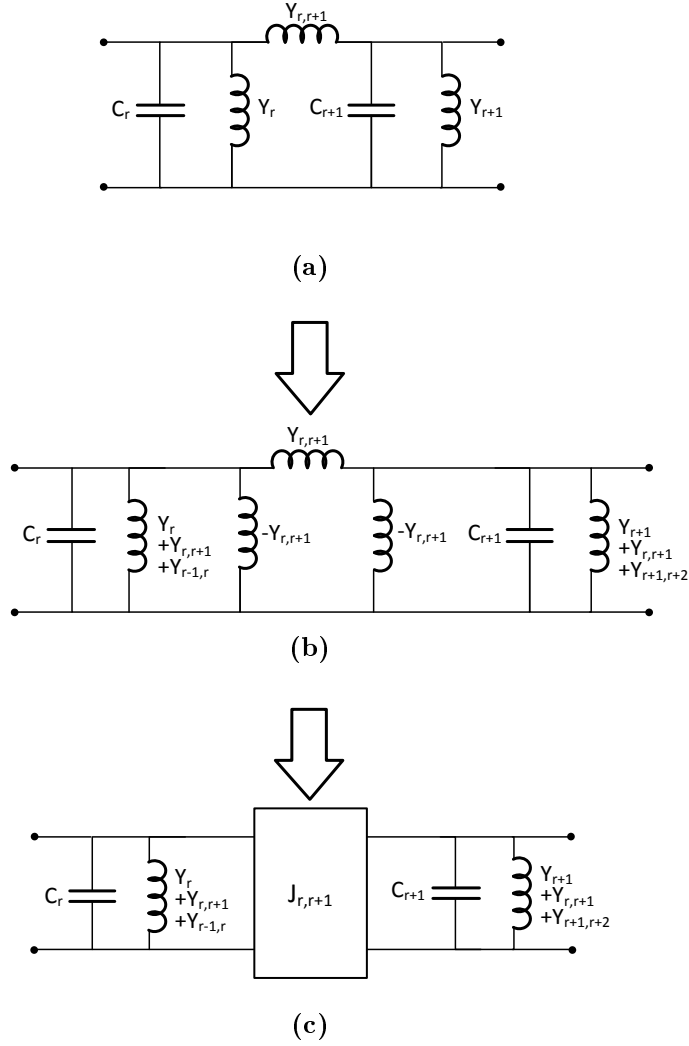


**Figure 2.10:** The extraction of an embedded admittance inverter from a section of the equivalent combline filter circuit. (a) The circuit represents two inductively coupled combline resonators, where the susceptance of the distributed inductance of the first resonator is  $\frac{-Y_r}{\tan\theta}$ . (b) The adapted lumped circuit. (c) The distributed circuit of the combline filter.

$$\theta = \left( \frac{\omega}{\omega_0} \right) \cdot \theta_0. \quad (2.31)$$

The frequency dependence of the inverters is removed by scaling the whole admittance network with  $\frac{\tan(\theta)}{\tan(\theta_0)}$ . This approximation holds only for narrowband filters, because in the vicinity of the center frequency the scaling factor is equal to unity.

Assuming narrow BW and by applying the backwards BPF transformation to the distributed model in Fig. 2.10c, the following is derived [16]

$$BW = k \cdot \frac{\theta_0 \cdot \tan(\theta_0)}{\tan(\theta_0) + \theta_0 (1 + \tan^2(\theta_0))}, \quad (2.32)$$

where  $k$  represents a constant that depends on the resonator geometry. The graph of

(2.32) given in Fig. 2.11 shows that there is a BW maximum at  $\theta_0 = 53^\circ$ . Around this point the BW degradation is a minimum as the resonator frequency is tuned. Therefore the filter should be designed with resonator line lengths of  $53^\circ$  at the centre tuning frequency, to enable optimal tuning range with minimum BW degradation. An octave tuning range ( $35^\circ - 70^\circ$ ) can be achieved with only 20% BW deviation ( $\Delta BW$ ) across the range.<sup>6</sup>

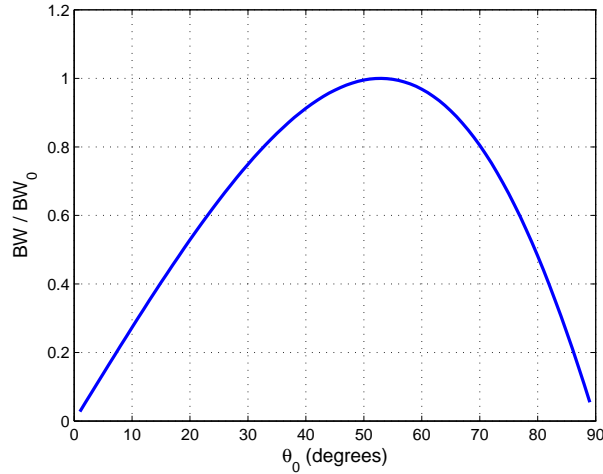


**Figure 2.11:** The normalised bandwidth ( $BW/BW_0$ ) of a combline filter for different resonator electrical lengths ( $\theta_0$ ), calculated with equation (2.32).

The factor  $\frac{\tan(\theta)}{\tan(\theta_0)}$ , used to scale the whole network, causes the terminal conductance to be frequency dependant. This consequently leads to a mismatch at the I/O terminals as the frequency changes, causing  $L_R$  to change. Tuning the centre frequency over an octave changes the terminal conductance with a ratio of 3.9:1.

This effect is minimised when a redundant impedance transforming network is introduced at the I/O terminals. It is realised with an inverter calculated by equations (27-29) in [16]. It is found that for optimal tuning with lowest degradation of  $L_R$ , the electrical length should be  $45^\circ$  at the design frequency. The result is a 0.87:1 variation in the terminal conductance over an octave tuning range ( $30^\circ - 60^\circ$ ).

In a practical realization of this design technique for a  $2^{nd}$  order filter, the authors of [16] achieve a tuning range from 3.2 to 4.9 GHz (0.53 of an octave) with a small deviation of 12.3% in the passband BW and  $L_R > 8dB$  across the tuning range. A systematic approach for this optimum design technique is given in [17].

In order to achieve constant BW in the tuning range, the  $M$  between adjacent resonators must be inversely proportional to the frequency while the  $Q_e$  is proportional. In [18] a new type of combline filter is designed using stepped-impedance lines for the resonators and lumped inductors for the terminal coupling transformers. The changes made to the conventional combline model deals with the frequency dependence of the coupling.

<sup>6</sup>Note that the BW deviation is calculated as the difference between the minimum and maximum BWs, divided by the maximum BW. I.e.  $\Delta BW = \frac{BW(\text{maximum}) - BW(\text{minimum})}{BW(\text{maximum})}$ .

The result of this type of filter in [18] gives a 3.2%  $\Delta BW$ , but this is across a very narrow tuning range of 0.16 of an octave. The return loss is also well preserved.

Another filter topology widely used is the interdigital filter with its tunable configuration shown in Fig. 2.12. In [19] a frequency tunable interdigital filter is designed. A tuning range of 0.9 of an octave is achieved, but with a poor  $\Delta BW$  around 70%.

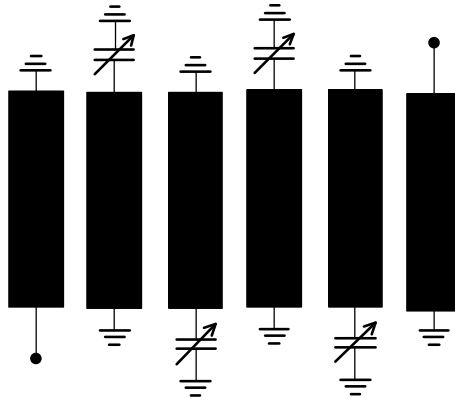


**Figure 2.12:** Schematic of an interdigital filter with frequency tuning ability.

## 2.5.2 Frequency and bandwidth tuning

The previous tuning approaches does not give the means to control the BW, but optimises the design to keep the absolute BW constant over the frequency range.<sup>7</sup> A new technique to tune the absolute BW, as well as the center frequency, is developed in [2].

The inductive coupling between adjacent resonators in a simple combline configuration can be represented by a distributed inductor as shown previously (Fig. 2.10a). In [20] a new coupling network (Fig. 2.13) is proposed for BW tuning. The idea is to tune the coupling between adjacent resonators continuously by the means of varactor diodes in order to control the BW of the filter response. Here the inductors represent distributed inductances with characteristic admittances  $Y_r$ ,  $Y_{c1}$  and  $Y_{c2}$ , while  $Y_{bw}$  is the tunable admittance that controls the BW of the circuit.

The following are the two extreme states of the BW control subnetwork by which the operating principle is analysed:

- When  $Y_{bw} \rightarrow 0$  (open-circuit) the coupling admittance between the two resonators is  $Y_c^{(0)} = Y_{c1}/2 + Y_{c2}$ . In this state the filter corresponds to the conventional 2<sup>nd</sup> order filter given in the circuit of Fig. 2.10a.
- When  $Y_{bw} \rightarrow \infty$  (short-circuit) the BW control subnetwork becomes a  $\Pi$ -network. By absorbing the distributed admittances  $Y_{c1}$  into the filter resonators, the coupling

<sup>7</sup>Absolute BW refers to the passband BW at a specific tuned frequency.

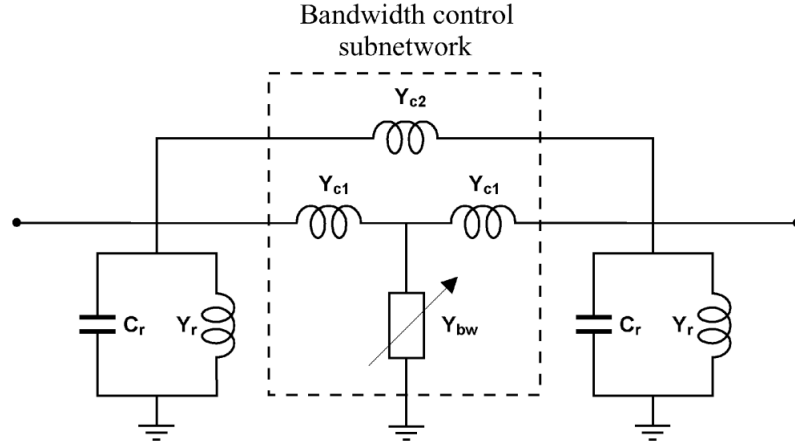


**Figure 2.13:** BW control subnetwork between two adjacent parallel resonators. In principle this configuration is a  $2^{nd}$  order BPF. Illustration taken from [2].

admittance becomes  $Y_c^{(\infty)} = Y_{c2}$  and thus results in a  $2^{nd}$  order filter again. Therefore not only does the BW change but also the center frequency of the filter, making the resonance frequency a function of the BW control subnetwork.

The coupling between resonators is directly proportional to the coupling admittance  $Y_c$  and therefore continuous BW tuning is achieved as  $Y_{bw}$  is tuned from 0 to  $\infty$ .

To obtain maximum BW tuning with a fixed center frequency, the resonator's capacitance ratio needs to be tuned between these two states as [2]

$$\frac{C_r^{(\infty)}}{C_r^{(0)}} = \frac{Y_r + Y_{c1} + Y_{c2}}{Y_r + 0.5Y_{c1} + Y_{c2}}. \quad (2.33)$$

This is realised by replacing the resonator capacitance  $C_r$  with a varactor diode. It is desirable to have an even larger capacitance ratio so that not only the BW is tunable (at a fixed position) but also the center frequency.

By using the equation (2.32) derived in [16], the FBW ratio can similarly be obtained as

$$\frac{FBW^{(\infty)}}{FBW^{(0)}} = \frac{Y_r + Y_{c1} + Y_{c2}}{Y_r + 0.5Y_{c1} + Y_{c2}}. \quad (2.34)$$

In [2] the BW control subnetwork is implemented with a coupling reducer between the two combline resonators shown in Fig. 2.14. The coupling reducer implements the working of  $Y_{bw}$  and is realised with a varactor-loaded transmission line with capacitance  $C_{cr}$  and characteristic admittance  $Y_{cr}$ . This is similar to the normal combline resonator, but with different resonant frequency. The admittance is therefore

$$Y_{bw} = j(2\pi f C_{cr} - \frac{Y_{cr}}{\tan\theta_{cr}}). \quad (2.35)$$

The significance of this particular network is that  $Y_{c2}$  and  $Y_{c1}$  is realised by the inductive coupling between the filter's in band resonators (original combline model) as well as between the adjacent resonators respectively.

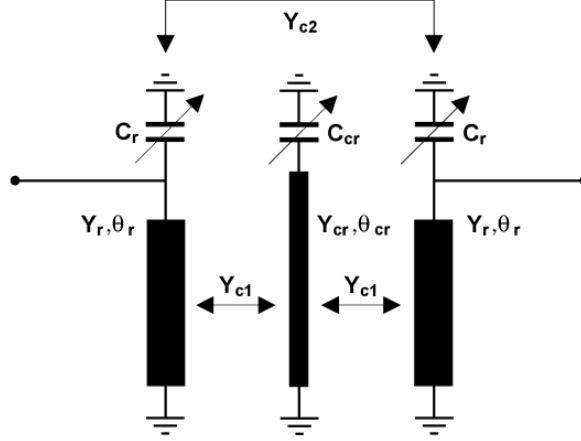


**Figure 2.14:** Schematic of  $2^{nd}$  order combline filter with detuned resonator for continuous BW and  $f_0$  tuning. Illustration taken from [2].

The downside of this design approach is that the BW control subnetwork is implemented with a detuned resonator that introduces out-of-band resonance. This resonance needs to be much lower than the filter's center frequency  $f_0$  in order to have good rejection near passband. Therefore the equation

$$f_{cr}^{max} = \frac{Y_{cr}}{2\pi C_{cr}^{min} \tan \theta_{cr}} \ll f_0 \quad (2.36)$$

needs to be satisfied where  $C_{cr}^{min}$  is the minimum capacitance value of the coupling reducer producing a maximum unwanted resonance at  $f_{cr}^{max}$ . Note that this is achieved with a low characteristic admittance  $Y_{cr}$  and a large electrical length  $\theta_{cr}$  ( $< 90^\circ$ ). It is also found that moderate to low- $Q$  varactors should be used for the detuned resonators in order to reduce the unwanted resonance peaks.<sup>8</sup>

The proposed tuning technique for BW and center frequency tuning is implemented in [2], where a  $3^{rd}$  order combline filter is constructed in suspended stripline technology as shown in Fig. 2.15. The filter is tuned in frequency over almost an octave in the UHF band (470-862 MHz), with the maximum and minimum BW a function of the frequency, producing a 40% BW tunability at the best instance (550 MHz). The insertion loss is below 10 dB in most instances and the return loss above 10 dB. From the results it is also observed that as the BW decreases (with a constant  $C_r$  value for all resonators) the insertion loss increases. The main reason for this effect is the mismatching between the source/load terminals and the I/O resonators. This can be overcome by introducing two additional I/O variable coupling reducers to rematch the filter as it is tuned.

<sup>8</sup>The influence of the  $Q$ -factor on the filter response will be discussed in the next section.

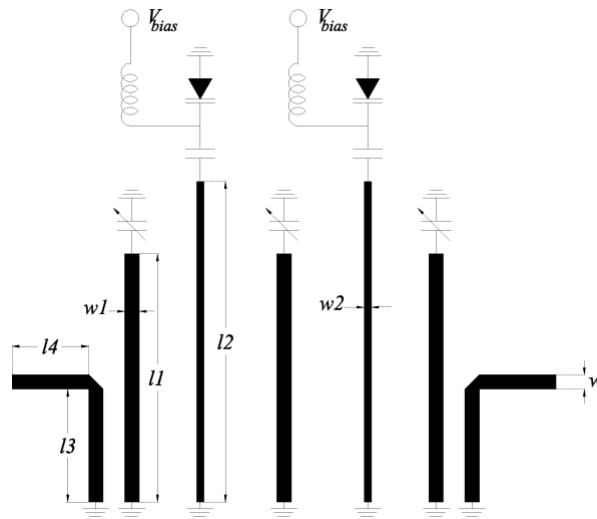


**Figure 2.15:** Constructed 3<sup>rd</sup> order combline filter with continuous BW and  $f_0$  tuning capabilities. Illustration taken from [2].

Another tune-all filter is designed in [21] to give a 2<sup>nd</sup> order response, using a hairpin filter topology. The frequency range is 0.19 of an octave with a 35% BW tunability at 2 GHz. The insertion loss is maintained below 4 dB and the return loss above 7 dB. The disadvantage of this type of filter is that an higher order filter is not as easy to realise, due to the fact that the coupling between hairpin resonators must also be controllable.

In [22] enhanced slow-wave resonators are used to realise tune-all filters.<sup>9</sup> Series varactors, coupling the resonators, are used to tune the BW while shunt varactors, which reduces the resonator size, are used to tune the centre frequency. The authors of [22] designed a 2<sup>nd</sup> order filter that has 0.44 of an octave frequency range (in the UHF band) while a BW tunability of up to 36% is achieved. The insertion loss is maintained below 5 dB and the return loss above 10 dB. This filter seems to have the best achieved results amongst the afore mentioned filters, taking all the facets into account.

### 2.5.3 Filter reconfigurability

Reconfigurability refers to filters that has switchable states of fixed frequency responses, opposed to tunable filters that has continuous reconfigurability. Reconfigurable devices are limited to a finite number of states, where the number of states are proportional to the number of switching components used.

The traditional way of switching between filter responses is by using a conventional switched filter bank [23]. This consist of multiple fixed frequency filters for the various filtering states. This type of device is usually not cost effective and very large in size.

<sup>9</sup>A slow-wave resonator is a type of resonator loaded at both ends of the distributed inductance. This gives a larger frequency separation between the first and second resonant modes, by bringing the even and odd mode group velocities closer to each other. Refer to [10].

In recent years research on reconfigurable filters has widely been done because of electronic switching components such as p-i-n diodes and MEMS (microelectromechanical systems). These components are used to switch between the filtering states.

This type of filters are well documented in [24, 25, 26, 27, 28, 29] and is not applicable for the aim of this thesis.

## 2.6 Quality factor and filter losses

The Q-factor of a filter is an indication of its ability to store energy. More specifically for a resonator circuit it is defined as [8]

$$Q = 2\pi \cdot \frac{(\text{energy stored in resonator})}{(\text{energy dissipated per cycle})}. \quad (2.37)$$

The  $Q$  of a resonator without any loading affects caused by external circuitry, is referred to as the unloaded quality factor ( $Q_u$ ) and is described by the above equation. In a filter network the resonators will always be coupled to other circuitry and so the resonator is characterized with the loaded quality factor ( $Q_L$ ). When a resonator has no internal losses and is coupled to an external load, the coupling is characterised by the external quality factor ( $Q_e$ ). The relationship between these  $Q$ -factors are given by

$$\frac{1}{Q_L} = \frac{1}{Q_e} + \frac{1}{Q_u}. \quad (2.38)$$

A resonator inherently has losses due to the microwave components. For a lossy series LC resonator the Q-factor can be defined [8] as

$$Q_u = \frac{\omega_0 L}{R} = \frac{1}{\omega_0 RC} \quad (2.39)$$

where  $R$  represents the series parasitic resistance. For a lossy parallel LC resonator it is

$$Q_u = \frac{R}{\omega_0 L} = \omega_0 RC \quad (2.40)$$

where  $R$  represents the parallel parasitic resistance. Note that the  $Q_u$  is measured at a specific frequency and in the case of a resonator it is defined at resonance. Equations (2.39) and (2.40) are based on the fact that at resonance there are an exchange between the inductive and capacitive components, where the average magnetic energy is equal to the average electric energy [8].

The significance of the  $Q_u$  is that it gives an indication of the losses in a filter. The higher the  $Q_u$  of a resonator the lower the losses. This can be approximated by the

equation

$$L_A(f_0) = \frac{4.343}{FBW \cdot Q_u} \sum_{i=1}^n g_i \quad (2.41)$$

proposed by Cohn [30], for a coupled resonator prototype filter with insertion loss  $L_A$  at the center frequency  $f_0$ , where  $g_i$  is the lowpass prototype element value of the corresponding resonator. Note that this is only true for uniform resonators. From this equation we can also see that the narrower the BW, the larger the insertion loss. On the other hand, the lower the order of the filter, the lower the loss.

In Fig. 2.16 the passband of a 4<sup>th</sup> order Chebyshev prototype filter for different  $Q_u$  values are plotted. It is observed that higher loss (or lower  $Q_u$ ) results in poorer selectivity at the passband edges. This effect is referred to as the filter's roll-off because the passband edges are rounded.

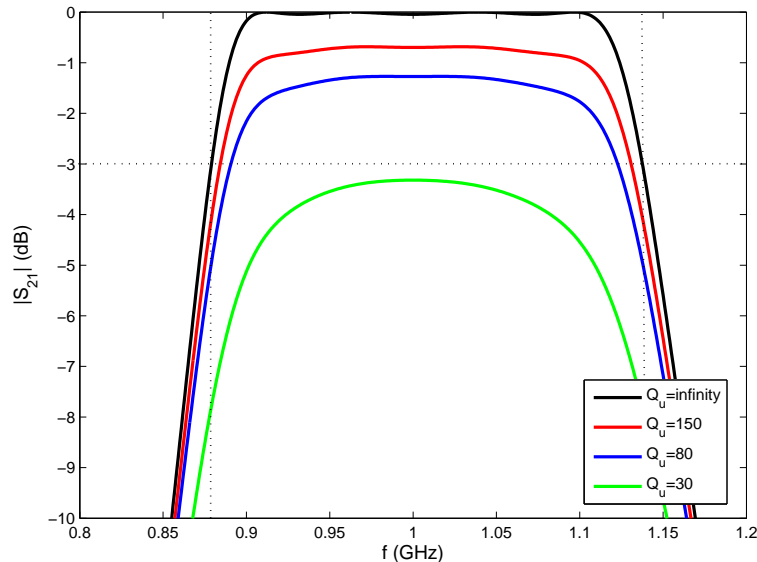


**Figure 2.16:** The affect of resonator dissipation on a 4<sup>th</sup> order Chebyshev filter with 20% FBW at 1 GHz.

In classical filter synthesis, as given in the previous sections, it is assumed that all prototype components are lossless. This leads to significant roll-off when losses are introduced as shown in Fig. 2.16. A common technique used to overcome this problem is the predistortion technique [31]. When losses are introduced in a filter, the poles of the transfer function are moved towards  $-\sigma$  on the complex plane. What this technique does is to take this shift, given a specific  $L_R$ , into account when designing the prototype filter. The result without losses is a filter response that has peaks in the transmission coefficient at the band edges, which in turn is flattened out as losses are introduced.

Another technique to deal with dissipation is the lossy filter synthesis developed in [32]. Here component losses are taken into account with the design of the prototype filter,



opposed to the classic lowpass prototype. This synthesis produces a passband with the same edge selectivity as in the lossless case, but only with higher insertion loss. The trade-off here is that the order of the filter is increased.

In the previous section it is shown that capacitors are normally replaced by varactor diodes for filter tunability. The simplest model of a varactor is a capacitor with a series resistance. The  $Q$ -factor of a varactor-loaded transmission line resonator (see Fig. 2.9a) is dependent on the line length, the intrinsic impedance, attenuation of the transmission line and the series resistance of the varactor [15]. In [19] it is shown that the line length and series resistance are the two significant influences of dissipation in such a resonator. In addition, the varactor's series resistance is a function of the biased voltage applied to the diode. For a high- $Q$  varactor the transmission line should be as long as possible ( $< 90^\circ$ ) to achieve good insertion loss, but this in turn limits the tuning range. In [33] it is shown that the tuning range of a filter decreases as the order of the filter increases and also as the  $Q$  of the tuning elements decreases. Therefore it is a constant trade-off between losses (also performance) and tunability.

The  $Q$  of a tunable filter can be improved by strategically placing the varactor diodes, but this is not always possible due to the filter layout or the controllable functionality. An example of this is a shunt varactor that is used to suppress a signal, opposed to a series varactor where the current at passband frequencies flow through, leading to dissipation.

The most common approach to deal with losses in tunable filters is the use of negative resistance circuits. The idea is to use active devices, such as transistors with some feedback circuitry, exhibiting negative resistance to compensate for the series resistance of the varactor diode [15]. This technique has been investigated in [34, 35]. The advantage of this is not only that the passband shape is restored, but also that wider tuning range is achievable. The downside of this active circuit approach is that it introduces non-linearity and more noise to the filter, which is a big concern for radio astronomy application.

## 2.7 Conclusion

A brief introduction to the Butterworth, Chebyshev, Elliptic and Gaussian functions was given. To realise these responses two classic filter syntheses were given, namely the lumped element form and distributed element form. The advantage of the distributed element synthesis is that the BW and centre frequency can be extracted directly from the prototype. This is of great benefit for tunable filter design. The disadvantage of the synthesis is that it is based on narrowband approximations which limits the accurate design of wideband filters.

Various tuning techniques for narrowband filters were introduced. It was found that for coupled resonator filters, the BW varies as the frequency is tuned. This is because

coupling between resonators are not frequency invariant as is the ideal inverters used in the prototype model.

A technique proposed by Hunter and Rhodes [16] for frequency tuning with constant absolute BW was given, followed by comparisons of other techniques. It was shown that BW tuning is not as straight forward as frequency tuning. A technique using detuned resonators [2] for BW tuning was introduced and compared to other BW tuning results found in literature.

All these techniques uses the varactor diode as tuning element. Through-out literature it seems that this is the most popular tuning element for planar microwave filters.

These tuning elements always add more dissipation to microwave filters. Therefore the significance of the Q-factor in filters was also discussed. It was shown how filter responses changes as losses are introduced. Different techniques to compensate for these effects were briefly mentioned.

In conclusion, some of the most widely used tuning techniques for planar filters were given in this chapter. There are more applications and different implementations, but are based mainly on these techniques and does not necessarily have much significance for the aim of this thesis. In the next chapter a moderate BW filter is designed with tunability based on the techniques given in this chapter.

The aim, however, is to find the best possible wideband tunable filter for the front-end of the KAT-7 system. In Chapter 4 wideband filters will be introduced and discussed in the light of some of these tuning techniques.

# Chapter 3

## Implementation of Tunable Narrowband Filters

### 3.1 Introduction

The purpose of this chapter is to implement filter tunability, by using varactor diodes in a coupled resonator filter with moderate BW. Following the literature review of the previous chapter, a frequency tunable combline filter is designed.

In this chapter the formulation and extraction techniques for the design parameters of coupled resonator filters, are presented. This is followed by a thorough design of the filter using these techniques. The simulated and measured results are presented and good correlation is found with the theory. The chapter ends with insight from the design process using varactor diodes, while recommendations are made for further improvement of the design with respect to the KAT-7 specifications.

### 3.2 Formulation and extraction of design parameters

The coupling coefficient and external quality factor are the two basic building blocks for the design of coupled resonator filters. The distributed models of these filters are shown in Fig. 2.7. The model consist only of resonators and inverters. The resonators are designed to have resonance at the filter centre frequency, while the inverters are designed for the specific design parameters ( $k$ 's and  $q_e$ 's) according to the filter specifications.

In this section the design parameters are defined with regard to the distributed filter model. Methods are derived for extracting these parameters from the measurable  $s$ -parameters of the circuit models. These methods are followed by the realisation of the corresponding inverters in microwave structures.

### 3.2.1 Coupling coefficient

The coupling coefficient, introduced in the previous chapter, is related to the mutual coupling between two inductors according to the definition given by (2.19). It is defined in order for maximum coupling to yield  $M = 1$  and for no coupling  $M = 0$ .

The coupling coefficient is also defined in a dual way for mutual coupling between two capacitors as

$$M_{i,i+1} = -\frac{C_m}{\sqrt{C_i C_{i+1}}}, \quad (3.1)$$

where  $C_m$  is the mutual capacitance between adjacent capacitors  $C_i$  and  $C_{i+1}$ . Note that  $M$  varies between -1 and 0. For this reason capacitive coupling is usually referred to as negative coupling, while inductive coupling is referred to as positive.

An equivalent lumped element circuit model for two inductive coupled  $LC$  resonators, is given in Fig. 3.1. It is shown in Appendix A that the solution to the nodal equations of this circuit yields two natural frequencies  $\omega_1$  and  $\omega_2$ . With these frequencies, known as eigenmodes, it is shown that the coupling coefficient can also be represented as

$$M = \frac{\omega_2^2 - \omega_1^2}{\omega_2^2 + \omega_1^2}, \quad \text{with } \omega_2 > \omega_1. \quad (3.2)$$

Coupling between resonators in close proximity is seldom only inductive or only capacitive, but usually a mixture of the two. It is shown in [10], using the same circuit principles, that (3.2) also holds for capacitive or mixed coupling between resonators.

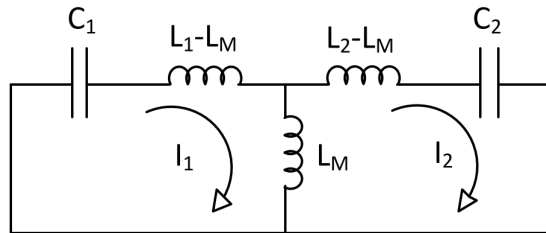


**Figure 3.1:** Equivalent circuit for the inductive coupling between two synchronously tuned series resonators.

Following equation (3.2) it is possible to extract the coupling coefficient between two coupled resonators, by determining the network's eigenmodes. In [36] it is shown using field theory that this method is applicable for any coupled microwave resonators, regardless of their structure, as long as it's synchronously tuned.

The eigenmodes of a physical structure can be extracted by coupling lightly into the structure and measuring the transmission coefficient. The light coupling refers to external circuitry coupling into a structure without loading the structure itself. The structure is excited just enough so that transmission may be observed.

In Fig. 3.2a a simulated example of this is shown. The two strips in the center of the substrate are the capacitive loaded resonators, as introduced in the previous chapter. Perpendicular to it are the two terminal strips on opposite sides. These terminal strips are also referred to as feeds. Small capacitive coupling occurs between the feed and resonator. This coupling is just enough to excite the structure without changing the characteristic impedance of the resonator strip.

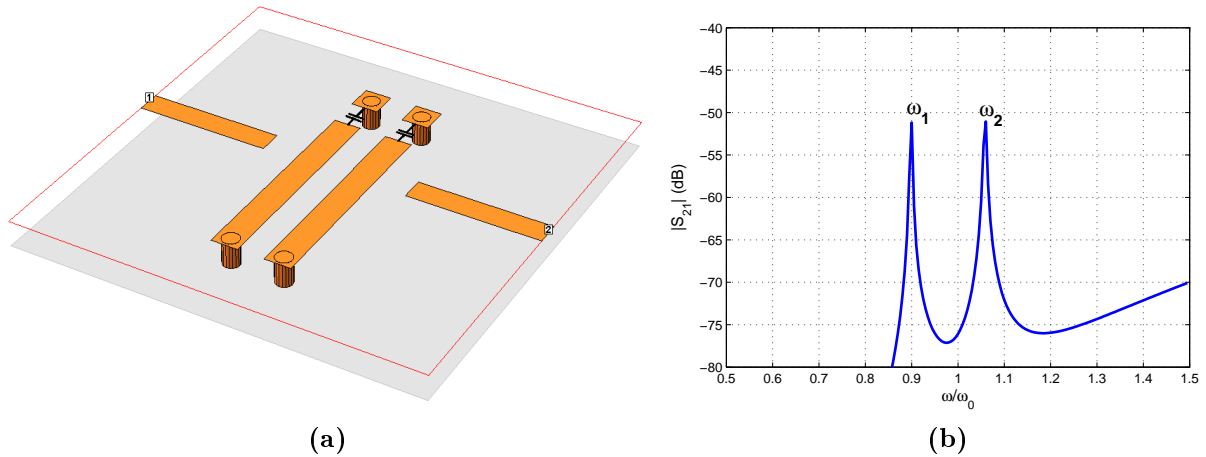


**Figure 3.2:** The method of extracting the coupling coefficient from two coupled resonators using an EM solver. (a) The microstrip layout of two lightly coupled resonators. The two centre strips are the capacitive-loaded resonators with the perpendicular two terminal strips on either sides known as feeds. The feeds are connected to port 1 and 2 as indicated by the labels. (b) The EM simulated results of the structure’s transmission coefficient. Note that the two peaks are the eigenmode frequencies.

An EM solver may be used to calculate the transmission coefficient of the structure, in order to obtain its eigenmodes. In this example Sonnet is used to solve the microwave structure of Fig. 3.2a. The  $s_{21}$  results are plotted in Fig. 3.2b and two peaks are observed. These peaks are the two eigenmode frequencies  $\omega_1$  and  $\omega_2$  of the coupled resonators. Using (3.2) along with these results, the coupling coefficient of the two coupled resonators are known.

### 3.2.2 External quality factor

The external quality factor is defined in the previous chapter as the measure of coupling from a loaded external circuit into a lossless structure. More specifically in coupled resonator filters it is a measure of the coupling from the terminal (normally  $50 \Omega$ ) into the I/O resonator.

Fig. 3.3 shows a circuit model of such coupling, where  $R$  is the resistance of the terminal and  $X$  the admittance of the lossless series LC resonator. The reflection coefficient at this terminal is

$$s_{11} = \frac{jX - R}{jX + R}. \quad (3.3)$$

The resonator is lossless and therefore the magnitude of the reflection is always equal to

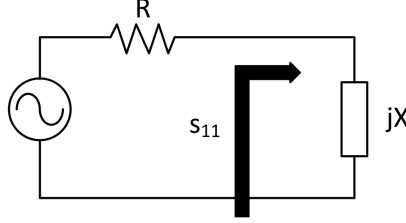


**Figure 3.3:** Equivalent circuit for the coupling between a terminal load and I/O resonator.

1. Following this, the phase of the reflection coefficient in (3.3) is derived as

$$\phi_{s_{11}} = -2 \cdot \tan^{-1} \left( \frac{X}{R} \right). \quad (3.4)$$

The group delay of  $s_{11}$  is defined at resonance [10] as

$$\tau_{s_{11}}(\omega_0) = - \left. \frac{\partial \phi_{s_{11}}}{\partial \omega} \right|_{\omega=\omega_0}. \quad (3.5)$$

Expanding this partial derivative and substituting with (3.4) gives

$$\begin{aligned} \tau_{s_{11}}(\omega_0) &= - \left[ \frac{\partial \phi_{s_{11}}}{\partial X} \cdot \frac{\partial X}{\partial \omega} \right]_{\omega=\omega_0} \\ &= - \left[ \frac{\partial}{\partial X} \left( -2 \cdot \tan^{-1} \left( \frac{X}{R} \right) \right) \cdot \frac{\partial X}{\partial \omega} \right]_{\omega=\omega_0} \\ &= - \left[ \left( \frac{-2}{1 + (X/R)^2} \cdot \frac{1}{R} \right) \cdot \frac{\partial X}{\partial \omega} \right]_{\omega=\omega_0}. \end{aligned} \quad (3.6)$$

At resonance  $X(\omega_0) = 0$  and therefore

$$\tau_{s_{11}}(\omega_0) = \frac{2}{R} \cdot \left[ \frac{\partial X}{\partial \omega} \right]_{\omega=\omega_0}. \quad (3.7)$$

In the previous chapter the external quality factor is defined in (2.22) for a series LC resonator. Substituting this with the susceptance slope parameter in (2.15) gives

$$Q_e = \frac{x}{R}. \quad (3.8)$$

Substituting this and the definition for the reactance slope (2.13) into (3.7), leads to

$$Q_e = \frac{\omega_0 \cdot \tau_{s11}(\omega_0)}{4}. \quad (3.9)$$

This equation enables the extraction of the external quality factor from the group delay of any type of resonator. The group delay can be calculated directly from the measured reflection phase using (3.5). This method is also accurate for lossy microwave resonators and is commonly used for the design of coupled resonator filters.

Fig. 3.4 shows two common ways of coupling into a capacitive-loaded microstrip resonator. The first is a coupled-line coupling (Fig. 3.4a), where a non-resonating line is used to couple into the resonator. The  $Q_e$  is dependent on the width of the line and the gap between the line and resonator. The second is a tapped-line coupling (Fig. 3.4b), where a  $50 \Omega$  feed line is coupled directly unto the resonator. Here the  $Q_e$  is dependent on the tapping position of the line from the resonator's ground.

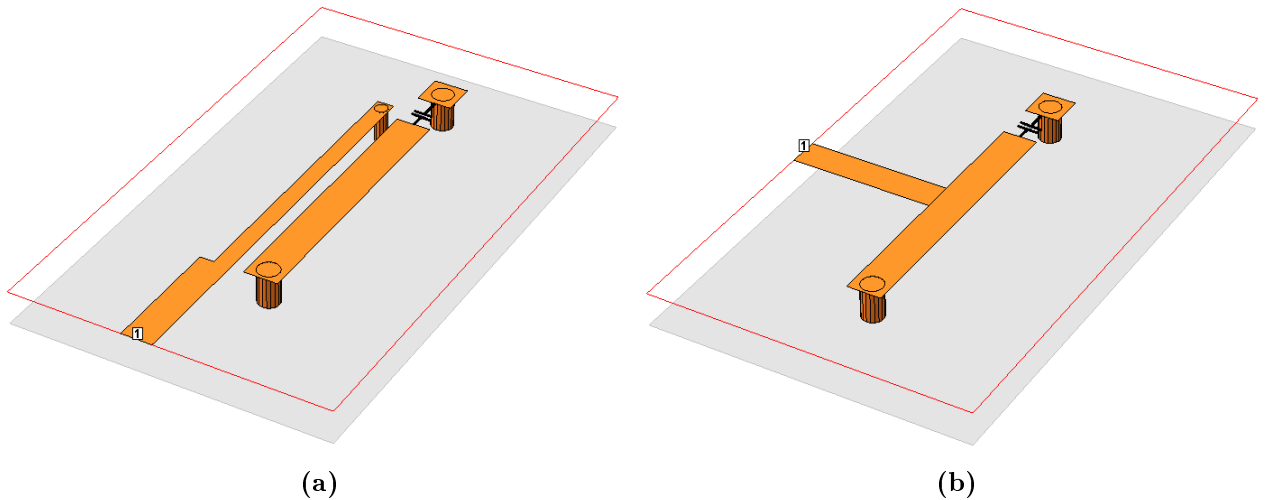


**Figure 3.4:** Common I/O coupling structures used for realising microstrip filters. Both structures consists of a feed between the labelled port 1 and a capacitive-loaded resonator. (a) Coupled-line feed and (b) tapped-line feed.

The normalised group delay of such a feed structure is plotted in Fig. 3.5. Note that the group delay peaks at resonance and therefore the external quality factor of such a microwave structure may be known by calculating (3.9).

### 3.3 Design of tunable combline filter

In this section a tunable combline filter is designed for frequency tuning. Following the theory discussed in the previous chapter, the filter is designed to achieve minimum absolute BW variation across the tuning range.

The specifications for the KAT-7 filter, given in Chapter 1, not only requires frequency tuning but also BW tuning. However, the filter design in this section is not specifically

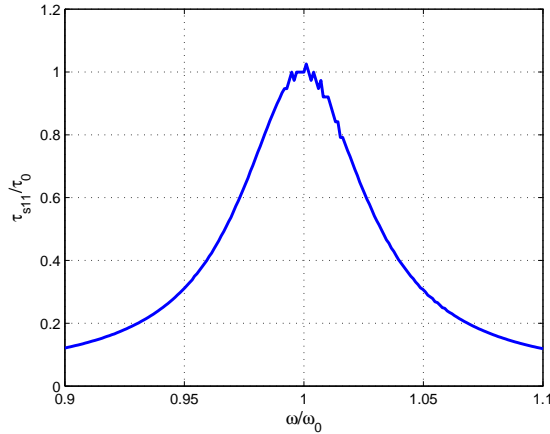


**Figure 3.5:** A typical response of the normalised group delay of the reflection coefficient of a type of coupling structure as shown in Fig. 3.4.

intended to satisfy these specifications, but to explore tunability using varactor diodes.

In order for the investigation of tunability to be applicable for the final KAT-7 filter, the specifications for this design need to be in the same frequency band. Therefore the design frequency is chosen at 1.53 GHz. The FBW is 20%, which according to [9] is on the limit of breakdown in BW accuracy, due to the narrowband approximations of the coupled resonator synthesis. The order of the filter is chosen to be low ( $n = 3$ ), because the insertion loss should not be too high, resulting in a passband with poor roll-off (refer to Section 2.6). The return loss must be 20 dB at the design frequency. The tuning range of the filter is not specified because it is dependent on the varactor diode used. All these specifications are summarised in Table 3.1.

**Table 3.1:** Specifications for tunable combline filter.

Parameter	Description	Value
$f_0$	Centre of tuning range (design frequency)	1.53 GHz
$FBW$	Fractional bandwidth	20%
$n$	Order of filter	3
$L_R$	Return loss	20 dB
$\frac{f_{max} - f_{min}}{f_{min}}$	Tuning range in octaves	As high as possible

The Chebyshev response is chosen due to its balance between high selectivity and group delay distortion. The normalised design parameters, for a 3<sup>rd</sup> order Chebyshev filter with 20 dB return loss, are found in [11] as

$$q_{e1} = q_{e3} = 1.311, \quad (3.10)$$

$$k_{12} = k_{23} = 0.6699. \quad (3.11)$$



This is denormalised with (2.25) and (2.26) to give

$$Q_{e1} = Q_{e3} = 6.56, \quad (3.12)$$

$$M_{12} = M_{23} = 0.134. \quad (3.13)$$

Before starting with the design of the filter, an appropriate substrate needs to be chosen. There are two main characteristics to consider, namely the relative permittivity ( $\epsilon_r$ ) and the substrate thickness. Both influences the effective permittivity<sup>1</sup> ( $\epsilon_{eff}$ ), with the former more significantly than the latter [8]. This is used to calculate the guided wavelength ( $\lambda_g$ ) in the material at a specific frequency

$$\lambda_g = \frac{c}{f\sqrt{\epsilon_{eff}}}, \quad (3.14)$$

where  $c$  is the speed of light in a vacuum ( $\approx 3 \cdot 10^8$  m/s). Therefore the higher  $\epsilon_{eff}$  the shorter is the wavelength and thus for an high  $\epsilon_r$  substrate (usually ceramic based) a more compact filter is obtained.

The thickness of the substrate influences the width of a microstrip line significantly. The width of a line, for a given characteristic impedance, is wider for a thicker substrate. The E-fields of a wide line are more concentrated between the line and ground, resulting in less capacitive coupling between two such lines close to one another. This is beneficial for inductive coupling between adjacent lines because higher coupling can be obtained for the same distance between lines, than is achievable with a thin substrate.

Following this a CER-10 substrate from Taconic is chosen for the design. This substrate has a permittivity of 10 and a thickness of 1.53 mm. This is chosen to ensure a compact filter while maintaining enough distance between resonators, in order to realise the layout of the varactor diodes' biasing network.<sup>2</sup>

### 3.3.1 Resonator design

A schematic for a combline resonator is given in Fig. 2.9a. To achieve minimum BW deviation across the tuning range, the electrical length of the resonator's transmission line must be  $53^\circ$  at the design frequency. If the characteristic impedance of the line is chosen as  $50 \Omega$  (same as the terminal impedance), the resonator's lumped capacitance ( $C_r$ ) is calculated according to (2.29) as 1.57 pF.

This value is a good benchmark for the choice in varactor diode, that is used for tuning the resonator's resonant frequency. The total capacitance of the varactor, in the middle

<sup>1</sup>The effective permittivity determines the phase velocity of a propagating wave in microstrip.

<sup>2</sup>The choice for larger gaps between resonators will be more clear following the design of the biasing network.

of its tuning range, should be more or less 1.57 pF. The  $Q$  of the varactor must also be considered along with its capacitance ratio (i.e. the highest capacitance divided by the lowest).

For a wide frequency tuning range, the capacitance ratio needs to be high. In most of the varactors commercially available, the  $Q$  is lower for a higher capacitance ratio. Note also that the  $Q$  is higher for varactors with lower capacitance, but in this design the capacitance is fixed by the electrical length according to (2.29). The characteristic impedance of the line may be increased to assist in this, but then the physical lines become very thick on the substrate, leaving no room for optimisation to compensate for parasitic effects.

Following these insights the BBY52-02W varactor diode from Infineon is chosen. It is a high- $Q$  varactor with a total diode capacitance ranging from 1.1 to 2.45 pF. The SCD80 package is chosen because it is very small and therefore has low parasitic inductances.

The next step is to look at the biasing of a varactor. The varactor is basically a P-N junction diode, that is reversed biased<sup>3</sup> in order to change the E-field across the junction. This change inherently causes a variation in capacitance. A graph of the capacitance as a function of the reversed biasing voltage is shown in Fig. 3.6. The reversed biasing voltage is referred to as the biasing voltage ( $V_b$ ) of a varactor.

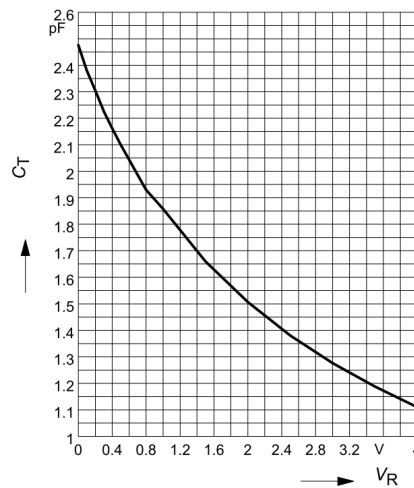


**Figure 3.6:** The total capacitance ( $C_T$ ) of the BBY52 varactor diode against the reversed biasing voltage ( $V_R$ ). This graph is taken from the datasheet provided by Infineon.

Two possible ways of biasing a varactor diode in this specific resonator are shown in Fig. 3.7. Both work on the same principle where a capacitor ( $C_b$ ) is used to block the DC signal and a RF choke to block the RF signal. The networks are identical when viewing it only at DC. At the higher frequencies, in this case L-band, one need to look at the current paths. The main difference come in when the component packages are

<sup>3</sup>Reversed biasing a P-N junction diode refers to a positive voltage applied to the cathode with the anode grounded.

considered. The BBY52-02W varactor has package terminals of 0.3 mm in width, whereas a common surface mount RF capacitor has a width of 0.8 mm. The strip width of a  $50\ \Omega$  transmission line on the chosen substrate is 1.44 mm, calculated with the TXLine calculator from Applied Wave Research. The surface current flows along the edges of a strip and therefore when the 0.3 mm terminals of the varactor is mounted on the 1.44 mm width line, the current path is longer. Based on this the network in Fig. 3.7a is chosen.

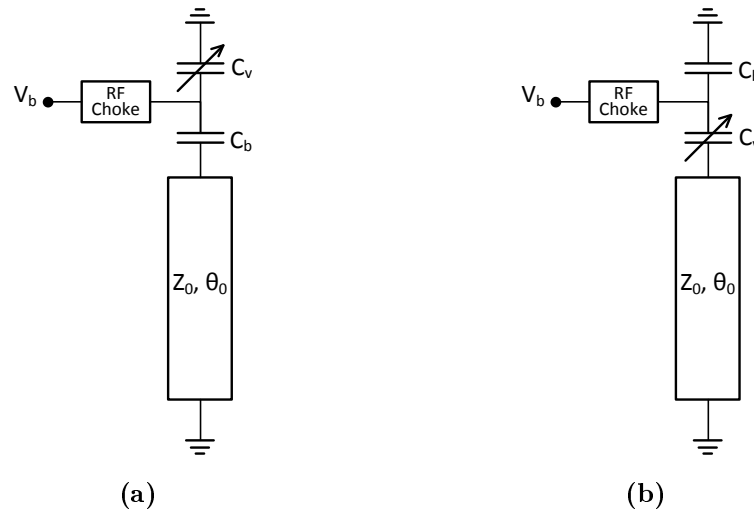


**Figure 3.7:** The schematics of two possible biasing networks for a varactor diode in a capacitive-loaded transmission line resonator.

An inductor is commonly used to act as a RF choke, but in the L-band this is not as simple. The inductor needs to be large enough to act as a high impedance in the L-band, but the higher the inductance the lower is the package's self-resonating frequency (SRF). In this frequency range there is always a trade-off between the inductance and the SRF. On the other hand, for a higher performance component (e.g. high SRF) the cost always increases drastically.

An advantage of the varactor diode is that it doesn't consume much power, since the DC current is negligibly small. Therefore a sufficiently large resistor may be used to choke the RF signal, because the DC current is very small causing no significant voltage drop across the resistor and biasing the varactor. A  $100\ k\Omega$  resistor is chosen which is large enough to create an open-circuit for the RF signal.

The DC block is implemented with a capacitor  $C_b$  as shown in Fig. 3.7. A large capacitor is required so that it doesn't decrease the overall capacitance and limit the tuning range. Thus a trade-off exists, because the higher the capacitance the lower is the Q which is also not desirable. Therefore a  $20\ pF$  capacitor is chosen from Dilabs, with a 0603 footprint.

After choosing all the components, the transmission line parameters of the resonator needs to be optimised due to parasitic effects. Using the circuit model for the varactor

package as shown in Fig. 3.8, along with the Spice model of the chip (provided by Infineon) and the s-parameters of the DC block (provided by Dilabs), a complete model for the biasing network is obtained. Note that the losses of the varactor are included in the Spice model of the chip.

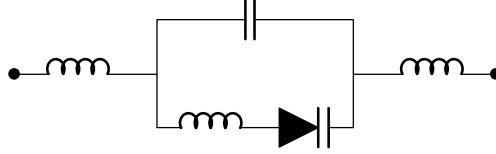


**Figure 3.8:** The typical schematic of the parasitic components of a varactor diode package.

This complete model is simulated with Applied Wave Research’s Microwave Office (MWO) to determine the total input capacitance range of the grounded varactor in series with the DC block. Biasing the varactor between 6 to 0V produces an equivalent resonator capacitance ( $C_r$ ) between 1.11 to 2.94 pF.<sup>4</sup> This capacitance range is the final fixed resonator capacitance values used for the design of the complete resonator.

The lowest tuned centre frequency ( $f_1$ ) is achieved when the capacitance is a maximum ( $C_{rmax} = 2.94$  pF) and the highest frequency ( $f_2$ ) when the capacitance is a minimum ( $C_{rmin} = 1.11$  pF). Implementing these into (2.29) respectively, yields

$$f_1 \tan \theta_1 \cdot C_{rmax} = \frac{1}{2\pi \cdot Z_0} \quad (3.15)$$

and

$$f_2 \tan \theta_2 \cdot C_{rmin} = \frac{1}{2\pi \cdot Z_0}. \quad (3.16)$$

Substituting equation (2.29), for the design frequency ( $f_0$ ) with corresponding capacitance  $C_{r0}$ , into (3.15) and (3.16) gives

$$f_1 \tan \theta_1 \cdot \frac{C_{rmax}}{f_0 \tan \theta_0} = C_{r0} \quad (3.17)$$

and

$$f_2 \tan \theta_2 \cdot \frac{C_{rmin}}{f_0 \tan \theta_0} = C_{r0}, \quad (3.18)$$

respectively.

From these equations it is clear that if  $C_{r0}$  is chosen to be low, then both  $f_1$  and  $f_2$  will be low. Therefore the optimal value for  $C_{r0}$  need to be chosen so that  $f_0$  is right in

<sup>4</sup>The maximum biased voltage of the varactor is 7 V according to the manufacturer’s datasheet. To be safe it will not be driven above 6 V.

the middle of  $f_1$  and  $f_2$ . Using the relationship between frequency and electrical length given in (2.31), the equations (3.17) and (3.18) are plotted in Fig. 3.9.

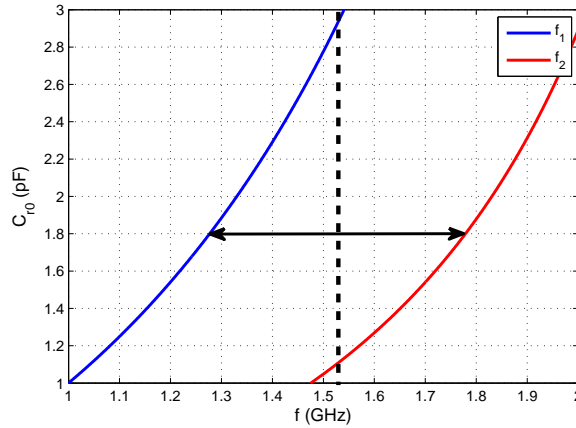


**Figure 3.9:** The values of the capacitance at the design frequency ( $C_{r0}$ ) corresponding to the lower ( $f_1$ ) and upper ( $f_2$ ) tuning frequency limits. For the filter response to be tuned symmetrically around the design frequency of 1.53 GHz (dashed line), the capacitance value should be 1.8 pF.

Note that  $f_1$  and  $f_2$  is symmetrical around the design frequency of 1.53 GHz, where  $C_{r0} = 1.8$  pF (at  $V_b = 1.5V$ ). This is therefore the optimal design capacitance giving lower and upper frequency limits of  $f_1 = 1.28$  GHz and  $f_2 = 1.78$  GHz. With this new capacitance value the characteristic impedance of the resonator's line is calculated as  $43 \Omega$ , using (2.29).

The complete microstrip layout of the resonator is shown in Fig. 3.10. The transmission line of the resonator has dimensions  $l_r \times w$  and the node where the varactor ( $C_v$ ), RF choke ( $R_c$ ) and DC block ( $C_b$ ) are connected has dimensions  $l_n \times w_n$ . The node should be as small as possible in order to keep its distributed inductance low, but large enough to solder the components on in the fabrication. The higher the added inductance, the shorter  $l_r$  must be for the same resonance frequency. The vias, illustrated by the circles in Fig. 3.10, has a diameter indicated by  $\phi_{via}$ . The via also adds inductance, which is inversely proportional to its diameter. A strip of five vias are used at the bottom of the resonator to ground it. These vias theoretically has a total inductance that is five times smaller than a single via. Note that the strip connected to the left of  $R_c$  is a DC line and has no specific dimensions.

The resonant frequency is determined from  $s_{21}$ , calculated with Sonnet, by lightly coupling the resonator with two terminal strips (as discussed in the previous section). Using this method the resonator dimensions are optimised for  $f_0 = 1.53$  GHz and given in Table 3.2. Note that the separation between adjacent vias, on the grounded side of the resonator strip, is one width of a via.

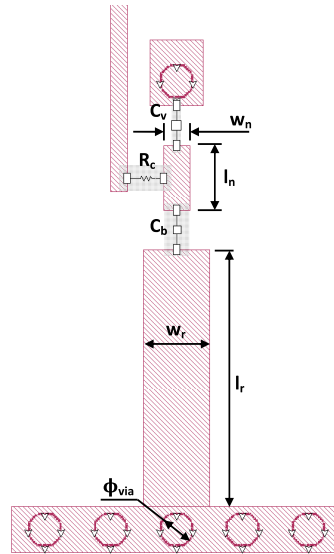


**Figure 3.10:** Microstrip layout of the complete resonator with dimension parameters. Note that the bottom strip is grounded with five vias and the strip connected to the left of  $R_c$  is a DC line.

**Table 3.2:** The physical dimensions of microstrip resonator shown in Fig. 3.10, with resonant frequency at 1.53 GHz.

Parameter	Description	Value (mm)
$w_r$	Width of resonator line	2
$w_n$	Width of biasing node	0.8
$l_r$	Length of resonator line	7.95
$l_n$	Length of biasing node	2
$\phi_{via}$	Diameter of vias	1

### 3.3.2 Coupling design

The 3<sup>rd</sup> order Chebyshev response only require one value (given in (3.13)) for both coupling coefficients in the coupled resonator prototype. The coupling coefficient is inversely proportional to the distance between two resonators. Using the simulation based extraction technique given in the previous section, the coupling coefficient between two resonators (see Fig. 3.11a) is determined and plotted in Fig. 3.11b. At the desired coupling ( $M = 0.134$ ) the gap between the resonator strips ( $s$ ) is 1.82 mm. Note that this is enough space to fit the DC line and RF choke comfortably in between the resonators, as seen in Fig. 3.11a.

The external quality factor for the input and output resonators are also of the same value, given in (3.12). The external coupling may be implemented using a feed structure as shown in Fig. 3.4. Note that  $Q_e$  must be quite low due to the moderate BW specification and therefore an high coupling structure is preferable. For this reason the feed structure in Fig. 3.4b is chosen for the design.

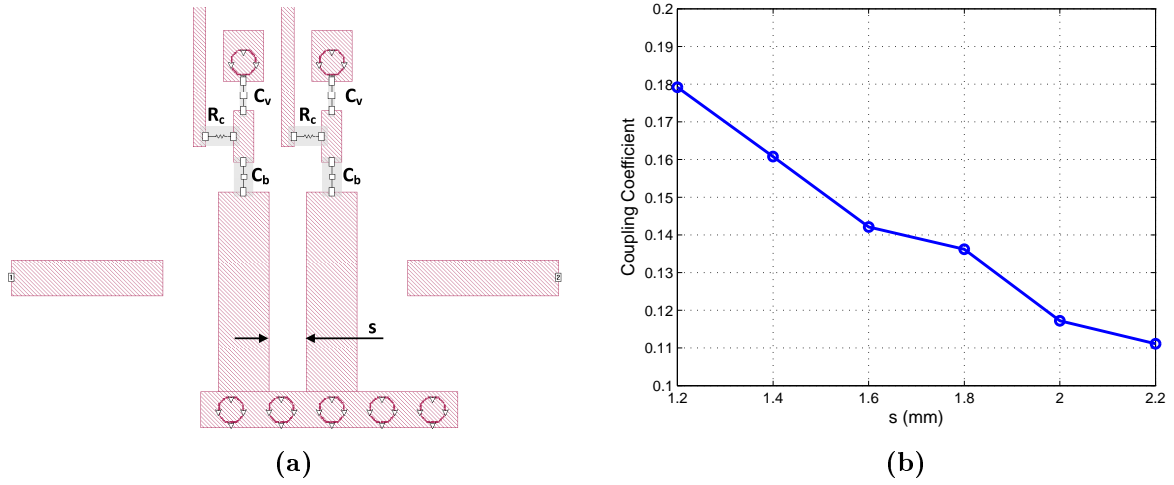


**Figure 3.11:** (a) Two coupled resonators with lightly coupled feeds. (b) The coupling coefficient of the resonators as a function of the gap ( $s$ ) between them.

Using the extraction technique presented in the previous section, the  $Q_e$  is determined for various feed offsets for the simulated structure in Fig. 3.12a, with the results plotted in Fig. 3.12b. Note that the  $50\ \Omega$  feed line has a width ( $w_f$ ) of 1.45 mm. The length is chosen to be 8 mm, so that a SMA connector may be mounted on it with enough clearance from the resonator. It is found that for the desired external quality factor ( $Q_e = 6.56$ ), the feed offset ( $l_{offset}$ ) must be 3.74 mm.

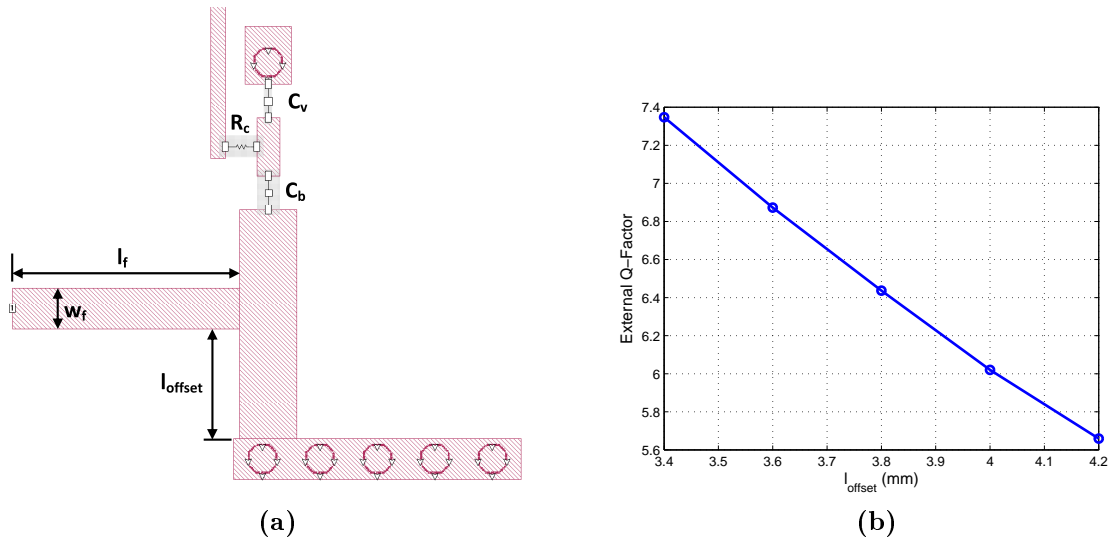


**Figure 3.12:** (a) The resonator with a tapped-line feed. (b) The  $Q_e$  as a function of the feed offset ( $l_{offset}$ ).

The resonance of the resonator is changed due to the loading affect of the feed. Therefore, by optimising the offset of the feed, the resonator length must simultaneously be changed in order to obtain the correct  $Q_e$  and  $f_0$ . The optimised values are found as  $l_r = 8.35$  mm and  $l_{offset} = 3.85$  mm.

### 3.3.3 Optimisation of complete microwave structure

The coupling structures designed in the previous subsection, cannot be placed together as it is to produce the correct filter response. The structures load one another and therefore changes the designed characteristics. For instance if the second resonator is placed together with the input feed and resonator, it changes the resonant frequencies and external coupling. Therefore to overcome this the coupling resonator prototype for this filter is considered, as shown in Fig. 3.13.

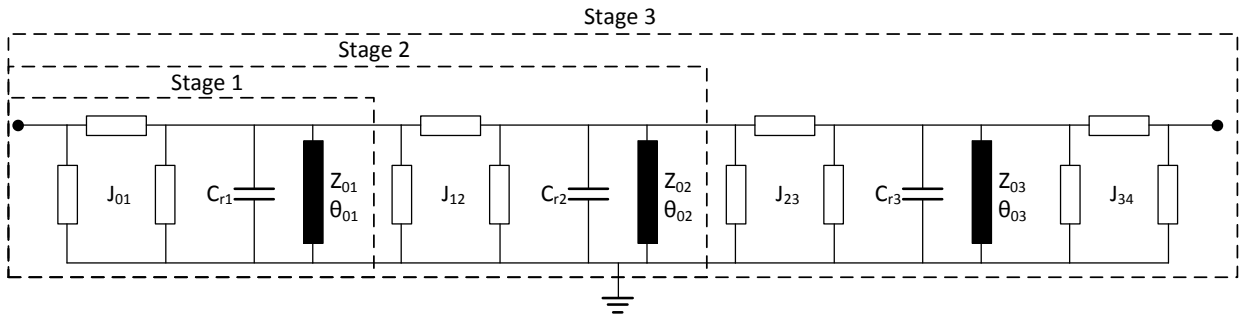


**Figure 3.13:** The 3<sup>rd</sup> order coupled resonator prototype circuit. Note that the three indicated “stages” are the different optimisation stages.

Here the admittance inverters are implemented with frequency independent admittances. The design equations in (2.27) are used to determine each component value according to the filter specifications. The prototype resonator is implemented with the combline resonator (capacitive-loaded transmission line). The new susceptance slope parameter is calculated as

$$b = \frac{\omega_0 C_r}{2} + \frac{\theta_0}{2Z_0 \sin^2 \theta_0}. \quad (3.19)$$

The idea is to optimise the microstrip structure, for the specific stage as indicated in Fig. 3.13, in order to match the group delay of the corresponding prototype section. The first stage (feed and input resonator) is already completed in the previous subsection.

In stage 2 a second resonator is added to the feed and input resonator. In this stage the main parameters that are optimised are the 1st and 2nd resonator lengths ( $l_{r1}$  and  $l_{r2}$ ), along with slight changes to  $l_{offset}$  and  $s$ .

In stage 3 the third resonator, along with its feed, is added to stage 2 and optimised to form the final filter layout shown in Fig. 3.14. Here the grey boxes represent the component packages. In Sonnet the package dimensions are important for the EM solver to determine the component’s terminal impedances. The optimised dimensions of the combline filter is given in Table 3.3.



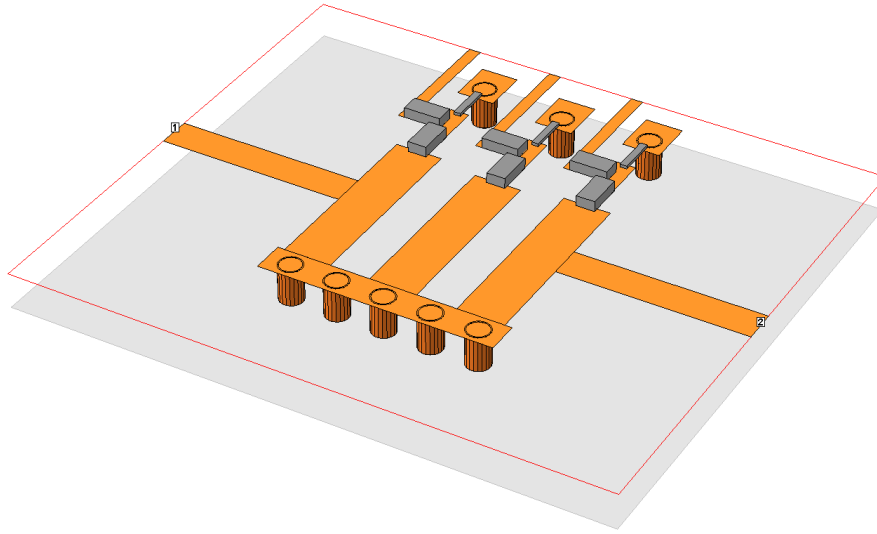


**Figure 3.14:** The simulation layout of the tunable combline filter. The grey boxes represent the component packages.

**Table 3.3:** The final dimensions of the tunable combline filter shown in Fig. 3.14. (Refer to Fig. 3.10, Fig. 3.11a and Fig. 3.12a for clear reference of the dimension parameters.)

Parameter	Description	Value (mm)
$w_r$	Width of the resonator lines	2
$w_n$	Width of all the biasing nodes	0.8
$w_f$	Width of the feed lines	1.45
$l_{r1}, l_{r3}$	Length of the input and output resonator lines	8.15
$l_{r2}$	Length of the 2nd resonator line	7.8
$l_n$	Length of all the biasing nodes	2
$l_f$	Length of the feed lines	8
$l_{offset}$	Offset of the feed lines	3.8
$s$	Gaps between adjacent resonators	1.7
$\phi_{via}$	Diameter of the vias	1

### 3.4 Results of tunable combline filter

The complete tunable combline filter is simulated with Sonnet, shown in Fig. 3.14. The simulated results for different biasing voltages are plotted in 3.15a-b. Note that there exists a transmission zero (i.e.  $s_{21} = 0$ ) on the upper side of the attenuation slope. This is caused by the resonator's transmission line that short-circuits the signal at that frequency. If the resonators are coupled only at the point between the capacitor and transmission line (as in the prototype circuit), then the transmission zero should be found at the frequency where the electrical length of the line is  $180^\circ$ .

The tuning range of the simulated results is found to be from 1.284 to 1.794 GHz (0.4 of an octave), which is close to what was anticipated with the design values (i.e.  $f_1 = 1.28$  GHz and  $f_2 = 1.78$  GHz). The  $\Delta BW$  across this range is 23.5%. According

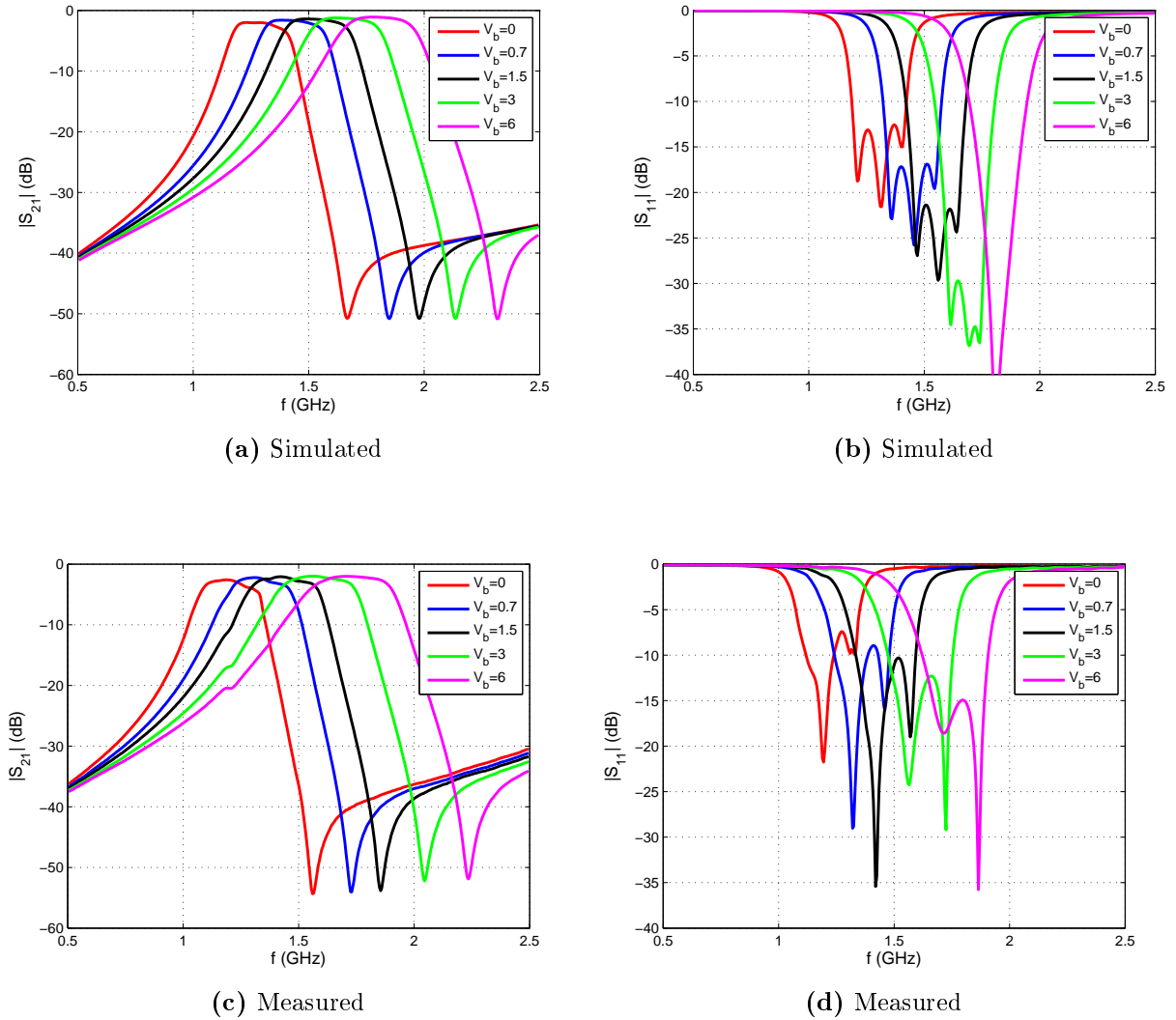


**Figure 3.15:** The tuned responses of the Sonnet simulations (a) - (b) and measurements (c) - (d) of the fabricated filter. Note that  $V_b$  represents the biasing voltage.

to the theoretical model (see Fig. 2.11) the  $\Delta BW$  should be 5.3% for the same tuning range if  $\theta_0 = 53^\circ$ .

There are two possible reasons for the large deviation in BW of the designed filter. The first is that the length of the coupled transmission lines is only 7.8 mm long, which is  $38^\circ$  at  $f_0$  and is much smaller than the optimal length. Calculating the theoretical  $\Delta BW$  for this length (with (2.32)), yields 18.5% and is much closer to the obtained 23.5%. In the design of the resonator only the line length is optimised to compensate for the influence of the parasitics of the component packages, as well as the via inductances. The result is therefore shorter resonator lines.

The second reason might be because this filter has a moderately wide FBW of 20%. The approximation made in [16] is for narrowband filters where  $BW \ll f_0$ . Therefore this might also add to the inaccuracy of  $\Delta BW$ .

Overall the simulated results meets the specifications listed in Table 3.1.

The filter is fabricated in-house with a milling machine and the vias are made with through-hole plating. A photo of the fabrication is shown in Fig. 3.16. The DC network is implemented using voltage division to tune each varactor separately with potentiometers. Note from the photo that the whole top part of the board layout (from the white bonding wires upwards) is the DC network.

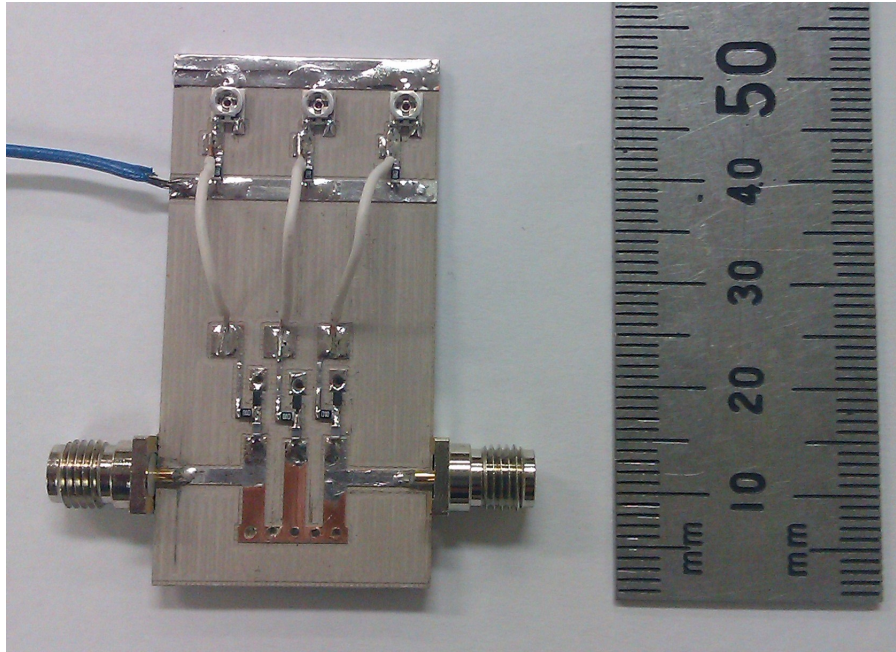


**Figure 3.16:** Photo of the fabricated tunable combline filter.

The measured results given in Fig. 3.15c-d, shows a frequency shift from the simulated results. At the design frequency the passband is shifted lower with 102 MHz.

The overall tuning range is from 1.192 to 1.711 GHz (0.44 of an octave). Note that the insertion loss is 2 dB at the design frequency, which is 0.6 dB higher than the simulation. The reason for this is mainly because of the nominal value for the series resistance of the varactor. This value is used in the varactor's Spice model that is implemented in Sonnet. According to the manufacturer the nominal value is  $0.9 \Omega$ , but may be as high as  $1.7 \Omega$  and therefore leading to a higher  $L_A$ .

It is noted in the graph of  $s_{11}$  (Fig. 3.15d) that there are not three poles present, as is expected from the 3<sup>rd</sup> order Chebyshev response. From the observation of  $s_{11}$  and  $s_{22}$  in Fig. 3.17a (for  $V_b = 1.5V$ ), it seems that not all resonators are synchronously tuned. The resonators are therefore separately tuned in order to obtain the design frequency. These measurements are plotted in Fig. 3.17b, along with the simulated response at  $V_b = 1.5V$ . For the measured instance the first and second resonators are both set to  $V_b = 2.4V$  and the third resonator to  $V_b = 3V$ . Therefore it seems that the third resonator's varactor diode does not respond the same as the other two, causing poorer  $L_R$  than expected.

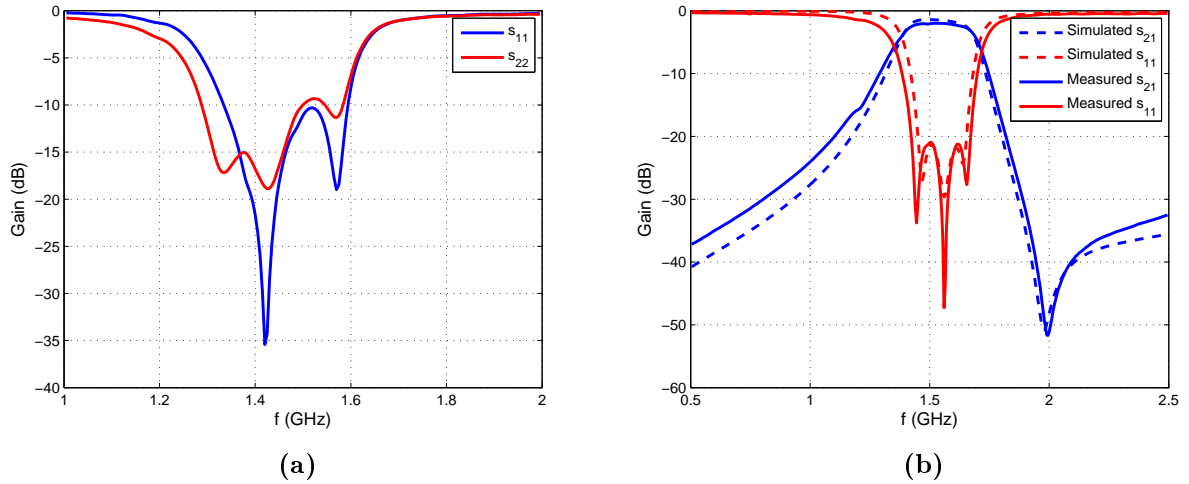


**Figure 3.17:** Investigation of symmetry in fabricated filter. (a) The reflections at port 1 and port 2 for  $V_b = 1.5V$ , seem to be unsymmetrical due to a detuned resonator. (b) The measured response where resonator 1 and 2 are both set to  $V_b = 2.4V$  and resonator 3 is set to  $V_b = 3V$ . The dashed lines are the simulated response with all resonators tuned at  $V_b = 1.5V$ .

### 3.5 Conclusion

This chapter started with the circuit formulation and extraction techniques for the design parameters of coupled resonator filters. A tunable combline filter was designed using these techniques. Varactor diodes were discussed and implemented in the filter for the frequency tunability. The measured results were found to be shifted in frequency from the simulated results because of tolerances in the varactor diodes. Despite the frequency shift, good agreement is found with the theory.

The modelling of the component parasitics are a critical part of the design. The reason for the difference in the insertion loss between the simulated and measured results, may be related to the equivalent series resistance which is too low in the Spice model of the varactor.

The accuracy of the component modelling is also determined by the EM solver. This refers to the coupling between the terminals where a component is mounted, as well as the terminal impedance of the physical package of the component. Sonnet takes these affects into consideration and therefore can be trusted for accurate EM calculations of planar structures, containing surface mount components.

It was found that the coupled transmission lines had to be shortened to compensate for the parasitic inductances, caused by packaging and vias. Therefore it is preferable to choose smaller capacitance values for the varactor diodes, in order to maintain the specified  $f_0$  without the need of changing the initial coupling line length, which in this case was  $53^\circ$ .

The design of this filter was a good exercise to gain experience and insight into tunable microstrip filters. However, this design is limited to  $f_0$  tuning and a narrow BW.

In order to obtain a wider BW, the coupling coefficients of this filter needs to be increased. This causes very narrow gaps between lines and makes it hard to realise the biasing network of the varactors. It also restricts the capability of BW tuning, because the coupling cannot be controlled with the detuned resonator approach [2] discussed in the previous chapter.

Therefore to realise the KAT-7 specifications, either a new BW tuning approach is required, or a new filter synthesis capable of producing wide bandwidths with controllable  $f_0$  and BW.

# Chapter 4

## Wideband Filters

### 4.1 Introduction

The purpose of this chapter is to look at different wideband filters applicable for the KAT-7 specifications. Therefore in each reviewed synthesis, the scope for tunability is also discussed.

There are three main sections in this chapter. The first section reviews the coupled resonator synthesis with regard to wideband implementations. In the second section the well-known *Richards' transform* is introduced followed by a brief discussion of the exact synthesis for coupled-line filters. In the last section a transversal filtering-section, based on signal-interference techniques, is reviewed and results of significant implementations are summarised.

This chapter is concluded with a comparison of the reviewed syntheses and a possible design approach is proposed to achieve the KAT-7 specifications with.

### 4.2 Coupled resonator filters

The general synthesis of coupled resonator filters have been discussed in Section 2.4 and a practical implementation was done in the previous chapter. In this section the coupled resonator synthesis is discussed with regard to wideband filters. Approximations used in the synthesis is discussed and possible solutions are reviewed.

#### 4.2.1 Wideband implementation

The focus has been primarily on parallel coupled-line filters thus far. It is worth mentioning that there exists another class of filters that has half-wavelength resonators, which are coupled at the ends of the lines as shown in Fig. 4.1. These filters produce very narrow BWs and as a result the former class of filters are more applicable for this work.

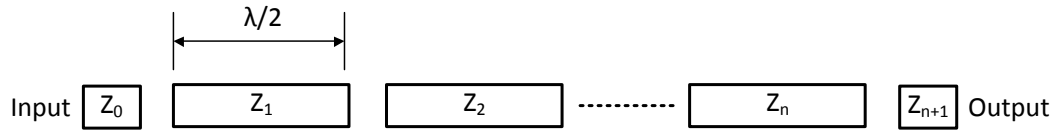


**Figure 4.1:** The microstrip layout of a  $n^{\text{th}}$  order end-coupled half-wavelength resonator filter.

The coupled resonator synthesis is a very suitable design approach for tunable filters. This is not only due to the simplicity of design, but also because both the  $f_0$  and BW of the filter response can be controlled directly in the prototype circuit.

Up until this point the synthesis has only been applied to narrowband specifications. In [37] it is shown how a BW of one octave is achieved by using an interdigital filter that is realised in stripline.

Wide BW is achieved in a coupled resonator filter with high coupling coefficients. In a coupled-line filter this is realised with very narrow gaps between adjacent microstrip lines.<sup>1</sup> These gaps are usually constrained by the fabrication process. Therefore it becomes difficult to achieve the wide BW required by the KAT-7 specifications, for implementations bounded by single layer planar topologies.

An alternative approach to this type of realisation, is the use of multilayer technology such as low-temperature co-fired ceramics (LTCC) or liquid crystal polymer (LCP). This enables resonators to be coupled broadside and leads to much tighter coupling. However, the disadvantage of this approach is that implementing tunability becomes almost impossible, due to the integration of varactor diodes between layers.

A more fundamental problem to the coupled resonator synthesis, is the narrowband approximations it is based on. The building blocks for the prototype filter consist of resonators and inverters. The resonator may be of any type, where only the resonance and slope parameter are of importance. An inverter is determined by the slope parameters of the adjacent resonators as well as the prescribed coupling coefficient between them, as given in (2.24) and (2.27). None of these parameters are defined as being dependent on frequency and as a result neither is the inverter.

The inverter represents the coupling between resonators as explained in Section 2.4. Mutual coupling is inherently dependant on frequency and thus only at resonance does the inverter model give an exact representation of the coupling.

Consequently this is the significant narrowband approximation in the coupled resonator synthesis. The main result is an inaccurate prediction of the realised BW for a

<sup>1</sup>It is interesting to note that the combline structure requires narrower gaps than the interdigital filter for wideband realisations.

wideband filter. Note that the margin of error in BW is dependent on the type of realised coupling structure. Therefore the error may be very small with other implementations. According to [9] the breakdown in synthesis is generally for  $FBW > 20\%$ .

An exact representation of an impedance/admittance inverter is an impedance/admittance step, given that its terminals are matched [9]. This property is exploited in a stepped-impedance filter shown in Fig. 4.2.

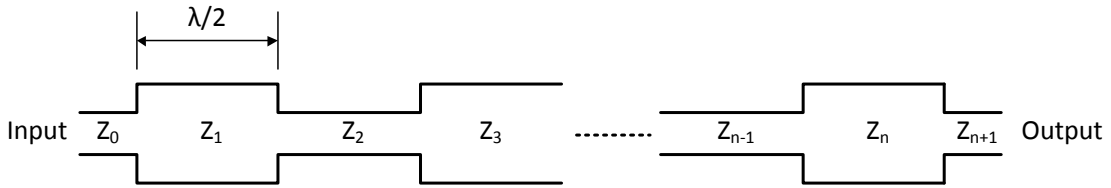


**Figure 4.2:** The microstrip layout of a  $n^{th}$  order stepped-impedance half-wavelength resonator filter.

The basic concept is that an impedance step represents an inverter of the prototype circuit shown in Fig. 2.7a, while the line section (between steps) is half a wavelength long in order to represent a resonator. With this approach a very wide passband is achievable, but the design itself is limited and results in a physically large structure. It is also not possible to implement tunability with varactor diodes in this topology.

### 4.2.2 Improved equations for coupled-lines

In the previous chapter it was shown how the coupling coefficient is implemented with adjacent coupled lines, for the design of coupled resonator filters. This implementation requires optimisation and thus for large structures become a time-consuming process.

A more direct implementation method of the coupling coefficient, is to calculate the required even- and odd-mode characteristic impedances of the coupled lines as [8]

$$Z_{0e} = Z_0 (1 + JZ_0 + (JZ_0)^2), \quad (4.1)$$

$$Z_{0o} = Z_0 (1 - JZ_0 + (JZ_0)^2), \quad (4.2)$$

where  $Z_{0e}$  and  $Z_{0o}$  denotes these impedances respectively. Note that  $J$  is the parameter of the admittance inverter that represents this coupling section. With (4.1) and (4.2) the gap widths between microstrip lines can be calculated as shown in [10].

In [8] the derivations of (4.1) and (4.2) are done based on the approximation that  $\sin\theta \approx 1$ , where the line length  $\theta$  is in the vicinity of  $90^\circ$  in the passband. This is obviously not ideal for wideband specifications, in which case it will result in an inaccurate



prediction of the realised filter BW.

Therefore with this approach (from here on referred to as the *classical method*) there are two approximations concerning the implementation of the inverters of a prototype circuit. The first is the  $\sin\theta \approx 1$  approximation used to obtain the physical coupling between lines. The second is the contrast between inverters and coupled-line sections with regard to its dependence on frequency, as discussed in the previous subsection.

In [7] new accurate formulas are derived for the even- and odd-mode characteristic impedances

$$Z_{0e} = \frac{JZ_0^2 \sin\theta}{\sin^2\theta - (JZ_0 \cos\theta)^2} \left[ \left( JZ_0 + \frac{1}{JZ_0} \right) \sin\theta + 1 \right], \quad (4.3)$$

$$Z_{0o} = \frac{JZ_0^2 \sin\theta}{\sin^2\theta - (JZ_0 \cos\theta)^2} \left[ \left( JZ_0 + \frac{1}{JZ_0} \right) \sin\theta - 1 \right]. \quad (4.4)$$

This is done by setting the ABCD parameters of the equivalent circuit, containing an ideal admittance inverter in Fig. 4.3a, equal to that of the coupled-line section in Fig. 4.3b. Note that when  $\theta = 90^\circ$  (the line length at resonance) these equations are the same as the initial equations (4.1) and (4.2), which confirms the validity of the derivation.

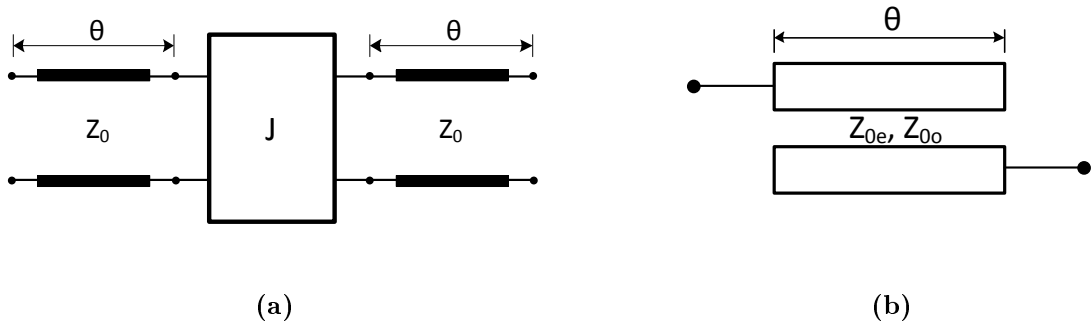


**Figure 4.3:** (a) The equivalent circuit, containing an ideal admittance inverter, of (b) the coupled-line section.

To obtain a more accurate prediction of the passband response, the coupling structure is calculated with

$$\theta = \frac{\pi}{2} \left( 1 \pm \frac{FBW}{2} \right). \quad (4.5)$$

This means that the new even- and odd-mode characteristic impedances are calculated at the band-edges rather than the centre frequency. Therefore an exact equivalence between the circuits in Fig. 4.3 is assured at the band-edges. It must be noted that the symmetry around  $\theta = 90^\circ$  in the trigonometric expressions of (4.3) and (4.4), ensures a single solution for  $Z_{0e}$  and  $Z_{0o}$  respectively at both cut-off frequencies.

This method only deals with the narrowband approximation for a special case of

filters, where open-circuited  $\lambda/4$  coupled-line sections (Fig. 4.3b) are used to realise the inverters. The authors of [7] demonstrates this method by applying it to a common filter layout known as the parallel-coupled half-wavelength resonator filter shown in Fig. 4.4.

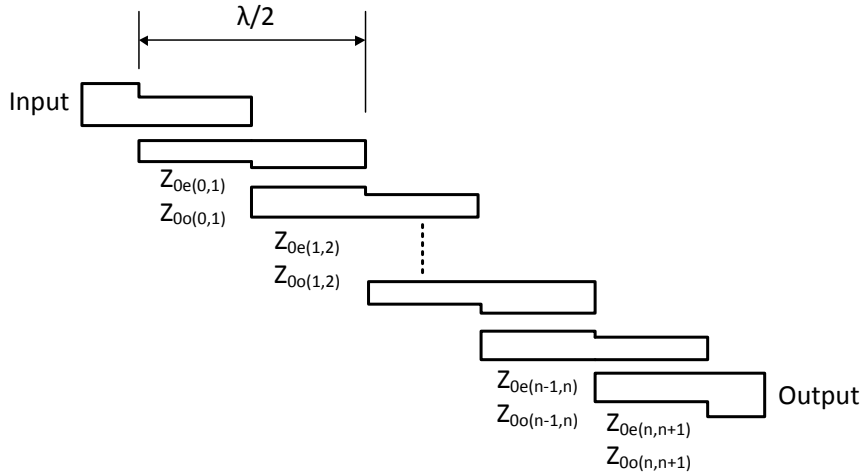


**Figure 4.4:** The microstrip layout of a  $n^{th}$  order parallel-coupled half-wavelength resonator filter.

The results of  $3^{rd}$  and  $5^{th}$  order realised filters [7] are given in Table 4.1. Very good agreement is found between the simulated and measured responses. In Table 4.1 the results are compared with that obtained from the filters designed with the classical method.

From the results it is clear that the new equations makes a substantial difference in the realised filter BW. One can also see the dramatic effect the narrowband approximations have in the classical implementation, with up to a 24% BW deviation for the  $5^{th}$  order filter. Note also that the margin of error in the BW prediction increases as the filter order is increased, due to an increase in the number of coupling sections.

The proposed method may possibly also be applied to interdigital and combline filters. This may be done by changing the coupled-line section to fit the specific filter layout, by deriving similar equations for  $Z_{0e}$  and  $Z_{0o}$ .

**Table 4.1:** The results obtained in [7] for  $3^{rd}$  and  $5^{th}$  order coupled-line filters. They are designed with the classical implementation method [8], as well as the new improved method [7]. The FBW of all the filters are designed for 50%. Note how small the measured BWs are for the filters designed with the classical method.

Filter order	Designed BW	Classical [8]	Improved [7]
3	50%	41%	48.2%
5	50%	38%	44%

An improved synthesis is proposed in [38] for coupled-line filters based on [7], by the same authors of the previous work. Here the insertion loss function of the filter is derived

for synthesising Chebyshev responses up to the 9<sup>th</sup> order. This function is then used to determine conditions for the dimensions of the coupled-line sections.<sup>2</sup>

The proposed method yields better accuracy than the previous. For instance for a 5<sup>th</sup> order filter designed for  $FBW = 50\%$ , the BW obtained with this method [38] is 47.5%, the previous method [7] yields 44% and the classic method [8] a very low 38%. These new methods doesn't completely resolve the approximation problem, but does improve the results substantially compared to the classical approach.

Reviewing the coupled resonator synthesis in view of wideband applications, it is clear that there exists a need for a more accurate approach as well as the ability to realise these filters in planar structures, without being restrained by the fabrication processes.

### 4.3 Exact synthesis based on Richards' transformation

Distributed transmission line elements are of great importance for the realisation of microwave filters. Lumped prototype circuits are commonly used in the design of filters as shown in Chapter 2. Therefore it is beneficial to find equivalences between distributed and lumped elements. The coupled resonator theory introduced in Section 2.4 make use of such equivalences, but is unfortunately based on narrowband approximations.

In 1948, Richards found an equivalence between lumped and distributed elements that is frequency independent. This approach is called the Richards' transformation [39] and is defined with Richards' variable<sup>3</sup>

$$S = j\Omega = j\tan\theta. \quad (4.6)$$

By applying the transformation to a short-circuited transmission line of input impedance

$$Z_{sc} = jZ_0\tan\theta, \quad (4.7)$$

gives

$$Z_{sc} = S \cdot Z_0. \quad (4.8)$$

Note that this looks similar to the Laplace representation of an inductor ( $sL$ ). Therefore a short-circuited or open-circuited (obtained in similar manner) transmission line may be represented in the  $S$ -domain as an inductor or a capacitor, respectively.

When applying Richards' variable ( $S$ ) to a lumped circuit, a distributed circuit is obtained consisting of short- and open-circuited lines, with characteristic impedances differing according to its equivalent lumped values. Note that these lines are all of the same length (commensurate lines) and therefore are limited in application. Nevertheless,

<sup>2</sup>This synthesis [38] is beyond the scope of this work and therefore is only briefly described.

<sup>3</sup>Richards' variable is only considered here for the lossless case.

this transformation is one of the fundamental contributors to modern filter theory.

In [40], Wenzel derives equivalent lumped circuits for coupled transmission line structures, using Richards' transform. These equivalent circuits enable one to formulate lumped prototype circuits for various coupled-line filters. Wenzel uses this in [3] to derive an exact synthesis for combline and interdigital filters. This approach is independent of the BW and therefore is of great significance for the design of wideband filters.

The synthesis starts by applying Richards' transformation to the filter response specifications.<sup>4</sup> Using this along with the specified transmission zeros (i.e. the loss pole locations), the input admittance polynomial of the filter network is derived in the Z-plane [41].

By removing each pole individually from this polynomial, a LC circuit is formed that produces the specified filter response. This circuit is the prototype circuit for the filter and it is similar to the LC ladder prototypes introduced in Section 2.3, although in the S-domain.

Richards' transformation is backwardly applied to this prototype circuit, in order to obtain the equivalent distributed network in the frequency domain. Note that the element values of the prototype circuit are used to determine the admittances of the transmission lines.

In [3] Wenzel also designs a wideband combline filter with 40% BW, using the exact synthesis. The equivalent circuit in the S-domain is shown in Fig. 4.5. Very good agreement is found between the theory and measured results.

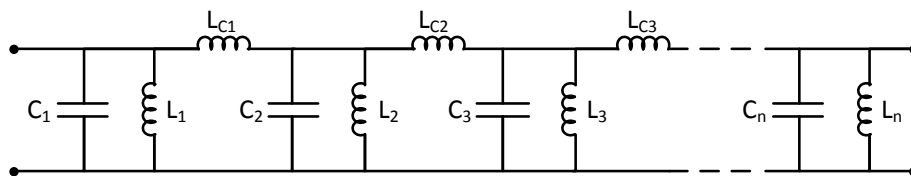


**Figure 4.5:** The equivalent circuit for a combline filter proposed by Wenzel [3]. Note these elements are distributed lumped elements in the S-domain.

Implementing tunability in a combline filter that is designed by the exact synthesis, is not as straight forward as for the coupled resonator approach used in the previous chapter. One need to bear in mind that the exact synthesis is not build on the BW and  $f_0$ , and therefore are not directly controllable parameters.

Referring to the paper by Hunter and Rhodes on combline filters [16], it is shown in

<sup>4</sup>For the purpose of this work the techniques used for the exact synthesis will not be discussed in detail. Refer to [3] for a complete descriptive overview.

Fig. 2.10 that the prototype circuit<sup>5</sup> is manipulated to obtain resonators and inverters that enables tunability. By using narrowband approximations, the physical combline filter is obtained from this manipulated circuit.

In the case of Wenzel’s synthesis, exact equivalent circuits are used to obtain the physical combline filter. The “resonators” in this filter are not specifically designed to be resonators of same characteristics, therefore one cannot tune the filter synchronously. Not only does the coupled-lines have different admittances, but lumped capacitors has to be forced into the design to enable some kind of tunability.<sup>6</sup>

The exact synthesis is highly appropriate for the design of wideband filters, but the disadvantage is that constructive tunability is not realisable.

## 4.4 Signal-interference techniques

A transversal signal-interference filtering-section is introduced in [42]. This section consists of two transmission lines connected in parallel as shown in Fig. 4.6, with the characteristic impedances and electrical lengths of lines referred to as  $Z_1$ ,  $Z_2$  and  $\theta_1$ ,  $\theta_2$ , respectively.<sup>7</sup>

The filtering characteristics of this transversal-section is based on the principle of constructive signal-interference in the passband and destructive signal-interference in the stopband. This action is repeated periodically with frequency, due to the periodicity of transmission lines.

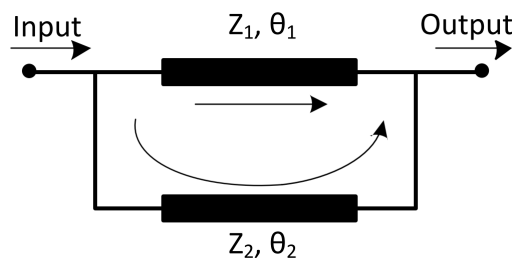


**Figure 4.6:** A transversal signal-interference filtering-section consisting of two parallel transmission lines.

The s-parameters of this section may be derived through standard two-port parameters. First the ABCD-parameters of each line (or path) are determined, followed by its translation into admittance parameters [10]. Since the upper and lower paths are connected in parallel, the admittance parameters may be added together to obtain the complete section’s admittance parameters. The final s-parameters of the section are found by translating these admittance parameters.

<sup>5</sup>Note that this prototype circuit is in the frequency domain.

<sup>6</sup>Note that the capacitors in Fig. 4.5 are distributed capacitors in the  $S$ -domain.

<sup>7</sup>Note that  $\theta_1$  and  $\theta_2$  are frequency dependant parameters, but if a specific value is assigned without stating the frequency, then the assumption is at  $f_0$ .

Applying the condition that the transmission coefficient is a maximum at  $f_0$  (for constructive signal-interference), given that the difference between  $\theta_1$  and  $\theta_2$  is always a multiple of  $2\pi$ , and by using additional symmetry requirements for the filter response around  $f_0$ , the following conditions are derived and are given in [42] to be met in the design of the transversal-section:

$$Z_0 = \frac{Z_1 Z_2}{Z_1 + Z_2}, \quad (4.9)$$

$$\theta_1(f_0) = m \cdot \frac{\pi}{2}, \quad (4.10)$$

$$\theta_2(f_0) = \theta_1 + k \cdot 2\pi. \quad (4.11)$$

Here  $m$  and  $k$  may be any natural integers (1, 2, 3, etc.) and  $Z_0$  represents the terminal impedance (or reference impedance).

The filtering responses are plotted in Fig. 4.7 for different values of the integers  $m$  and  $k$ . Note that the BW increases with an increase in  $m$  or a decrease in  $k$ , however, with an increase in  $k$  the unwanted passbands increases. The unwanted passbands, also referred to as spurious passbands, are caused by the periodicity of the transmission lines. The frequency responses with  $m = 1$  ( $\theta_1 = 90^\circ$ ) have a period of  $2f_0$  and with  $m = 2$  ( $\theta_1 = 180^\circ$ ) the period is  $f_0$ .

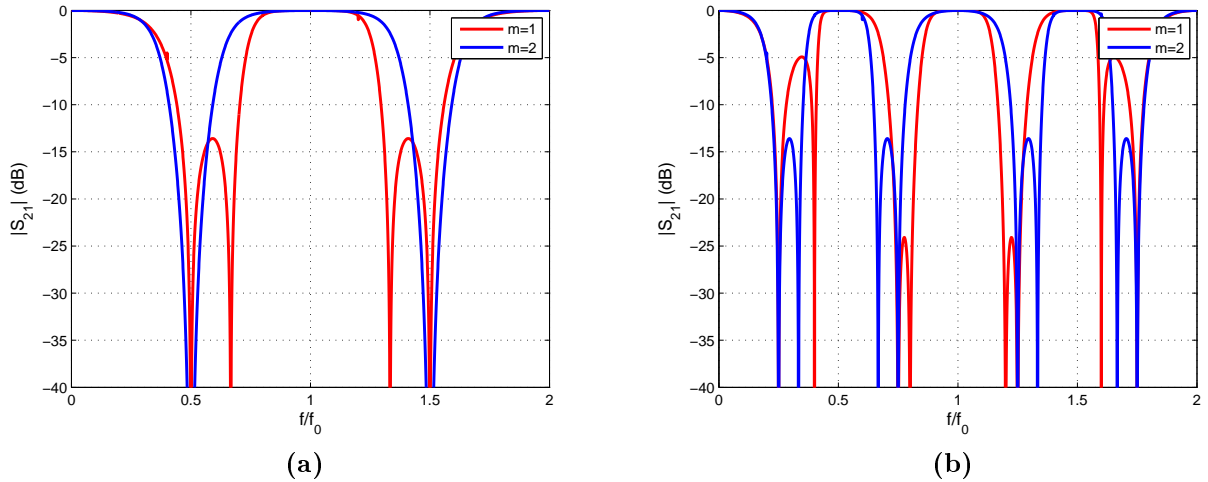


**Figure 4.7:** The transmission responses of the transversal-section with (a)  $k=1$  and (b)  $k=2$ , while the equations (4.9), (4.10) and (4.11) are met with  $2Z_0 = Z_1 = 100\Omega$ .

It is also shown in [42] that when the impedance  $Z_1$  increases while maintaining (4.9), the BW increases and higher stopband rejection is achieved. However, the trade-off is that the transmission zeros (closest to the passband) moves away from the passband, causing the selectivity of the attenuation slopes to decrease and also the BW of the stopbands to decrease.

Higher selectivity may be achieved by cascading these filtering-sections together [42], due to the increase in the passband transmission poles. It is reported in [6] that by using a  $\lambda_g/4$  line with characteristic impedance  $Z_0$  between cascaded sections, higher out-of-band rejection is achieved at the expense of lower return loss in the passband. Open-circuit stubs may be used to introduce more transmission zeros in the stopband in order to obtain higher rejection [5, 6].

### Two cascaded transversal-sections

In [42], two transversal-sections with different filtering characteristics are cascaded through a  $\lambda_g/2$  line with characteristic impedance  $Z_0/2$ . The first section is designed for  $m = 1$  and  $k = 2$  to produce a moderate BW (refer to Fig. 4.7b). The second section is designed for  $m = 1$  and  $k = 1$  to produce a wider BW (refer to Fig. 4.7a), in order to suppress the first section's spurious passbands adjacent to the centre passband, when cascading these sections together. Therefore the result is that the stopbands are wider, without significantly affecting the first section's passband. The use of the cascading  $\lambda_g/2$  line extends the stopbands even further, but unfortunately makes the filter very large in physical size. The FBW is measured to be 27.6% and  $f_0 = 5$  GHz. The lower and upper spurious passbands are rejected above 20 dB from 2.3 to 7.3 GHz.

The characteristic impedances have a significant role in the filtering characteristics such as the BW, rejection and  $L_R$  of a transversal filter. The ratio between the impedances may be very large for such a filter and therefore become difficult to realise in microstrip. The designed filter in [42] has a ratio of 4.2 between the highest and lowest impedance lines.

The advantage of the transversal-type filter is that the insertion losses are minimised because there are no coupling gaps causing mismatching and radiation losses. Therefore the losses are only contributed by the dielectric and conductor losses.

### Coupled-line transversal-section

The transversal filters are generally very large in size, as determined by (4.10) and (4.11). The size of such a filter is reduced in [4], by replacing the upper line ( $\theta_1$ ) in Fig. 4.6 with a coupled-line section. The coupled-line section consists of two short-circuited lines coupling in an interdigital configuration as shown in Fig. 4.8a. The coupling section changes the phase characteristics of the signal and therefore equation (4.11) no longer hold for constructive interference. In this configuration the two signal paths has line lengths of  $\theta_1 = 90^\circ$  and  $\theta_2 = 270^\circ$ , compared to the smallest solution for the transversal-section that is  $\theta_1 = 90^\circ$  and  $\theta_2 = 450^\circ$ . Therefore the section as a whole is much smaller than the conventional transversal-section.

An example of such a section's calculated response is given in Fig. 4.8b. Here the

characteristic impedance of the lower line is  $Z_2 = 66\Omega$ , while the even- and odd-mode characteristic impedances of the coupled-lines are  $Z_{1e} = 41\Omega$  and  $Z_{1o} = 96\Omega$ , respectively. The coupling coefficient is estimated to be  $M \approx 0.49$ .<sup>8</sup> This coupling is very tight and may be difficult to realise in microstrip.

An ultra-wideband (UWB) filter is designed and measured in [4] using this configuration. The result is a FBW of 110% and  $f_0 = 6.85$  GHz. The measured insertion loss is found to be 0.8 dB.

Unfortunately this filtering-section only produces UWB responses which are much wider than the KAT-7 specifications. Nevertheless, the response calculated in Fig. 4.8b has very good out-of-band rejection and a stopband that extends to DC. Therefore this type of filter may be used in cascade with a conventional transversal-section, in order to produce a wideband filter response with high out-of-band rejection. In principle this should produce a more compact and wider passband filter than the one designed in [42].

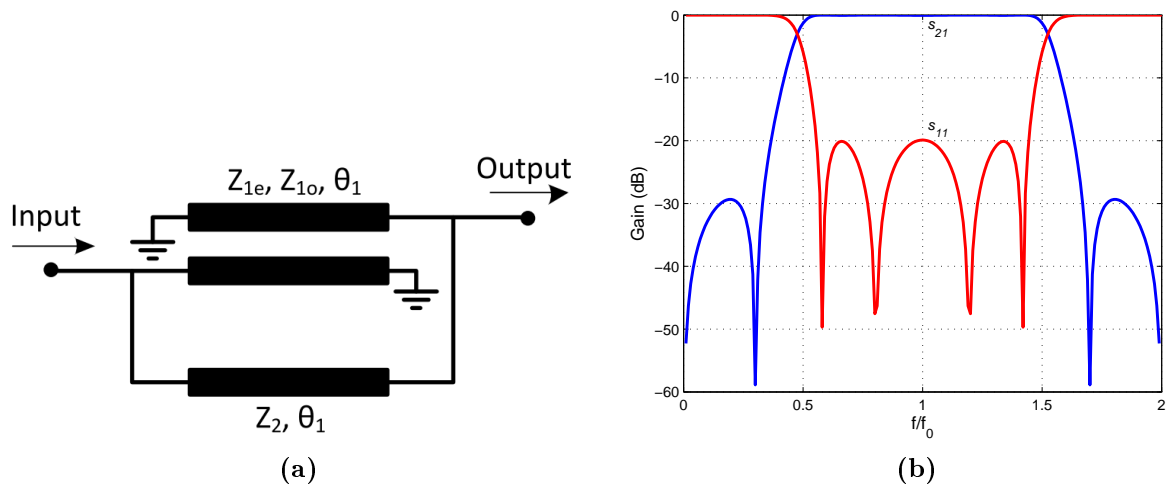


**Figure 4.8:** (a) The schematic of a transversal-section consisting of short-circuited coupled-lines in parallel with another transmission line, as proposed in [4]. (b) An example of the calculated s-parameters of such a filtering-section. Here the coupled-line section has a length of  $\theta_1 = 90^\circ$  and even- and odd-mode characteristic impedances of  $Z_{1e} = 41\Omega$  and  $Z_{1o} = 96\Omega$ , respectively. The lower line has a length of  $\theta_2 = 270^\circ$  and characteristic impedance of  $Z_2 = 66\Omega$ . Note that the coupling coefficient for the coupled-lines is approximately  $M \approx 0.49$ .

### Interdigital fed transversal-section

Interdigital coupling sections with  $\lambda_g/2$  open-circuited stubs are used in [5] to couple into a single transversal-section as shown in Fig. 4.9. The coupling section with its stub introduces extra transmission zeros and therefore good out-of-band rejection is obtained. The simulated and measured results prove to be very good. A FBW of 61% is achieved

<sup>8</sup>The coupling coefficient is extracted from a coupled transmission line circuit in MWO, by using the method for extraction given in the previous chapter.



and  $f_0 = 4$  GHz. The lower and upper spurious passbands are rejected above 18 dB from DC up to 10 GHz. Therefore with this configuration there is no need to cascade sections for the sole purpose of out-of-band rejection.

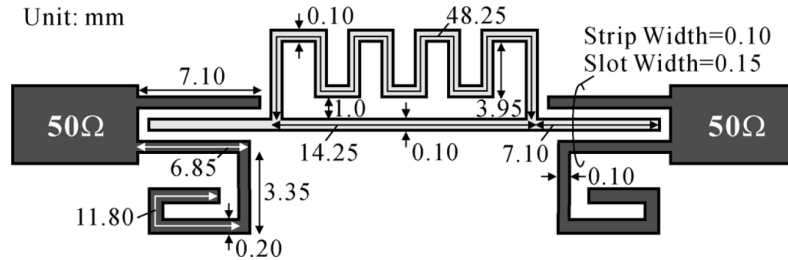


**Figure 4.9:** The microstrip layout of a transversal-type filter proposed in [5]. The filter consists of terminals coupling in an interdigital configuration into a transversal-section. The feeds are asymmetrically loaded with  $\lambda_g/2$  open-circuited stubs to produce transmission zeros in the stopband. The illustration is taken from [5].

### Perturbed ring-resonators in cascade

In [6] a different approach is used to implement a cascaded transversal-type filter. The derivation of this filter is based on the operation of a ring-resonator fed with tapped-lines as shown in Fig. 4.10a. The principle is that a ring with a circumference of  $\lambda_g$  produces a notch (transmission zero) at the resonant frequency and at odd-multiples thereof, given that it is excited at the specific positions as indicated in Fig. 4.10a.

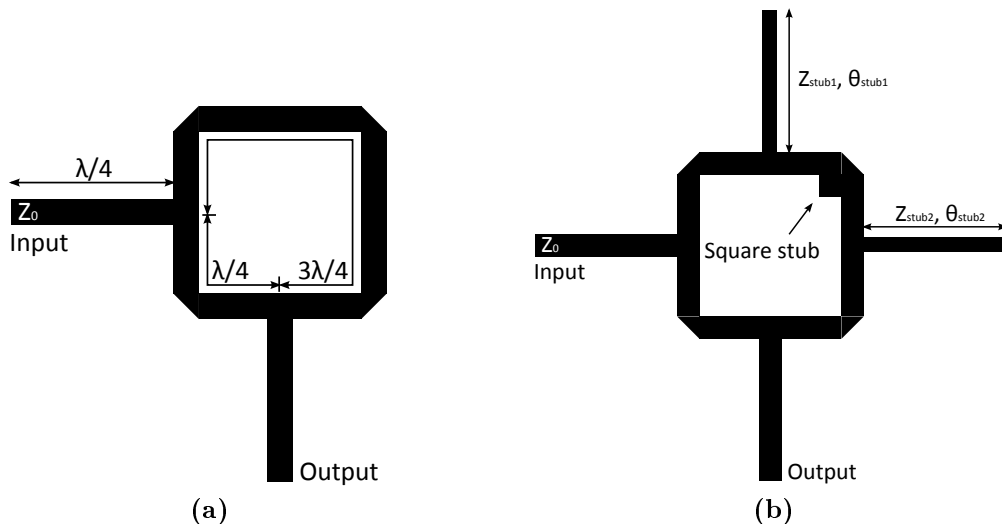


**Figure 4.10:** (a) The microstrip layout of a ring-resonator with tapped-feed lines and a circumference of  $\lambda_g$ . (b) The ring-resonator of (a) are loaded with two open-circuit stubs and one square stub, as proposed in [6].

The ring-resonator on its own is unique in that it has degenerate modes that may resonate at the same frequency. This means that there exists two resonances at the same

frequency, but with orthogonal field distribution [10]. These type of resonators are referred to as dual-mode resonators.

For a symmetrical excitation of the ring, as the one in Fig. 4.10a, only one type of field distribution is forced and therefore only one mode exists at resonance. Therefore the degenerate modes are excited when the resonator's symmetry is disturbed. This phenomena is referred to as perturbation. By adding only one of the stubs shown in Fig. 4.10b with lengths  $\theta_{stub1}$  and  $\theta_{stub2}$  to the ring (first ignore the square stub), the ring is perturbed and the degenerate modes are split with one mode moving away from  $f_0$  to a lower frequency.

This is illustrated in Fig. 4.11, where the transmission coefficient is plotted for different stub lengths where  $Z_0 = 50\Omega$  and  $Z_{stub1} = Z_{stub2} = 64\Omega$ . First the second stub (doesn't matter which one due to symmetry) is removed and the coupling coefficient is given in Fig. 4.11a for different lengths of the first stub. Note that when both stubs have no length, the notch of the ring-resonator is found at  $f_0$  as expected. When  $\theta_{stub1} = 20^\circ$  one can observe the split of the two degenerate modes at  $f_0$  and  $3f_0$ , respectively. The degenerate modes that move to the lower frequencies are marked with 'X' and 'O', initially positioned at  $f_0$  and  $3f_0$  respectively. Note that when  $\theta_{stub1} = 90^\circ$  these two modes are positioned symmetrical around  $f_0$ .

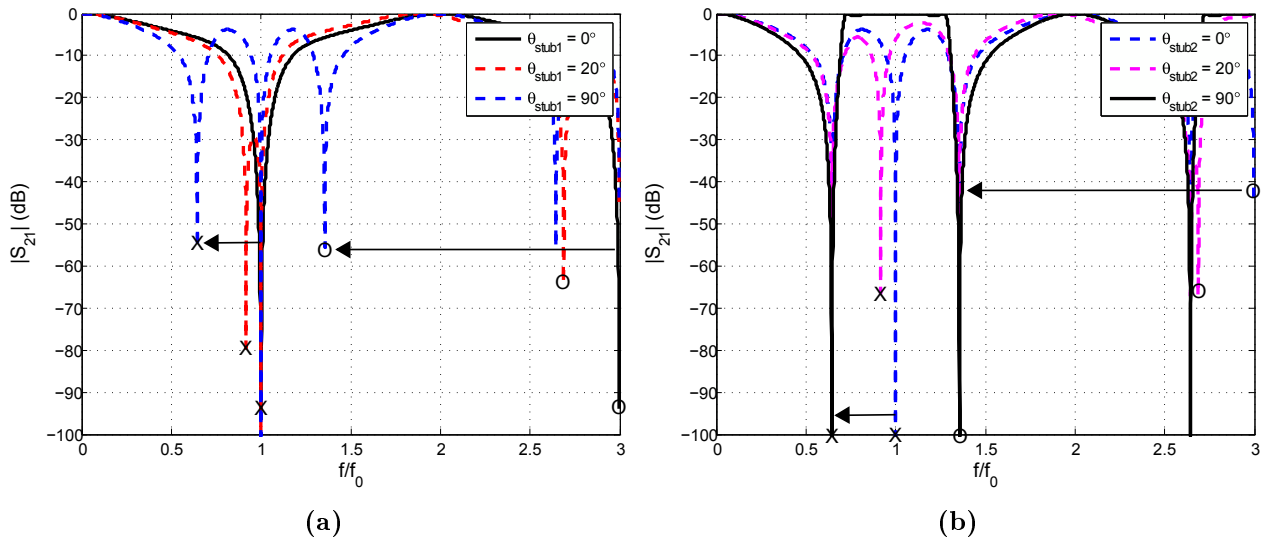


**Figure 4.11:** The transmission coefficient for the stub-loaded ring-resonator in Fig. 4.10b, with  $Z_0 = 50\Omega$  and  $Z_{stub1} = Z_{stub2} = 64\Omega$ . (a) The length of  $\theta_{stub1}$  is varied while  $\theta_{stub2} = 0^\circ$ . The degenerate modes marked with 'X' and 'O', which are initially positioned at  $f_0$  and  $3f_0$  respectively, are moved to lower frequencies as  $\theta_{stub1}$  increases. (b) Here  $\theta_{stub1} = 90^\circ$  while  $\theta_{stub2}$  is varied. The remaining degenerate modes, also marked with 'X' and 'O', are now moved to lower frequencies as  $\theta_{stub2}$  increases.

For  $\theta_{stub1} = 90^\circ$  the transmission coefficient is given in Fig. 4.11b for different lengths of the second stub. In this case the remaining degenerate modes at  $f_0$  and  $3f_0$  are also

moved lower and a symmetric passband is formed at  $f_0$ . The degenerate modes are not excited when the stubs have the exact same characteristics, due to the symmetrical positioning of the stubs on the resonator. However, for  $\theta_{stub1} = \theta_{stub2} = 90^\circ$  the first and third resonances are found at lower frequencies, symmetrically positioned around  $f_0$ .

This resonator is perturbed again, but with a square stub as indicated in Fig. 4.10b. This excites the degenerate modes and causes a small split in the transmission zeros, that consequently increases the out-of-band rejection. Three of these resonators are cascaded through  $\lambda_g/4$  lines to obtain more transmission zeros in the stopband, in order to increase the out-of-band rejection.

This filter is designed and fabricated in [6] where good agreement is found between the calculated and measured results. The FBW is 49.3% and  $f_0 = 6$  GHz. The insertion loss is lower than 1.6 dB and the return loss greater than 13.3 dB in the passband. Very good out-of-band rejection is obtained with  $|s_{21}| < -40$  dB from 2.75 to 9.08 GHz.

### Ring-resonator and transversal-section

Viewing the ring-resonator in Fig. 4.10a through the transversal approach, it is clear that there exists two parallel paths between the input and output lines. Therefore the shorter line can be compared with the upper path ( $\theta_1$ ) and the longer line with the lower path ( $\theta_2$ ) of the transversal-section in Fig. 4.6. However, the ring resonator corresponds to  $\theta_1 = 90^\circ$  and  $\theta_2 = 270^\circ$  which do not adhere to the condition in (4.11) for constructive signal-interference. From Fig. 4.11a where both stubs have zero length, it is clear that at  $2f_0$  this condition do exist and a passband is found. This corresponds to the conventional transversal-section where  $m = 2$  and  $k = 1$  as seen in Fig. 4.7a.

Therefore another explanation of the filter-section in Fig. 4.10b may be that the symmetrical  $\lambda_g/4$  stub-loading actually moves the passband of the transversal-section to half of its original centre frequency, reducing the overall physical size.

Therefore, the idea of degenerate modes in a ring-resonator give rise to the premise that it might be possible to strategically perturb any other transversal-section, in order to enhance the stopband characteristics. The perturbation might also be in the form of tuning elements, to move the transmission zeros and enabling tunability of the wideband filter characteristics.

## 4.5 Conclusion

The emphasis of this chapter was on wideband filters with regard to tunability. Three main syntheses were reviewed and the possibility of implementing tuning networks was investigated.

The coupled resonator synthesis was reviewed for wide bandwidths. Unfortunately the

building blocks of this synthesis is derived using narrowband approximations and therefore result in inaccurate wideband design. New design equations and techniques were reviewed and good improvement was found for the BW accuracy.

This synthesis is most beneficial for tunable filter design due to the direct controllability of the BW and  $f_0$ . However, this is not necessarily the case for wide BW filters. For an increase in BW, the gaps between resonators become very small and leads to difficulty in the fabrication process and implementation of the tuning networks. This is especially true for the implementation of detuned resonators (refer to Chapter 2), in order to control the BW. Therefore new tuning techniques are required for such tightly coupled resonator structures.

The exact synthesis of coupled-line filters was briefly introduced. Here there are no narrowband approximations and thus very accurate wideband filters may be designed. However, the synthesis is bounded by commensurate lines and therefore only a certain class of coupled-line filters may be designed. The synthesis is also bounded to purely distributed filters and lumped elements must be forced into the design, that will introduce some approximations.

The design is not based on the BW and  $f_0$  parameters and therefore cannot be controlled directly. The adjacent “resonators” are not symmetrical and thus not synchronously tunable. If tuning would be possible, there are still the issues of fabrication and implementation of tuning networks due to narrow gaps.

A transversal filtering-section was introduced through signal-interference techniques. This section proved to be very flexible in wide BWs, with various ways of implementation. The filter response has high selectivity due to transmission zeros at finite frequencies. The insertion loss proved to be very low due to the lack of mismatching and radiation caused by coupling gaps.

Though the filter response of the conventional transversal-section is repeated periodically, with spurious passbands found in close proximity to the fundamental passband, different techniques were reviewed to deal with this.

The transversal-sections may be matched to  $50\Omega$  and therefore makes cascading quite straight forward. Cascading sections together introduces more transmission zeros which leads to more out-of-band rejection. Stubs may also be used for the purpose of introducing transmission zeros.

It was found that by perturbing a ring-resonator, more versatility is added to the design. The ring-resonator can be viewed as a transversal-section, therefore, the conclusion is that perturbation may also be applicable to other transversal-type sections. By perturbing with tuning elements, the premise is that constructive tunability may possibly be introduced into such a wideband filter. Another advantage is that implementation of tuning networks should not be a problem due to the large physical size of these filters.

The significant filter syntheses regarding the KAT-7 specifications, were reviewed in this chapter. Thus, it is concluded that no tune-all wideband planar filter synthesis exists in current literature.

The most promising reviewed work for tunable wideband filters is that of the perturbed ring-resonators [6]. In the next chapter the potential of perturbation with tuning-elements are investigated for transversal-sections, in order to obtain a solution for the required KAT-7 filter.

# Chapter 5

## Prototype Filters for KAT-7

### 5.1 Introduction

The purpose of this chapter is to develop and design a tune-all wideband filter for the KAT-7 front-end. In the previous chapter the conclusion was made that there exists no synthesis for tune-all wideband filters in microstrip technology, although potential was found with the signal-interference techniques. The premise follows that tuning elements may be used to perturb transversal-sections, leading to the possibility of tunable wideband filters.

Therefore the starting point of the filter development in this chapter, is the investigation of tunability in transversal-sections through perturbation. A new tunable filtering-section is proposed and characterised. This is followed by the development of two prototype filters, consisting respectively of 4 and 6 of these filtering-sections in cascade. A systematic synthesis is proposed for the design by optimisation of these type of filters. Very good results are obtained in both the designs. The filters are fabricated and reasonably good agreement is found between the simulated and measured results.

The chapter is concluded with a summary of all the results and recommendations are made for future work.

### 5.2 Tunable transversal-sections based on perturbation

In this section the recommendations made in the previous chapter are investigated and different approaches for tunable filtering-sections are proposed. The aim is to enable tunability through varactor diodes with the concept of perturbation in a transversal-section.

### 5.2.1 Premise for the investigation of tune-all filtering-sections

In a ring of circumference  $\lambda_g$ , there are two possible resonant modes at  $f_0$  that may propagate in the structure [43]. These two modes are referred to as degenerate modes and their orthogonal field distributions are shown in Fig. 5.1. The X's and arrows in the illustration, respectively indicates the voltage and current absolute maxima at resonance.

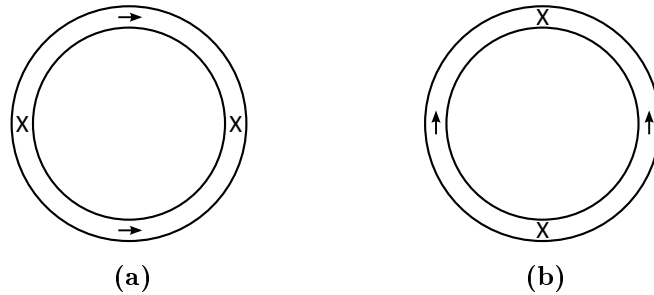


**Figure 5.1:** The two possible field distributions of the ring-resonator that may propagate at resonance, when the circumference of the ring is  $\lambda_g$ . The X's and arrows indicate the voltage and current absolute maxima, respectively.

When the ring's symmetry is disturbed, both of these resonant modes may be excited and will resonate at the same or nearly the same frequencies, depending on the influence of the disturbance. Viewing it in terms of the field distribution, it is simply a superposition of the two distributions shown in Fig. 5.1.

Loading the ring for instance with an open-circuit stub, the symmetry of the ring is disturbed in such a way that the degenerate modes are excited and therefore split in frequency. Note that to fully understand the loading of the ring, the phases of the fields should also be considered [43].

This disturbance technique is known as perturbation and is widely used in cavity structures. The concept of perturbing a ring-resonator in order to excite the degenerate modes, has briefly been discussed in Section 4.4. A wideband filter based on this approach was introduced by [6].

It is worth mentioning that by placing feed terminals orthogonally with respect to one another on the ring (see Fig. 4.10a), one of the terminals always has a maximum signal voltage while the other terminal is grounded. Therefore a notch (or transmission zero) is produced at  $f_0$ .

The premise for this work is that perturbing with tunable elements may lead to the possibility of moving these transmission zeros in the frequency domain. With this method it may also be possible to move the transmission zeros around a filter passband in such a way, that a tune-all capability is achieved in the filter.

Based on this premise, various filtering-sections will be investigated in the next subsection. This will be done through simulations of circuit models in MWO, where the

transmission lines are modelled by TEM-lines.

## 5.2.2 First proposed filtering-section

The centre frequency of filter responses have been calculated this far with (2.1). For transversal-sections the centre frequency is defined differently by

$$f_0 = \frac{f_{c1} + f_{c2}}{2}, \quad (5.1)$$

where  $f_{c1}$  and  $f_{c2}$  are the cut-off frequencies with  $f_{c1} < f_{c2}$ . The reason for this definition is due to the periodicity of conventional transversal-sections. Therefore the circuits investigated in this section will be designed with (5.1).

Note that  $f_0 = 1.53$  GHz is specified for the KAT-7 filter in Chapter 1, which is calculated with (2.1). However, the passband must stretch between the two cut-off frequencies and therefore  $f_0$  is only considered as a reference for the design.<sup>1</sup> In this section the design frequency is calculated with (5.1) as  $f_0 = 1.575$  GHz, in order to obtain the cut-off frequencies 1.2 and 1.95 GHz.

The first proposed tunable filtering-section is shown in Fig. 5.2a. This filtering-section is based on the stub-loaded ring-resonator (see Fig. 4.10b) proposed in [6]. It was shown in Fig. 4.11 that by changing the stub lengths, the positions of the transmission zeros are changed. In the new proposed filtering-section (Fig. 5.2a), the open-circuit stubs are replaced by stubs that are loaded with variable capacitors  $C_{s1}$  and  $C_{s2}$ , in order to tune the positions of the transmission zeros.

The line lengths are  $\theta_1 = 90^\circ$  and  $\theta_2 = 270^\circ$  and the characteristic impedances are chosen  $Z_1 = Z_2 = 50\Omega$  for simplicity of the ring-resonator characteristics. The BW and  $L_R$  are determined by the stub impedances  $Z_{s1}$  and  $Z_{s2}$ . The lower the impedances the wider is the BW, but at the expense of poor  $L_R$ . The parameters are chosen as  $Z_{s1} = Z_{s2} = 90\Omega$  and gives a BW that is slightly smaller than 750 MHz. When introducing the capacitor loads, the stub lengths become shorter in order to maintain the transmission zero positions, which then increases the BW to 750 MHz. Note that the stubs are designed to be identical, in order to have the degenerate modes at same frequencies for passband symmetry (refer to Fig. 4.11b).

The input impedance of a capacitor-loaded stub (in Fig. 5.2a) is given by

$$Z_{in} = Z_0 \frac{1 - \omega C Z_0 \tan \theta}{\omega C Z_0 + \tan \theta}, \quad (5.2)$$

where  $Z_0$  and  $\theta$  are the characteristic impedance and electrical length of the line, respectively.

---

<sup>1</sup>The transmission line electrical lengths and the frequency tuning ranges are determined according to  $f_0$ .



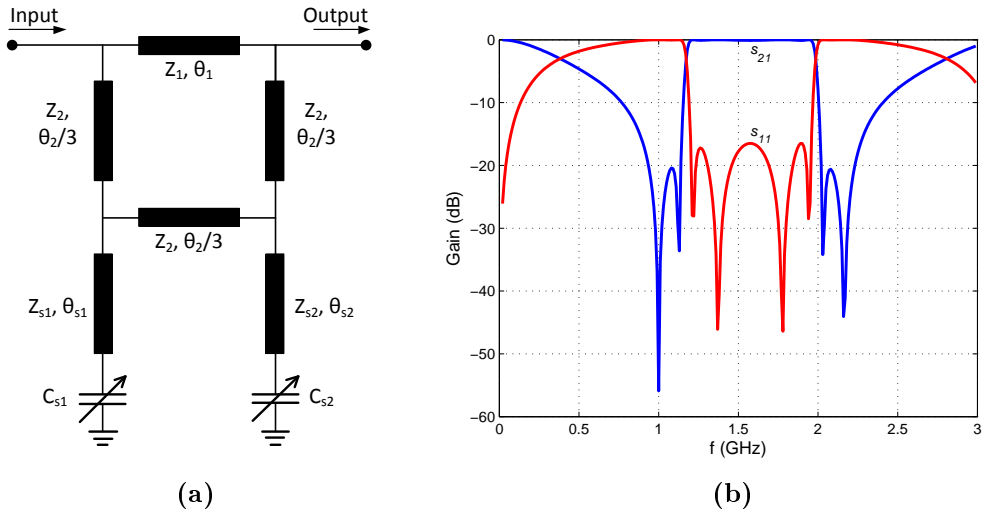


**Figure 5.2:** (a) The first proposed tunable filtering-section, consisting of a stub-loaded ring-resonator with tuning capacitors. (b) An optimised response for the filtering-section in (a) to meet the passband specifications of KAT-7. The parameter values are  $\theta_1 = 90^\circ$ ,  $\theta_2 = 270^\circ$ ,  $Z_1 = 43\Omega$ ,  $Z_2 = 47\Omega$ ,  $\theta_{s1} = \theta_{s2} = 60^\circ$ ,  $Z_{s1} = Z_{s2} = 80\Omega$  and  $C_{s1} = C_{s2} = 0.73$  pF.

The input impedance of a  $\lambda_g/4$  open-circuit stub is zero at  $f_0$ . Therefore replacing the fixed stub in Fig. 4.10b with a tunable stub, the input impedance (5.2) of the tunable stub must also be zero at  $f_0$ . Following this the capacitance is calculated as

$$C = \frac{1}{\omega_0 Z_0 \tan \theta_0}. \quad (5.3)$$

With optimisation of the circuit in MWO it is determined that for  $Z_{s1} = Z_{s2} = 90\Omega$ , the stub lengths must both be  $\theta_{s1} = \theta_{s2} = 60^\circ$  in order to obtain a ripple passband from 1.2 to 1.95 GHz. Therefore using (5.3) the capacitor values are calculated to be  $C_{s1} = C_{s2} = 0.65$  pF. The filter response for these values are given by the black line in Fig. 5.3a.

By tuning either of the capacitors, the excitation of the degenerate modes are changed. The position of each degenerate mode ( $1^{st}$  and  $3^{rd}$  modes of the ring-resonator) corresponds to the characteristics of one of the capacitor-loaded stubs. For example by increasing  $C_{s1}$  the one pair of degenerate modes around the passband are moved to lower frequency positions. This corresponds to an increase in the equivalent stub length as was shown in Fig. 4.11a.

This tuning effect is illustrated in Fig. 5.3, where both capacitors are changed from 0.53 to 0.79 pF to decrease the centre frequency of the passband. Here the return loss is maintained across the tuning range above 10 dB. Note that the passband is asymmetrical if  $C_{s1} = C_{s2} \neq 0.65$  pF.

For BW tuning the premise is that the degenerate modes must be split through asym-

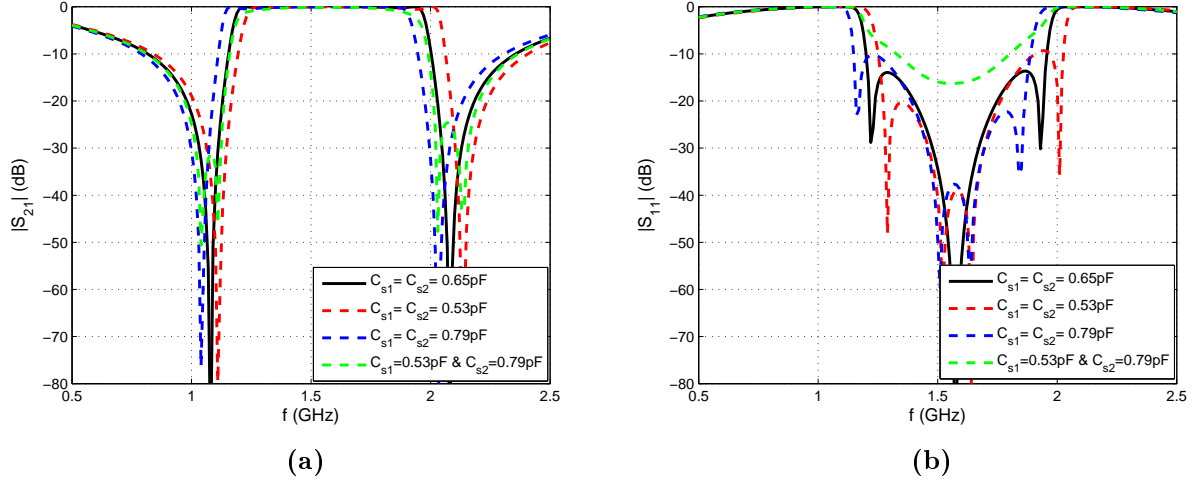


**Figure 5.3:** The (a) transmission coefficient and (b) reflection coefficient of the proposed tunable filtering-section in Fig. 5.2a, for different capacitor values. The parameter values of the filtering-section are  $\theta_1 = 90^\circ$ ,  $\theta_2 = 270^\circ$ ,  $Z_1 = Z_2 = 50\Omega$ ,  $\theta_{s1} = \theta_{s2} = 60^\circ$  and  $Z_{s1} = Z_{s2} = 90\Omega$ .

metrical tuning, causing two of the transmission zeros to move closer to  $f_0$ . This is done by setting  $C_{s1} = 0.53$  pF and  $C_{s2} = 0.79$  pF, with the response shown in Fig. 5.3a. It is observed that the degenerate modes does in fact split and a pair of the transmission zeros around the passband moves closer to  $f_0$ , while the other pair moves away. Therefore the passband does decrease slightly, but it is also observed in Fig. 5.3b that the return loss deteriorates significantly, resulting in very poor roll-off at the band edges. Thus very poor BW tuning is achieved with this type of filtering-section.

Nevertheless it is worth showing that a very good response is achievable with this section, by optimising its impedances. The ring's line impedances ( $Z_1$  and  $Z_2$ ) are changed in order to perturb the resonator and therefore obtaining better out-of-band rejection. This is generally also done in transversal-sections to obtain better out-of-band rejection and to vary the BW, but is not always considered as perturbation due to a lack of insight into the equivalences to ring-resonators.

Due to the BW change caused by the line impedances, the stub impedances are also optimised in order to maintain the passband specifications. The new parameter values are  $Z_1 = 43\Omega$ ,  $Z_2 = 47\Omega$ ,  $Z_{s1} = Z_{s2} = 80\Omega$ ,  $\theta_{s1} = \theta_{s2} = 60^\circ$  and  $C_{s1} = C_{s2} = 0.73$  pF. The response accompanying these values is shown in Fig. 5.2b. For this TEM-model the return loss is 16.5 dB. A frequency tunability of 10% is achieved with very little change in the absolute BW. This is obtained by tuning both the capacitors from 0.59 to 0.97 pF, while maintaining  $L_R \geq 10$  dB. Note also the very high selectivity caused by the transmission zeros.

The first proposed tunable filtering-section has much potential for wideband frequency tunable filters. However, for this work BW tuning is also desired and therefore other

perturbation layouts of the ring-resonator should be investigated.

It has to be mentioned that for a transversal-section with  $\theta_1 = 90^\circ$  ( $m = 1$ ) and  $\theta_2 = 450^\circ$  ( $k = 1$ ), the same perturbation techniques may be applied. The problem, however, is that the out-of-band rejection is much worse than for the ring-type (i.e.  $\theta_1 = 90^\circ$  and  $\theta_2 = 270^\circ$ ). For other transversal-sections with longer lines (i.e. large  $m$  and  $k$ ), it is observed in Fig. 4.7b that more spurious responses appear close to  $f_0$  and the BWs are reduced, due to the periodicity of transmission lines. For the purpose of this work, therefore, it is not worth investigating any of these other transversal-sections, apart from the ring-resonator.

### 5.2.3 Second proposed filtering-section

The development of the second proposed tunable filtering-section consists of multiple steps, in order to obtain a fully tunable structure. First an open-circuit stub is connected half way on the lower path of a ring-resonator as shown in Fig. 5.4a. The structure is lightly coupled at the terminals in order to observe the perturbation effect more clearly on the transmission pole and zero positions.<sup>2</sup>

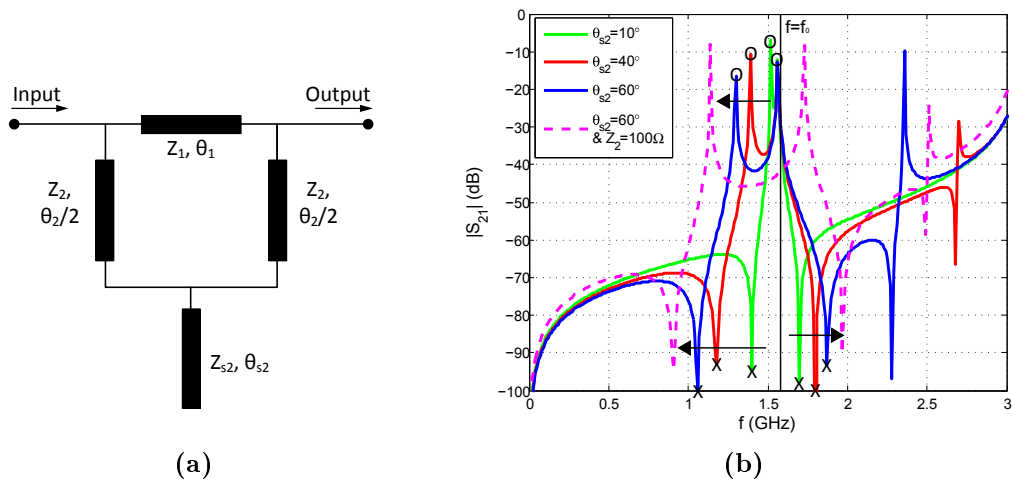


**Figure 5.4:** (a) A ring-resonator loaded with a single open-circuit stub. (b) The transmission coefficient of this filtering-section for different stub lengths, with the terminals lightly coupled. The parameter values are  $\theta_1 = 90^\circ$ ,  $\theta_2 = 270^\circ$ ,  $Z_1 = Z_2 = 50\Omega$  and  $Z_{s2} = 50\Omega$ , except for the dashed line where  $Z_2 = 100\Omega$ . The X's indicate the transmission zeros of the excited degenerate modes, while the O's indicate the transmission poles found between them.

The line lengths and characteristic impedances are again chosen as  $\theta_1 = 90^\circ$  and  $\theta_2 = 270^\circ$  and  $Z_1 = Z_2 = 50\Omega$  for simplicity of the ring-resonator characteristics. The characteristic impedance of the stub is arbitrarily chosen as  $Z_{s2} = 50\Omega$ . Note that the

<sup>2</sup>For these experiments series capacitors of 0.1 pF are used in MWO to couple into the circuits. Refer to Subsection 3.2.1 for an explanation of light coupling.

stub is not loaded with a capacitor in this case, because the perturbation affect at that position on the ring is first investigated. A tunable capacitor may be added later in the design.

In Fig. 5.4b the transmission coefficient of this circuit is plotted for different lengths of the stub ( $\theta_{s2}$ ). Note how the degenerate modes are split at  $f_0$  when the stub is introduced. The transmission zero that exists at DC is caused by the series capacitors, used to couple lightly from the terminals. This is not part of the structure itself and may be ignored. The transmission pole and zero pair found on the graph between 2 to 3 GHz, is a result of the perturbation of the pole at  $2f_0$ .

As  $\theta_{s2}$  increases, the degenerate modes are split causing the transmission zeros (marked with X's in Fig. 5.4b) to move away from  $f_0$ . A passband is formed between them which consists of two transmission poles marked with O's. Note that the lower pole position moves to lower frequencies as  $\theta_{s2}$  increases, while the upper pole remains at  $f \approx f_0$ .

The transmission poles indicate approximately how wide the passband is. For the aim of this investigation an even wider passband is required. Therefore the lower path's characteristic impedance must be increased in order to perturb the ring even more. This is done by setting  $Z_2 = 100\Omega$  and is shown in Fig. 5.4b with the dashed line. It is noted that not only does the lower pole move away from  $f_0$ , but also the upper pole.

The perturbation affect of the stub mainly tunes the lower transmission pole position and does not give enough tuning freedom for the passband. The upper transmission pole position, however, may be tuned by changing the impedance of either of the paths denoted by  $Z_1$  and  $Z_2$  and therefore enabling freedom for the tunability of the passband. For this reason the second step in the development of this filtering-section, is to insert a shunt variable capacitor ( $C_1$ ) on the upper path as shown in Fig. 5.5a, in order to possibly influence  $Z_1$ .

In Fig. 5.5b the transmission coefficient is plotted for different values of  $C_1$ , while the rest of the parameters remain the same as in the previous circuit (i.e.  $\theta_1 = 90^\circ$ ,  $\theta_2 = 270^\circ$ ,  $Z_1 = 50\Omega$ ,  $Z_2 = 100\Omega$ ,  $Z_{s2} = 50\Omega$  and  $\theta_{s2} = 60^\circ$ ). It is clearly observed that the lower pole (indicated with 'O') moves to lower frequencies as the shunt capacitor is introduced. This is contrary to what is required to make the circuit a tune-all filtering-section, because the upper pole is still not tunable.

Therefore the next step is to replace the shunt capacitor with a series capacitor (also denoted by  $C_1$ ), in order to try and tune the upper transmission pole position. The new circuit is shown in Fig. 5.6a, with its transmission coefficient plotted in Fig. 5.6b. As the capacitor is introduced and tuned to 4 pF, the upper pole (indicated with 'O') is in fact moved away from  $f_0$  to increase the BW. Note that the capacitor also introduces a transmission zero from DC, which is beneficial for the out-of-band rejection.

Therefore this circuit (Fig. 5.6a) exhibits tunability of the lower and upper poles,

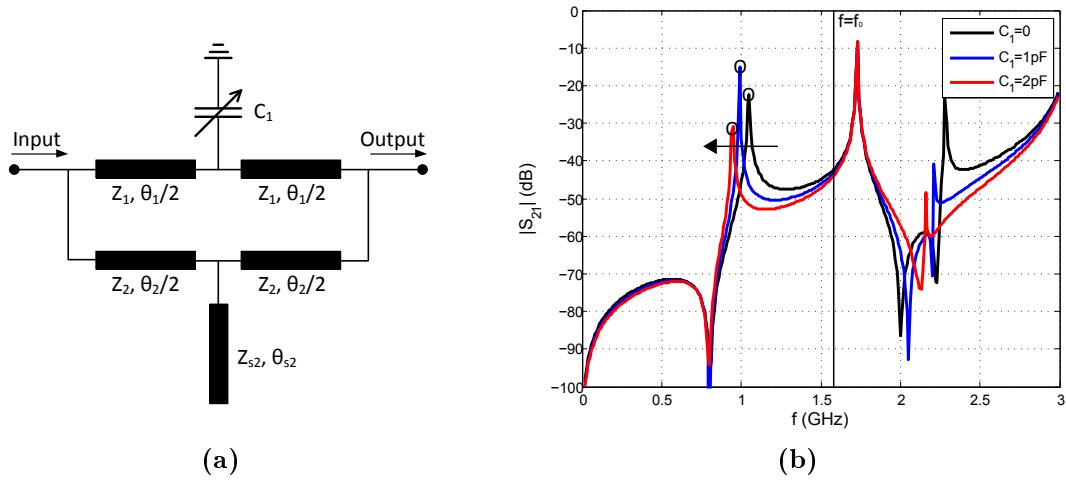


**Figure 5.5:** (a) A ring-resonator loaded with a single open-circuit stub on the lower path and a shunt capacitor on the upper path. (b) The transmission coefficient of this filtering-section for different capacitor values, with the terminals lightly coupled. The parameter values are  $\theta_1 = 90^\circ$ ,  $\theta_2 = 270^\circ$ ,  $Z_1 = 50\Omega$ ,  $Z_2 = 100\Omega$ ,  $Z_{s2} = 50\Omega$  and  $\theta_{s2} = 60^\circ$ . The O's indicate the lower transmission poles that are tuned with  $C_1$ .

through the perturbing affect of the stub and capacitor, respectively. This tune-all capability makes the circuit desirable over the former proposed tunable filtering-section. However, the open-circuit stub still has to be replaced by a tunable element and the network scaled to the correct centre frequency. This is done in the next section, where this circuit is optimised according to the KAT-7 specifications.

### 5.3 Prototype development

In this section the circuit in Fig. 5.6a is further developed to obtain a filter response with tune-all capabilities. The optimisation of the circuit is followed by a summary of its frequency behaviour with regard to its parameters. An attempt is also made to describe the network with two-port parameters.

This section is concluded with propositions for the use of the filtering-section in the design of a prototype filter, adequate for the KAT-7 front-end.

#### 5.3.1 Development of the tune-all filtering-section

The proposed filtering-section with tune-all capabilities is shown in Fig. 5.7a. Here a shunt capacitor ( $C_2$ ) is used to replace the stub in the preceding circuit (Fig. 5.6a).

The reason for not implementing a capacitor-loaded stub, as done with the circuit in Fig. 5.2a, is because perturbation with a shunt capacitor has quite similar results to the former. The capacitor also has a more realistic value without the transmission line. Note

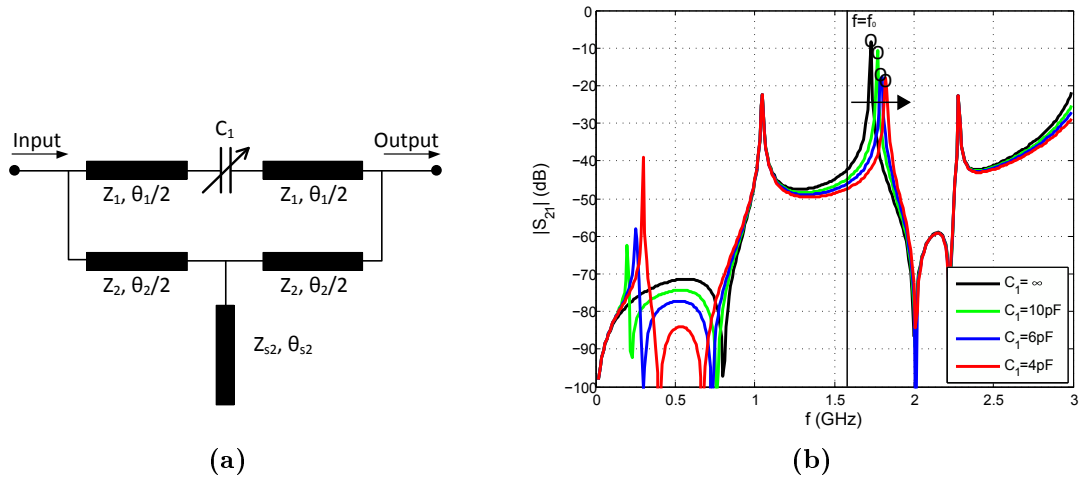


**Figure 5.6:** (a) A ring-resonator loaded with a single open-circuit stub on the lower path and a series capacitor on the upper path. (b) The transmission coefficient of this filtering-section for different capacitor values, with the terminals lightly coupled. The parameter values are  $\theta_1 = 90^\circ$ ,  $\theta_2 = 270^\circ$ ,  $Z_1 = 50\Omega$ ,  $Z_2 = 100\Omega$ ,  $Z_{s2} = 50\Omega$  and  $\theta_{s2} = 60^\circ$ . The O's indicate the upper transmission poles that are tuned with  $C_1$ .

that the capacitor is linear with frequency and therefore at higher frequencies does not have the same affect as an open-circuit stub.

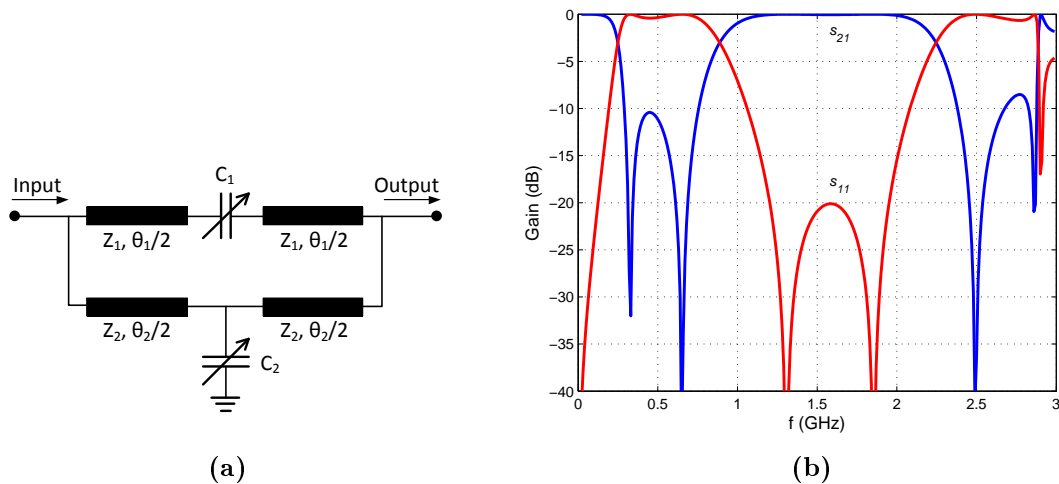


**Figure 5.7:** (a) Proposed filtering-section with tune-all capabilities. (b) The filter response of this TEM-circuit in MWO, with optimised parameter values given in Table 5.1.

It is decided to calculate the centre frequency with the initial formula (2.1) for further development of this circuit, because the filtering-section no longer exhibit pure signal-interference characteristics (e.g. symmetry in the filter response) and the KAT-7 specifications require it to be  $f_0 = 1.53$  GHz. It must also be noted that the passband (1.2 to 1.95 GHz) is specified at the ripple cut-off for the lossless TEM-circuit.

The parameter values of the circuit in Fig. 5.7a are optimised in MWO for  $f_{c1} = 1.2$

GHz,  $f_{c2} = 1.95$  GHz,  $L_R = 20$  dB and a symmetrical passband. The initial values of the previous circuit are also the initial values for the optimisation process, i.e.  $\theta_1 = 90^\circ$ ,  $\theta_2 = 270^\circ$ ,  $Z_1 = 50\Omega$ ,  $Z_2 = 100\Omega$ ,  $C_1 = 4$  pF and  $C_2 = 2.5$  pF. The shunt capacitor is chosen as  $C_2 = 2.5$  pF in order for the transmission poles to be at the same positions as the previous circuit (Fig. 5.6a), although some of the transmission zeros are moved slightly.

The whole network is scaled for the new centre frequency of 1.53 GHz and the result is  $\theta_1 = 87.4^\circ$ ,  $\theta_2 = 262.3^\circ$ ,  $Z_1 = 50\Omega$ ,  $Z_2 = 100\Omega$ ,  $C_1 = 4.1$  pF and  $C_2 = 2.6$  pF. Note that the circuit is no longer lightly coupled to the  $50\Omega$  terminals.

To be able to tune  $f_{c1}$  and  $f_{c2}$  higher or lower with  $C_2$  and  $C_1$ , without the transmission zeros around the passband disappearing, the capacitor values are both increased to  $C_1 = 7$  pF and  $C_2 = 4.7$  pF for  $FBW \approx 49\%$ .

In order to move the passband higher for the desired cut-off frequencies, the line lengths are decreased to  $\theta_1 = 81^\circ$  and  $\theta_2 = 212^\circ$ . Note that  $\theta_1$  is not scaled in comparison as low as  $\theta_2$ , because symmetry in the passband is required and therefore  $\theta_1$  is optimised. After this the impedances  $Z_1$  and  $Z_2$  are optimised to achieve the correct BW, with a slight change in  $C_2$ .

The final optimised values are given in Table 5.1 with the corresponding response of this TEM-circuit (in MWO) plotted in Fig. 5.7b. This state of the circuit is referred to as the design state with a centred response because it satisfies the passband requirements of  $f_0 = 1.53$  GHz and  $FBW = 49\%$ . A  $2^{nd}$  order quasi-Chebyshev response is obtained in the passband with  $L_R > 20$  dB. Note that a lowpass passband occurs at the lower frequencies, that is generally found in such transversal-type filters.

**Table 5.1:** The optimised parameter values of the TEM-circuit in Fig. 5.7a with filter response shown in Fig. 5.7b. The terminal impedance is  $Z_A = 50\Omega$ .

Upper path	Lower path
$\theta_1 = 81^\circ$	$\theta_2 = 212^\circ$
$Z_1 = 48.4\Omega$	$Z_2 = 94.4\Omega$
$C_1 = 7$ pF	$C_2 = 4.9$ pF

The required 20 dB out-of-band rejection from 0.89 to 1.1 GHz and from 2.1 to 2.5 GHz, are not met in this response. The selectivity of the attenuation slopes are also not nearly high enough, with a poor roll-off at the band edges. These specifications are addressed in the design phase of the prototype filters later in this chapter. The focus of the investigation in this subsection, is on the passband characteristics and the tunability thereof.

A key characteristic of this circuit is the dependence of the BW on the line impedances. This is illustrated in Fig. 5.8, where the FBW at  $|s_{21}| = -0.043$  dB ( $FBW_{ripple}$ ) and at

$|s_{21}| = -20$  dB ( $FBW_{20dB}$ ) are plotted respectively against the impedance ratio  $Z_2/Z_1$ . These results are given for various values of  $Z_1$ .

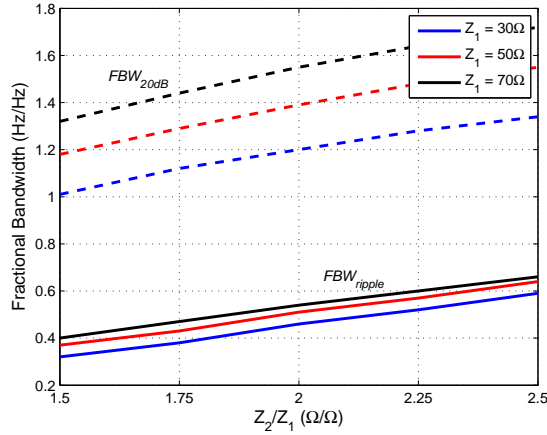


**Figure 5.8:** The FBW at  $|s_{21}| = -0.043$  dB ( $FBW_{ripple}$ ) and at  $|s_{21}| = -20$  dB ( $FBW_{20dB}$ ) are plotted respectively against the impedance ratio  $Z_2/Z_1$ , for different values of  $Z_1$ . Note that the terminal impedances are also changed according to  $Z_1$ , in order to maintain a minimum  $L_R$  of 20 dB in the passband.

The first thing to note here is that for high values of  $Z_2/Z_1$  the BW is increased. The second is that the distance between the  $FBW_{20dB}$  and the  $FBW_{ripple}$  is an indication of the selectivity. Therefore it is clear that for lower values of  $Z_1$  higher selectivity is achieved. However, due to the large difference between the two line impedances (for wide BW), the terminal impedance ( $Z_A$ ) is predominantly dependant on  $Z_1$ . Therefore the data in Fig. 5.8 is generated for different values of  $Z_A$  according to  $Z_1$ , in order to maintain a minimum  $L_R$  of 20 dB in the passband.

The most significant characteristic of this circuit is its tuning capability, illustrated in Fig. 5.9. Here the  $BW$  and  $f_0$  are plotted for different values of  $C_1$  and  $C_2$  respectively. It has to be made clear that  $\theta_1 = 81^\circ$  and  $\theta_2 = 212^\circ$  are determined for 1.53 GHz and does not change as the passband  $f_0$  changes.

Another key point of the data plotted in Fig. 5.9, is that the terminal impedance is also changed as the capacitance values are tuned away from the design values in Table 5.1. This is done in order to compare the passbands with equality, because without a change in  $Z_A$  the return loss deteriorates, leaving no ripple to measure the BW from.

The capacitor range of  $C_1$  is plotted from 3 to 40 pF, because at 4.5 pF the two lower transmission zeros (left of the passband) are at the same position and below this value they start to disappear, with the rejection level reducing significantly. For values greater than 40 pF the series capacitor become a short-circuit, having almost no effect on the passband as seen in Fig. 5.9a.

The capacitor range of  $C_2$  is plotted from 1 to 10 pF, because for smaller values than 1 pF the return loss become smaller than 15 dB. For values greater than 10 pF the lower



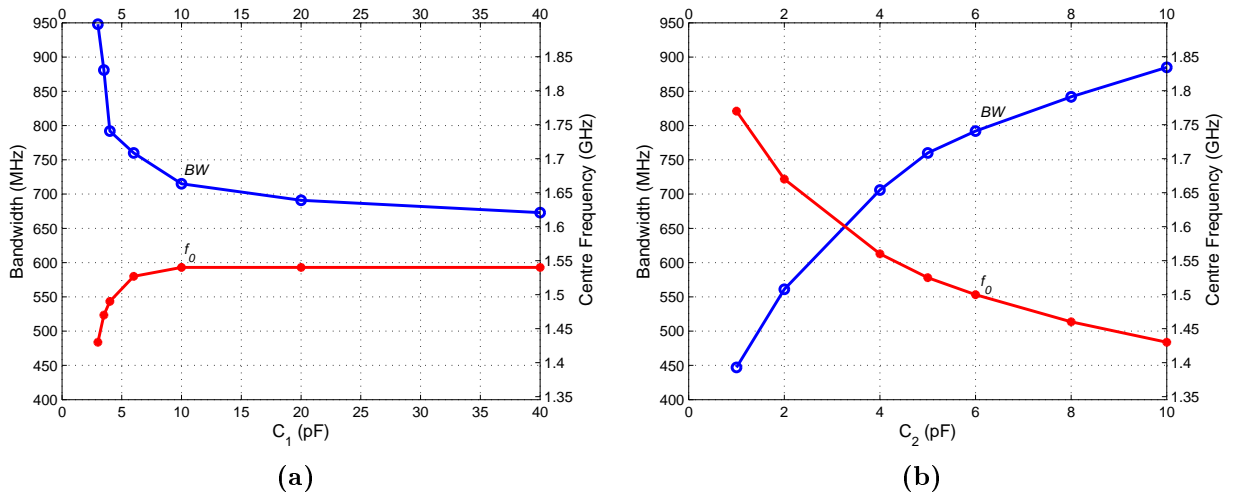


**Figure 5.9:** The tunability of the bandwidth and centre frequency with the (a) series capacitor and the (b) shunt capacitor. The design parameter values of the filtering-section (Fig. 5.7a) are  $\theta_1 = 81^\circ$ ,  $\theta_2 = 212^\circ$ ,  $Z_1 = 48.4\Omega$ ,  $Z_2 = 94.4\Omega$ ,  $C_1 = 7$  pF and  $C_2 = 4.9$  pF.

two transmission zeros disappear again, causing the out-of-band rejection to deteriorate.

It is clear from Fig. 5.9b that the lower cut-off frequency is controllable with  $C_2$ . Therefore as  $C_2$  increases the BW also increase while  $f_0$  shifts lower. However,  $C_1$  does not tune the upper cut-off independently, as expected from the previous subsection's analysis. It is seen in Fig. 5.9a that as  $C_1$  increases the BW decrease and  $f_0$  increase. This is opposite than  $C_2$ , although here  $f_0$  changes very little and therefore it is mainly the BW that is tuned with  $C_1$ .

This may be explained from the previous circuit's results in Fig. 5.6b. It is seen here that as the series capacitor value is changed, the transmission zero next to the lower cut-off move in the opposite direction than the upper pole. This influences the lower cut-off frequency and affectively changes the BW.

Nevertheless, with different combinations of both these capacitors, the  $f_0$  may be tuned for a fixed FBW and vice versa. This is clearly illustrated in Table 5.2, where the tuning results of this optimised circuit is given. Note that the tuning is limited by the capacitance range of  $C_1$ . Here  $\Delta BW = 15.8\%$  is achieved while maintaining  $f_0 = 1.53$  GHz and  $\Delta f_0 = 4.9\%$  (centre frequency deviation<sup>3</sup>) for a fixed  $FBW = 49\%$ .

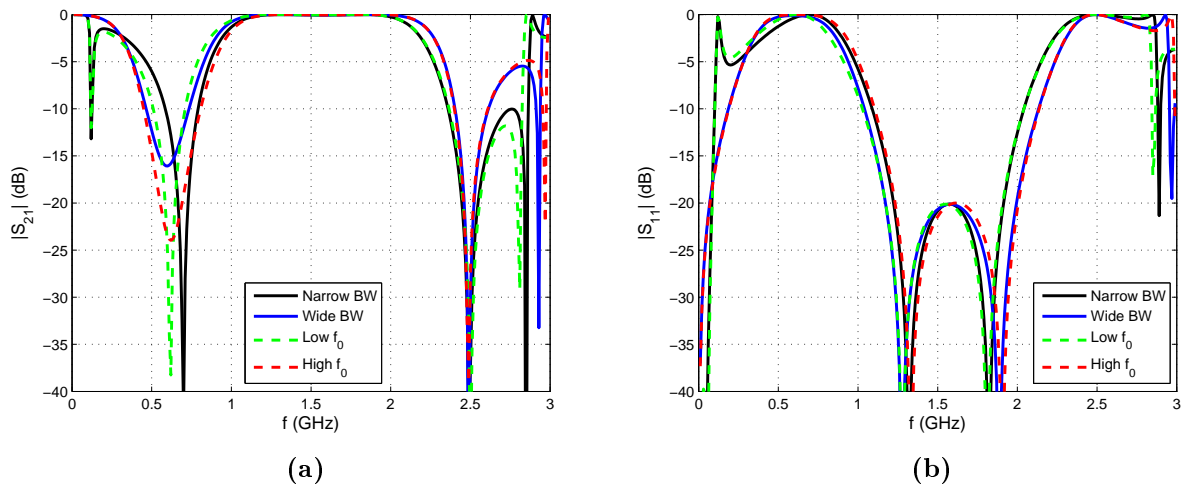
The corresponding filter responses are given in Fig. 5.10. Note that because  $L_R > 20$  dB, the ripple is very small (0.043 dB) and therefore one cannot clearly see  $f_{c1}$  and  $f_{c2}$  from these graphs. What is important to observe is that the lower transmission zero, adjacent to the passband, moves as the capacitors are tuned. The upper transmission zero, however, remains stationary at 2.5 GHz. Therefore as  $C_1$  is tuned the upper attenuation

<sup>3</sup>Note that the centre frequency deviation is calculated in the same manner as  $\Delta BW$ , given as  $\Delta f_0 = \frac{f_0(\text{maximum}) - f_0(\text{minimum})}{f_0(\text{maximum})}$ . This is the difference between the minimum and maximum  $f_0$ , divided by the maximum  $f_0$ .

**Table 5.2:** The tune-all results of the proposed filtering-section, for the design values given in Table 5.1.

Description	$C_1$ (pF)	$C_2$ (pF)	FBW (%)	$f_0$ (GHz)	$Z_A$ ( $\Omega$ )
Narrow BW	40	5.4	45	1.53	57.2
Wide BW	3	3.48	53.5	1.53	41.1
Low $f_0$	40	7.2	49	1.496	55.7
High $f_0$	3	2.95	49	1.573	42.3

slope changes.

**Figure 5.10:** The (a) transmission coefficient and (b) reflection coefficient for different tuned passband states, given in Table 5.2.

Following the design by optimisation of this filtering-section, the behaviour of the circuit in the frequency domain with regard to its parameter values, are summarised in Table 5.3. In the next subsection the circuit is analysed mathematically, in order to obtain a more concrete synthesis.

### 5.3.2 Network analysis of filtering-section

In this subsection the two-port parameters of the lossless filtering-section in Fig. 5.7a, are derived and analysed. The aim is to achieve a more comprehensive understanding of the working of this network, in order to make informed choices for the design of such a filtering-section.

The two-port parameters are derived in a few steps. First the ABCD-parameters of each of the 6 components in Fig. 5.7a are determined. The parameters of the 3 components of each path, upper and lower paths respectively, are cascaded together to obtain new ABCD-parameters. Both of these ABCD matrices are then converted to admittance parameters. The two paths are connected in parallel and therefore results in

**Table 5.3:** The behaviour of a filtering-section with regard to its parameter values. This table serves as guidelines for the optimisation of the filtering response. Note that the numbering of the transmission poles and zeros, respectively increases from the lower to higher frequency positions. Refer to the schematic and filter response in Fig. 5.7.

	Parameter description	Result in frequency response
1	$C_1$	Introduces 1 <sup>st</sup> transmission zero
2	Decrease in $C_1$	Move position of 2 <sup>nd</sup> transmission zero lower
3	Decrease in $C_1$	Move position of 2 <sup>nd</sup> transmission pole higher
4	$C_2$	Introduces 4 <sup>th</sup> transmission zero
5	Increase in $C_2$	Move position of 2 <sup>nd</sup> transmission zero lower
6	Increase in $C_2$	Move position of 1 <sup>st</sup> transmission pole lower
7	$Z_1$	Determines $L_R$ substantially. Passband matched for $\approx Z_A$ .
8	Decrease in $Z_1$	Increase the BW
9	Decrease in $Z_1$	Increase the selectivity
10	Increase in $Z_2$	Increase the BW
11	Both $\theta_1$ and $\theta_2$	Determines passband position ( $f_0$ )
12	$\theta_1$	Determines symmetry in passband

the addition of the two admittance parameter matrices, to obtain the complete network's admittance parameters

$$y_{11} = y_{22} = j \frac{\omega C_1 - 2\omega C_1 \sin^2 \theta_a + \frac{1}{Z_1} \cos \theta_a \sin \theta_a}{\cos \theta_a (\cos \theta_a - 2\omega C_1 Z_1 \sin \theta_a)} + j \frac{1 - 2\sin^2 \theta_b - \omega C_2 Z_2 \cos \theta_b \sin \theta_b}{Z_2 \sin \theta_b (\omega C_2 Z_2 \sin \theta_b - 2\cos \theta_b)} \quad (5.4)$$

and

$$y_{12} = y_{21} = j \frac{1}{\cos \theta_a (2Z_1 \sin \theta_a - \frac{1}{\omega C_1} \cos \theta_a)} - j \frac{1}{Z_2 \sin \theta_b (\omega C_2 Z_2 \sin \theta_b - 2\cos \theta_b)}. \quad (5.5)$$

Note that the parameter substitutions

$$\theta_a = \frac{\theta_1}{2} \quad (5.6)$$

and

$$\theta_b = \frac{\theta_2}{2} \quad (5.7)$$

are made to partially simplify these expressions.

The admittance parameters are converted to transmission and reflection coefficients [10] as

$$s_{11} = \frac{(Y_A - y_{11})(Y_A + y_{22}) + y_{12}y_{21}}{(Y_A + y_{11})(Y_A + y_{22}) - y_{12}y_{21}} \quad (5.8)$$

and

$$s_{21} = \frac{-2Y_A \cdot y_{21}}{(Y_A + y_{11})(Y_A + y_{22}) - y_{12}y_{21}}, \quad (5.9)$$

where  $Y_A$  is the admittance of both ports.

In order to simplify the expressions for  $s_{11}$  and  $s_{21}$ , the admittance parameters first need to be considered. It is clear that equations (5.4) and (5.5) consist of complex trigonometric expressions, which cannot be simplified to a more basic form. Substituting these equations into (5.8) and (5.9) to obtain  $s_{11}$  and  $s_{21}$ , lead to even more complex expressions.

Numerous trigonometric simplifications have been applied to these expressions, but nothing concrete is extractable. The parameter approximations  $\theta_2 = 2\theta_1$  and  $Z_2 = 2Z_1$  have also been applied, without any results. Applying parameter approximations limits the design of the filter characteristics and therefore are undesirable.

The most basic filter characteristic that may be found is a transmission zero location. This is done by setting  $|s_{21}| = 0$  and therefore from (5.9) it is clear that this translates into  $|y_{21}| = 0$ . Following this condition it is noted from (5.5) that at the frequency where the equation

$$\cos\theta_a(2Z_1 \sin\theta_a - \frac{1}{\omega C_1} \cos\theta_a) = Z_2 \sin\theta_b(\omega C_2 Z_2 \sin\theta_b - 2\cos\theta_b) \quad (5.10)$$

holds, a transmission zero may be found. No simplification is found for this expression either.

The two-port parameters of this network consists of very complex trigonometric expressions containing six degrees of freedom. Therefore no simplified mathematical expressions are obtained for this network, where the characteristics of the filter response are expressed in terms of the network parameters. Thus it is concluded that until another approach is discovered, the obvious way forward is to design the network by optimisation, using the knowledge obtained in the preceding investigations.

### 5.3.3 Proposition for a filter prototype for KAT-7

It is clear from the preceding investigations that the proposed filtering-section has much potential for a tune-all wideband filter. However, this network on its own does not meet all the filter specifications, in terms of the passband selectivity and out-of-band rejection (refer to Fig. 5.7).

To overcome this issue, the technique of cascaded sections may be implemented. In [6] this is done with the stub-loaded ring-resonators, where good out-of-band rejection is obtained as discussed in Section 4.4. As the number of cascaded sections increase,

the transmission zeros adjacent to the passband should also increase, yielding improved selectivity.

It is also reported that by cascading through a  $\lambda_g/4$  line with characteristic impedance the same as that of the terminals, higher out-of-band rejection is achieved, but at the expense of lower return loss in the passband [6]. It should be mentioned that because of an increase in the filtering-sections and as a consequence the varactor diodes, the insertion loss of the filter response will also be increased.

Another aspect that needs attention is the terminal impedance. Throughout the preceding investigations of the proposed tunable circuit, the value of  $Z_A$  has been changed (refer to Table 5.2) as the filter response is tuned. This is done to maintain the matching in the passband.

Therefore to preserve the return loss while tuning the filter response, tunable impedance inverters are required at the terminals. This is not desirable because it increases the complexity of the network, adds losses due to extra tunable elements and if implemented with coupled-lines, unwanted radiation will also add to the loss of energy.

The maximum impedance deviation according to Table 5.2, is only 0.82:1. For this instance it is found that when keeping  $Z_A = 50\Omega$ , the return loss deteriorates from 20 to 11.4 dB. It might be possible to improve this to above 15 dB in the design. Therefore it is decided not to implement matching circuits to compensate for this.

The trade-off, however, is that the selectivity of the attenuation slopes cannot be increased by changing  $Z_1$  according to Fig. 5.8. This is because  $Z_A$  is predominantly determined by  $Z_1$ . Nevertheless, as explained, the cascading of these sections should compensate for the selectivity.

In the next sections of this chapter, prototype filters consisting of these cascaded filtering-sections are designed in order to satisfy the KAT-7 specifications given in Table 1.1.

## 5.4 First prototype: 4 cascaded filtering-sections

In this section the first prototype filter is designed. The aim of this filter is to achieve optimal tunability in BW and  $f_0$ , while partially satisfying the KAT-7 specifications.<sup>4</sup>

The cascading of filtering-sections are investigated and design graphs are obtained for the 4 cascaded sections. Prototype circuits are developed and a structured design by optimisation are proposed for this filter type.

---

<sup>4</sup>The partial achievement of the specifications is due to trade-offs between optimal tunability and the attenuation slope selectivity.

### 5.4.1 Cascaded filtering-sections

The aim of cascading the filtering-sections is to increase the out-of-band rejection as well as the selectivity of attenuation slopes. As mentioned in the previous section, a  $\lambda_g/4$  line with characteristic impedance the same as the terminals, may be used to cascade these sections together. According to the results of the design in [6] this increases the out-of-band rejection.

#### Cascaded sections with $\lambda_g/4$ lines

In Fig. 5.11a the schematic of such a cascaded network is shown. The parameter values of the single section in Table 5.1, are used as a point of departure for the optimisation of the cascaded network.

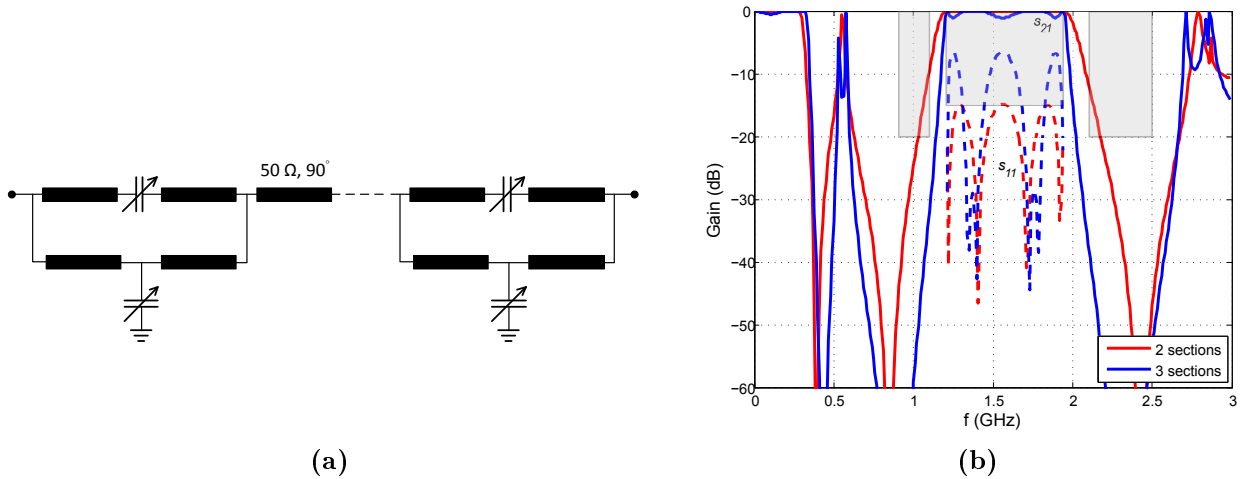


**Figure 5.11:** (a) The schematic of a TEM-circuit of filtering-sections cascaded with lines of  $Z_0 = 50\ \Omega$  and  $\theta_0 = 90^\circ$ . (b) The filter responses of the networks consisting of 2 and 3 cascaded sections with parameter values given in Table 5.4. The gray regions indicate the areas not adhering to the filter specifications. Note that  $s_{11}$  (dashed line) is only plotted in the passband.

The reason why the parameter values need to be optimised is due to mismatching. The input impedance at a terminal is not a constant  $50\ \Omega$  across the passband, for an optimised single section with the other terminal loaded with  $50\ \Omega$ . Therefore when connecting these sections in cascade (directly or through a line), the input impedance changes again. In order to achieve a type of equal-ripple transmission coefficient in the passband, the parameter values for the cascaded network need to be optimised. It has to be mentioned that the optimisations in the following investigations are done for various filtering characteristics. However, the one goal that remains the same throughout the investigations is the equal-ripple passband.

The response of the cascaded network in Fig. 5.11a with the parameter values of the single section network, has a much wider BW. Bear in mind that the guidelines for

optimisation in Table 5.3 are also applicable for the cascaded networks. Therefore the first parameter that is optimised is  $Z_2$ . The centre frequency of the passband is higher than required and thus the line lengths ( $\theta_1$  and  $\theta_2$ ) are increased. The final step is to obtain an equal-ripple passband with the best return loss, by changing  $Z_1$ .

These optimisation steps apply to any arbitrary number of sections cascaded with  $\lambda_g/4$  lines, given that the initial values in Table 5.1 are used. The optimised parameter values for the networks consisting respectively of 2 and 3 cascaded sections, are given in Table 5.4 with the corresponding responses shown in Fig. 5.11b.

**Table 5.4:** The optimised parameter values for the networks consisting respectively of 2 and 3 cascaded sections (Fig. 5.11a), with corresponding responses shown in Fig. 5.11b.

Parameter	Two sections	Three sections
$\theta_1$	$95^\circ$	$96^\circ$
$\theta_2$	$216.5^\circ$	$223^\circ$
$Z_1$	$42.5\Omega$	$37.3\Omega$
$Z_2$	$55.5\Omega$	$44.4\Omega$
$C_1$	$7pF$	$7pF$
$C_2$	$4.9pF$	$4.9pF$

The first thing to note is that the selectivity of the 3 section network is much higher, though at the expense of the return loss. It is expected that as the number of sections increase the return loss decreases. This is because each section has reflections on its own and thus by cascading the sections, all the reflections are accumulated resulting in poor return loss.

Note that the 2 section network has a 4<sup>th</sup> order equal-ripple passband, while the 3 sections has a 6<sup>th</sup> order type of equal-ripple passband. Therefore each added section introduces 2 more poles to the passband. For both networks the out-of-band rejection is much better as expected, than that of the single section's response in Fig. 5.7b.

The selectivity of the 2 section network is not as high as desired, i.e.  $|s_{21}| \leq -20dB$  at 1.1 and 2.1 GHz. The 3 section network has very high selectivity, but the return loss is only 6.6 dB oppose to the former network that is 14.8 dB. Therefore the 2 section network is much more applicable for a prototype filter.

### Direct cascaded sections

Another way to implement cascaded sections is by directly connecting the section terminals, as shown in Fig. 5.12a. The single section's parameter values given in Table 5.1 are used again for the initial values of the optimisation.

It is found with these values that the first transmission zero is too close to the second zero. This introduces an unwanted pole on the lower attenuation slope of the passband.

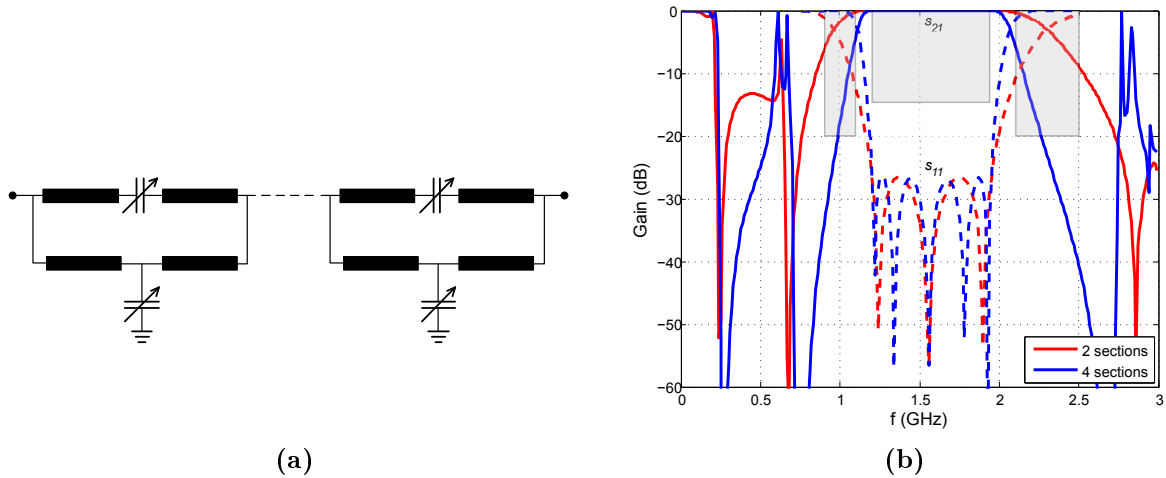


**Figure 5.12:** (a) The schematic of a TEM-circuit of direct cascaded filtering-sections. (b) The filter responses of the networks consisting of 2 and 4 cascaded sections with parameter values given in Table 5.5. The gray regions indicate the areas not adhering to the filter specifications. Note that  $s_{11}$  (dashed line) is only plotted at the passband frequencies.

Therefore to move the first transmission zero to lower frequencies,  $C_1$  is increased. The next step is to obtain a symmetrical passband by changing the length of  $\theta_1$ .

The centre frequency of the passband is lower than required and thus the line lengths ( $\theta_1$  and  $\theta_2$ ) are decreased. After this the BW is increased by increasing  $Z_2$ . The final step is to obtain an equal-ripple passband with the best return loss, by changing  $Z_1$ .

The optimised parameter values for the networks consisting respectively of 2 and 4 cascaded sections, are given in Table 5.5 with the corresponding responses shown in Fig. 5.12b. The 3 cascaded sections are not given because it seems like no acceptable response may be obtained for an equal-ripple passband. The reason is that the return loss is more than 40 dB in the passband for symmetry, which yields a very small ripple. Therefore the 3 dB BW must be very wide in order to obtain the correct ripple BW. This causes the transmission zeros to disappear and gives an unwanted response.

**Table 5.5:** The optimised parameter values for the networks consisting respectively of 2 and 4 cascaded sections (Fig. 5.12a), with corresponding responses shown in Fig. 5.12b.

Parameter	Two sections	Four sections
$\theta_1$	$95.5^\circ$	$94.7^\circ$
$\theta_2$	$192^\circ$	$201^\circ$
$Z_1$	$46.9\Omega$	$46.4\Omega$
$Z_2$	$115\Omega$	$89\Omega$
$C_1$	$10pF$	$10pF$
$C_2$	$4.9pF$	$4.9pF$

The reason why the 2 section network is included, is because it only has 3 reflection zeros and therefore is straight forward to obtain a lower return loss (with  $Z_1$  and  $Z_2$ ) for



an equal-ripple passband. Note from the responses in Fig. 5.12b that the return loss is optimised to be the same as the 4 section network, i.e. 27 dB.

It is interesting to note that for direct cascading, each added section increases the order of the filter response only by 1. From the results it is evident that the selectivity increases as the number of sections increase, but again at the cost of the return loss. Therefore the 4 section network is more desirable than the 2 sections, although it does not entirely satisfy all the filter specifications.

The large return loss of the 4 section network is beneficial for the tuning of the filter response, given that the terminal impedance remain unchanged. E.g. when tuning for the passband state with the worst mismatch<sup>5</sup>, i.e. for wide BW according to Table 5.2, the return loss deteriorates substantially. According to the filter specifications this should not be less than 15 dB. For these filter networks, it seems as if the return loss will determine the limits of the passband tunability.

Therefore, to compare the tunability of the 4 section network (Fig. 5.12a) with that of the 2 sections cascaded with a  $\lambda_g/4$  line (Fig. 5.11a), the BWs are tuned to 54% with fixed  $f_0 = 1.53$  GHz. To be fair in the results, the capacitance of  $C_1$  in the latter network is changed to be the same as the former network, which is 10 pF. The network is then optimised again for the correct centred response.

The tuning results of the two networks are plotted in Fig. 5.13. Note that the BW is measured according to the level of the ripple of the designed response. It is clear from the graph that the former network has a minimum return loss of 15.2 dB while the latter has a mere 5 dB. Therefore it is safe to conclude that for good tunability, the 4 section network (Fig. 5.12a) is more satisfactory than the 2 sections cascaded with a  $\lambda_g/4$  line (Fig. 5.11a).

It is clear that there exists a trade-off between the selectivity and tunability in these filtering networks. Therefore the aim of the first prototype filter is to achieve good tunability within the passband requirements. For this design the 4 section network (Fig. 5.12a) is chosen and developed in the next subsection.

The reason why a network consisting of 5 direct cascaded sections is not considered for this prototype, is because although the selectivity is higher, the return loss will consequently be lower and therefore result in poor tunability. Although the centred response of the proposed 4 cascaded sections does not have very high selectivity, it may be increased by choosing different design values for the capacitors. This is illustrated in the design graphs obtained in the next subsection.

---

<sup>5</sup>This is the state of the passband where either wide BW, low BW, high  $f_0$  or low  $f_0$  is tuned. For any of these states the terminals are mismatched and therefore the return loss deteriorates.

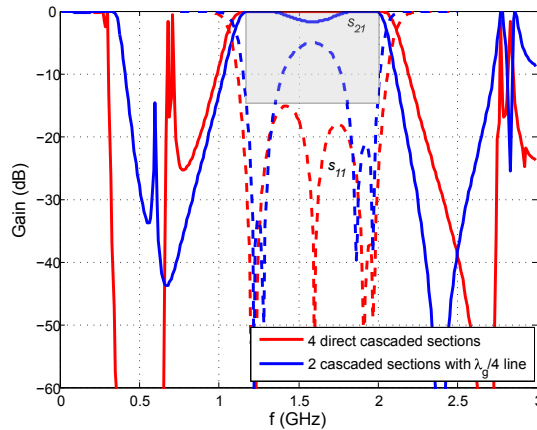


**Figure 5.13:** The tuned wideband responses of the networks consisting respectively of 4 direct cascaded sections (Fig. 5.12a) and 2 sections cascaded with a  $\lambda_g/4$  line (Fig. 5.11a). The former network is tuned here with  $C_1 = 5.5$  pF and  $C_2 = 5.7$  pF, while the latter is tuned with  $C_1 = 4.6$  pF and  $C_2 = 5.85$  pF. The gray region indicate the return loss specification.

## 5.4.2 Design of prototype circuit

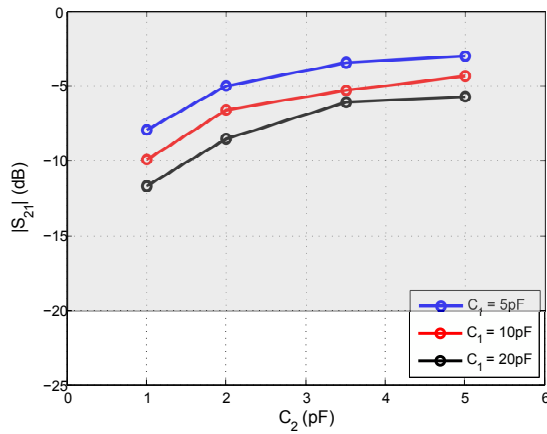
The first prototype filter that is designed for KAT-7 consists of 4 filtering-sections (Fig 5.7a) cascaded together to form a single network. In this subsection a prototype circuit, consisting of TEM-lines and ideal capacitors, is developed for the filter. All the results of the circuit are obtained with MWO.

The capacitor values that have been used up to this point, were chosen in the development phase of the single filtering-section. By changing these design values for the cascaded circuit, more versatility is found with the filter response. This is illustrated with the design graphs given in Fig. 5.14.

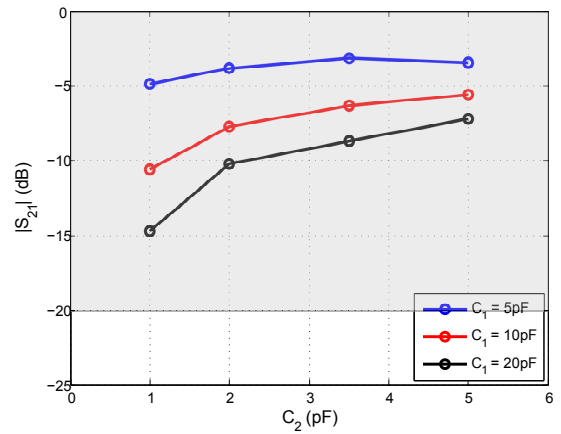
Here the network is optimised for the different capacitor values according to the pass-band requirements. The first four graphs indicate the out-of-band characteristics while the fifth graph the physical realisability. The capacitor range for  $C_2$  are chosen according to the results of reasonable filter responses. The upper limit is chosen because of the increasingly poor selectivity for larger capacitor values. The lower limit is chosen in order to obtain realistic values for  $Z_2$ . Note that optimal tunability with  $C_1$  is achieved when the design capacitance is between 8 to 10 pF. The graphs for  $C_1 = 5$  pF and 20 pF are only given to illustrate its influence on the filter characteristics.

Fig. 5.14a shows the measured  $|s_{21}|$  at 1.1 GHz, which indicates the selectivity of the lower attenuation slope. In similar manner is the upper slope at 2.1 GHz given in Fig. 5.14b. It is clear from these graphs that the selectivity of the 4 section network may be increased from its previous response shown in Fig. 5.12b, though all the filter specifications are not met for any of these capacitor values. Note that the gray regions on these graphs indicate the areas where the filter specifications are not met. Therefore

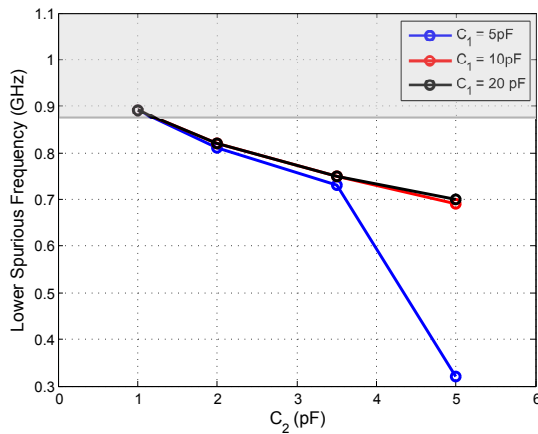
it is clear that  $C_1$  should be as large as possible, while  $C_2$  is as small as possible.



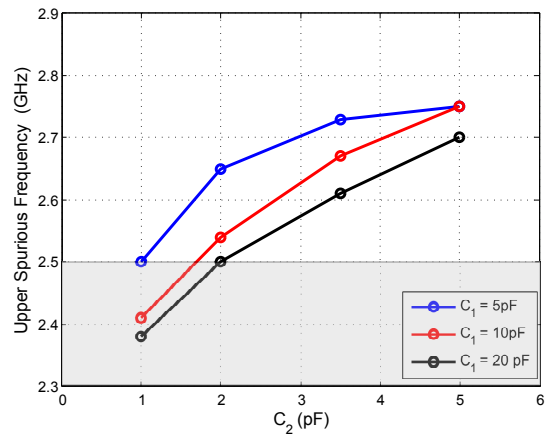
(a) Selectivity of lower attenuation slope at  $f = 1.1$  GHz



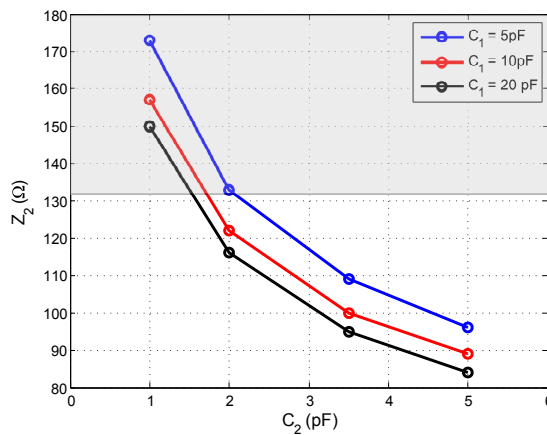
(b) Selectivity of upper attenuation slope at  $f = 2.1$  GHz



(c) Frequency where lower spurious passband starts, for  $|s_{21}| \geq -20$  dB



(d) Frequency where upper spurious passband starts, for  $|s_{21}| \geq -20$  dB



(e) Characteristic impedance of second line

**Figure 5.14:** The design graphs of different capacitor values for a filter network consisting of 4 cascaded sections. The TEM-network is optimised in each case for the correct passband specifications. The gray regions indicate the areas not adhering to the filter specifications.

Fig. 5.14c shows the frequency where the lower spurious response starts, for  $|s_{21}| \geq -20$  dB. Therefore the frequency samples are taken at  $|s_{21}| = -20$  dB. The lower spurious passband may not be closer to the designed passband, specified by  $f \leq 0.89$  GHz. The same concept applies to the upper spurious passband but for  $f \geq 2.5$  GHz, as shown in Fig. 5.14d.

For most of the capacitor values in Fig. 5.14c, the lower frequency specifications are met. Note that the sudden drop in frequency at  $C_1 = 5$  pF and  $C_2 = 5$  pF, is due to suppression of the lower spurious passband and therefore only a lowpass passband exists for  $f \leq 0.32$  GHz (refer to Fig. 5.12b). It is clear from both these graphs that the upper spurious passband is the most volatile of the two. Therefore to adhere to the specifications it is required that  $C_2 > 1.7$  pF for  $C_1 \leq 10$  pF.

The final graph (Fig. 5.14e) shows the impedance  $Z_2$  for different capacitor values. The purpose of this graph is to consider the realisability of this line width in microstrip. Bear in mind that the other line impedance  $Z_1$  is around  $50\Omega$  for passband matching. Therefore,  $Z_2$  cannot be too large because depending on the choice of substrate, either the one line will be too thick or other line too thin.

The first concern for the physical line width is the transition from the microstrip line to the relevant component package, such as from the shorter line ( $Z_1$ ) to the varactor diode ( $C_1$ ). The width of the pin of a typical surface mount varactor is around 0.3 mm. The width of the line should be as close as possible to this. However, if the shorter line has a width of 0.3 mm the longer line ( $Z_2$ ) will become unreasonably thin.

The second concern is the fabrication requirements. A rule of thumb is that the line width should not be smaller than 0.1 mm. Therefore based on the applicable line impedances the RO4003C substrate from Rogers is chosen, with characteristics given in Table 5.6. For a  $50\Omega$  line at  $f_0$  on this substrate the line width is 1.14 mm. The 0.1 mm limit yields a upper limit of  $132\Omega$  for the line impedances.

**Table 5.6:** Characteristics of the RO4003C substrate from Rogers.

Description	Value
Dielectric constant	3.38
Dissipation factor	0.0027
Dielectric thickness	0.508 mm
Copper thickness	34 $\mu\text{m}$

In Fig. 5.14e this limit is indicated by the gray region. Note that the line impedance become very large as the value of  $C_2$  is reduced. Thus to keep to the fabrication limit, it is required that  $C_2 > 1.7$  pF for  $C_1 \leq 10$  pF.

As mentioned before the capacitance value for  $C_1$  should be between 8 to 10 pF for optimal tuning. For maximum selectivity this value should be as high as possible and therefore  $C_1 = 10$  pF is chosen. According to the graphs of both the out-of-band rejection

and realisability, it is required that  $C_2 > 1.7$  pF for  $C_1 = 10$  pF. However, for maximum selectivity  $C_2$  should be as low as possible. In order to leave room for the parasitic affects of the circuit implementation,  $C_2 = 2$  pF is therefore chosen.

It has to be mentioned that for all these different capacitor values, the optimised responses yield more or less the same return loss. This is seen in the final optimised response shown in Fig. 5.15 where  $L_R = 26$  dB. The parameter values are given in Table 5.7. The selectivity at 1.1 GHz and 2.1 GHz is found to be  $|s_{21}| = -7$  dB and  $|s_{21}| = -7.6$  dB respectively. Note that the spurious responses are clear of the specifications indicated by the gray regions on either side of the passband.

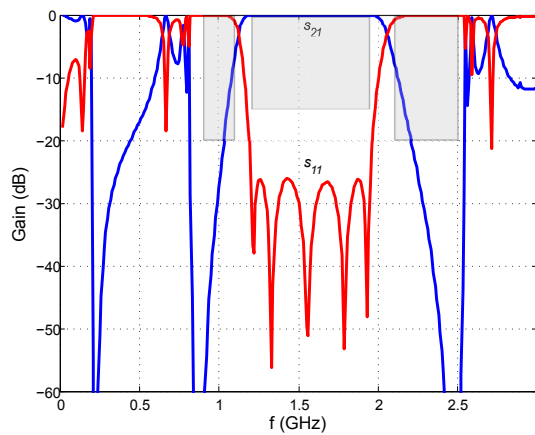


**Figure 5.15:** The filter response of the 4 section prototype circuit with the optimised parameter values given in Table 5.7.

**Table 5.7:** The optimised parameter values of the 4 section prototype circuit with filter response shown in Fig. 5.15. The terminal impedance is  $Z_A = 50\Omega$ .

Path 1	Path 2
$\theta_1 = 94.8^\circ$	$\theta_2 = 216.8^\circ$
$Z_1 = 45.4\Omega$	$Z_2 = 121.5\Omega$
$C_1 = 10$ pF	$C_2 = 2$ pF

The tunability of this circuit is illustrated in Fig. 5.16 where the four different pass-band states are given. The tuning results are summarised in Table 5.8. Each state is tuned in order to adhere to the minimum return loss specification. The tunability of the prototype circuit is determined as  $\Delta BW = 16.7\%$  while maintaining  $f_0 = 1.53$  GHz and  $\Delta f_0 = 5.5\%$  for a fixed  $FBW = 49\%$ . Again the passband is measured according to the ripple level of the centred response. These tuning results are even better than that of the single section summarised in Table 5.2, however, the return loss is lower.

From these results it is clear that the capacitor range for  $C_1$  is from 4.9 to 40 pF and for  $C_2$  it is from 1.64 to 2.27 pF. Note that the upper limit for  $C_1$  is not due to the return loss specification, but rather because beyond this value the capacitor has no more

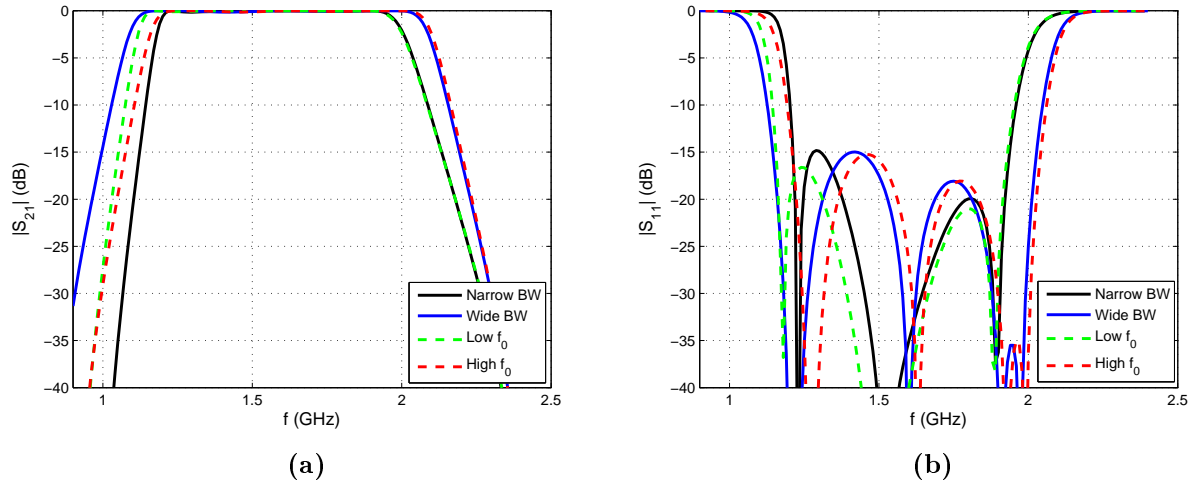


**Figure 5.16:** The (a) transmission coefficient and (b) reflection coefficient for different tuned passband states, given in Table 5.8.

**Table 5.8:** The tune-all results of the 4 section prototype circuit for the design values given in Table 5.7.

Description	$C_1$ (pF)	$C_2$ (pF)	FBW (%)	$f_0$ (GHz)	$L_R$ (dB)
Narrow BW	30	1.64	44.6	1.53	14.9
Wide BW	5.6	2.27	53.6	1.53	15.0
Low $f_0$	40	2.18	49	1.491	16.6
High $f_0$	4.9	1.68	49	1.579	15.3

significant influence on the passband. Also note the large capacitance ratio of  $C_1$ , i.e. 8.16. These values are used for the choices of the varactor diodes.

### 5.4.3 Biasing network

The implementation of the biasing network (of the varactor diodes) in this filter network is not a trivial exercise. There are two different varactors in the circuit that has to be biased independently, which poses careful consideration. Another aspect to consider is the fact that the one varactor is connected in series in the circuit.

In the design of the tunable combline filter in Chapter 3, the DC blocks are implemented with capacitors ( $C_b$ ), while the RF chokes are implemented with resistors ( $R_c$ ). In this subsection the same approach is followed, but for generic circuit layouts (i.e. no component values are specified).

To simplify the problem  $C_1$  and  $C_2$  must both have the “same” ground. In other words the filtering network is grounded at DC to form a reference for both varactors. This is illustrated in Fig. 5.17 with the resistors ( $R_c$ ) connected from the signal paths to ground. Here two possible implementations are given for the biasing networks in the prototype circuit.

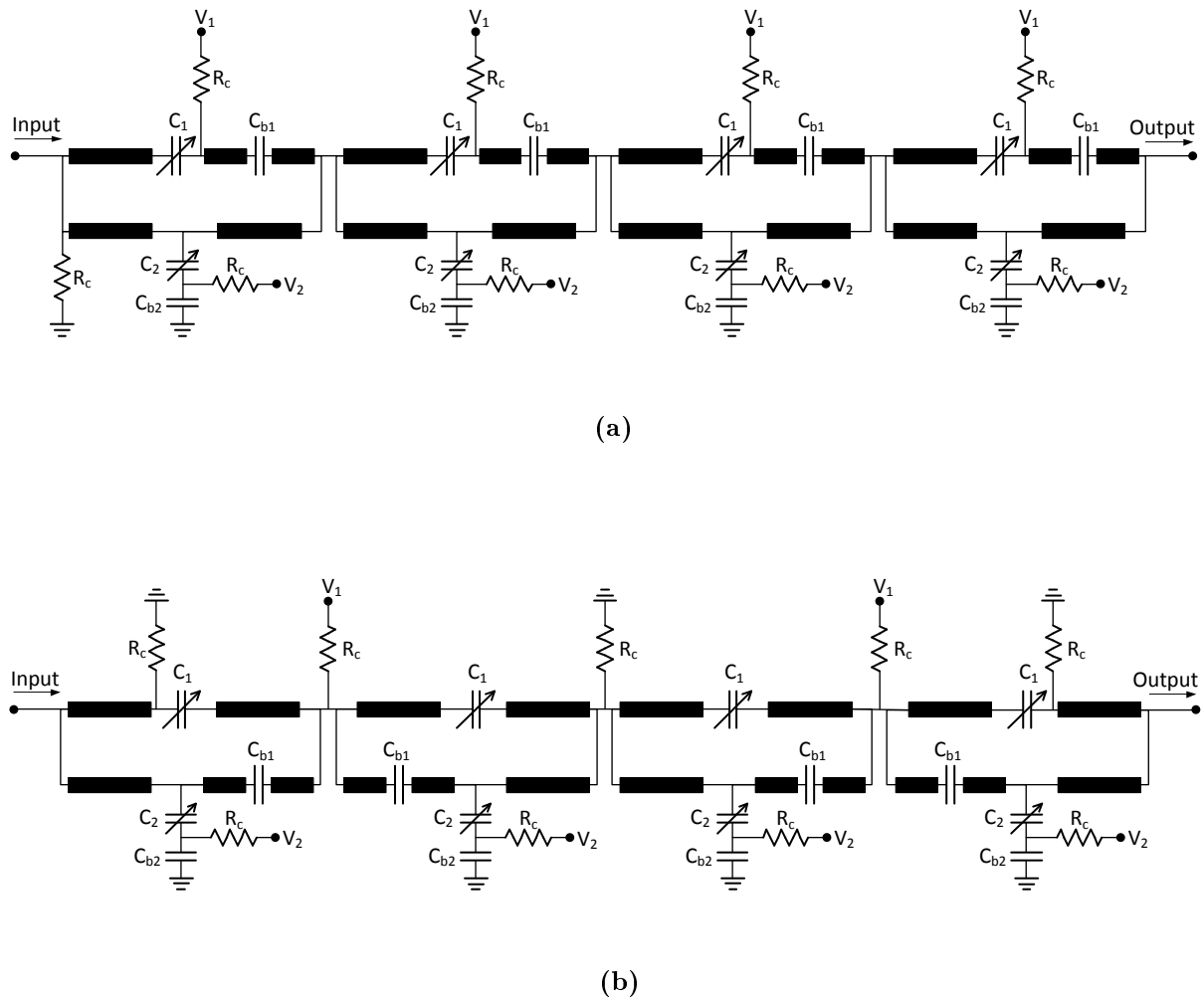


**Figure 5.17:** Possible implementations of biasing networks in the prototype circuit.

It has to be mentioned that the TEM-lines in Fig. 5.17, all correspond to the lines indicated in the single section network in Fig. 5.7a. The main difference between these circuits (Fig. 5.17) is the position of the DC block  $C_{b1}$ . In the first circuit (Fig. 5.17a) the series varactors ( $C_1$ ) each has its own DC voltage terminal. However, in the second circuit (Fig. 5.17b) they are biased in pairs. Note that the voltage applied to each series varactor, in both circuits, is the same and indicated with  $V_1$ .

A DC voltage ( $V_2$ ) is applied to the shunt varactors ( $C_2$ ) in both circuits, at the node where the varactor is grounded at RF through the DC block  $C_{b2}$ . Note that all the voltage terminals are isolated from the RF signals with resistors.

In order to make a decision between these two possible circuits, supposing that the RF chokes operate correctly, a few aspects of  $C_{b1}$  should be considered. That is the position of the capacitor on the TEM-line, both the series and parallel parasitic inductances caused by the capacitor's physical size, the capacitor's influence on the return loss and the influence of the component losses on the filter's insertion loss.

After extensive investigations it is clear that the second circuit layout is the most desirable for this filter design. The two overall motivations for this choice, are the return loss that is higher than that of the first circuit and the introduction of a transmission zero at DC, caused by the position of  $C_{b1}$ . The position best fit for  $C_{b1}$  on the lower path of the section, is at the node where the adjacent section is connected.

In the next subsections the components for this circuit are chosen and implemented in a microstrip layout.

#### 5.4.4 Components for filter network

The losses of the components, more specifically that of the varactor diodes, have a significant influence on the passband insertion loss and causes roll-off at the band edges, as explained in Section 2.6. The KAT-7 filter specifications, however, requires a flat passband. The varactors have different influences at different frequencies and therefore the passband flatness is easily altered.

This is illustrated in Fig. 5.18 where different resistors, denoted by  $R_{s1}$  and  $R_{s2}$ , are implemented in series with the capacitors  $C_1$  and  $C_2$ , respectively. Note that the results are obtained from the optimised TEM-circuit without the biasing network.

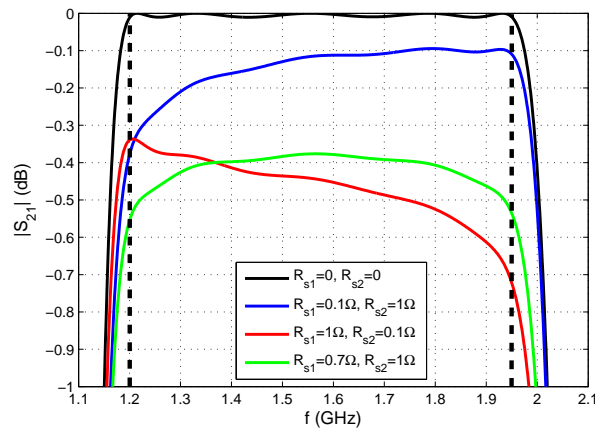


**Figure 5.18:** The insertion loss of the 4 section TEM-circuit for different resistors, denoted by  $R_{s1}$  and  $R_{s2}$ , that are connected in series with the capacitors  $C_1$  and  $C_2$ , respectively. The dashed lines indicate the two cut-off frequencies.

It is clear from the graph that the losses of  $C_1$  has a direct affect on the upper passband frequencies, while  $C_2$  on the lower frequencies. This is expected following the analysis of the single filtering-section. It is also found that in order to maintain a flat passband, the ratio between the series resistors must be  $R_{s1}/R_{s2} \approx 0.7$ .

The varactor diodes are chosen according to the capacitor values found in Subsection 5.4.2, i.e.  $C_1$  ranges from 4.9 to 40 pF and  $C_2$  from 1.64 to 2.27 pF. There are two main aspects to consider, namely the varactor's Q-factor and parasitic inductances.



The first aspect has been established with the specified ratio between the series resistors (i.e.  $R_{s1}/R_{s2} \approx 0.7$ ), although it is desirable to use as high as possible Q-factor varactor diodes. Note that the insertion loss illustrated in Fig. 5.18 will increase considerably when the substrate losses are introduced along with the lossy components of the biasing network.

The filter network is quite sensitive to the components and therefore to accurately model the circuit, Spice models or parasitic models of the varactors are required. The manufacturers Infineon, NXP and Skyworks give satisfactory information concerning the parasitics.

Note that the required range for  $C_2$  is within the capacitance range of the BBY52-02W varactor from Infineon (i.e. 1.1 to 2.45 pF), used in the design of the tunable combline filter (Chapter 3). The package SCD80 is very small and therefore the parasitic inductances are low. The series resistance in the L-band is around  $1\Omega$ , which is an acceptable value. Therefore this is the correct component for the design.

According to the required resistance ratio, the corresponding series resistance of  $C_1$  should be  $0.7\Omega$ . The BB198 varactor from NXP is therefore chosen with capacitance range from 5 to 52 pF. The reason for this choice is not only because of the  $0.7\Omega$  parasitic resistance, but also because this varactor has the same small package as the BBY52-02W.

Following the investigations of the implementation of the biasing network (see Fig. 5.17b), it is decided to make the DC blocks  $C_{b1}$  and  $C_{b2}$  the same. The capacitance should ideally be as high as possible in order not to affect the filter response and tunability. However, due to the package's inductive parasitics, an increase in capacitance decreases the component's SRF. After various trials it is concluded that 20 pF is a reasonable value for the design. Therefore the 20 pF capacitor with 0603 footprint from Dilabs is chosen. Measured s-parameters for this component are also provided by the manufacturer.

With the help of circuit simulations it is found that a  $100\text{ k}\Omega$  resistor (for the RF chokes) gives satisfactory isolation between the DC and RF circuitry. All the components are chosen and therefore the next step is to implement the circuit in microstrip.

### 5.4.5 Implementation of filter network

The general notion is to implement the complete filter network (Fig. 5.17b) directly in a microstrip structure. However, there are various parasitic effects of such a passive structure that will influence the filter characteristics significantly and thus requires optimisation.

A new complete circuit is developed in MWO with various microstrip elements as shown in Fig. 5.19. This circuit is developed in order to reduce the simulation time for the optimisation phases. The idea is that after optimisation of the microstrip circuit, it may be implemented directly in a complete microstrip structure. Note that the microstrip

elements in the circuit are calculated with equations developed by MWO, therefore avoiding full EM simulations.

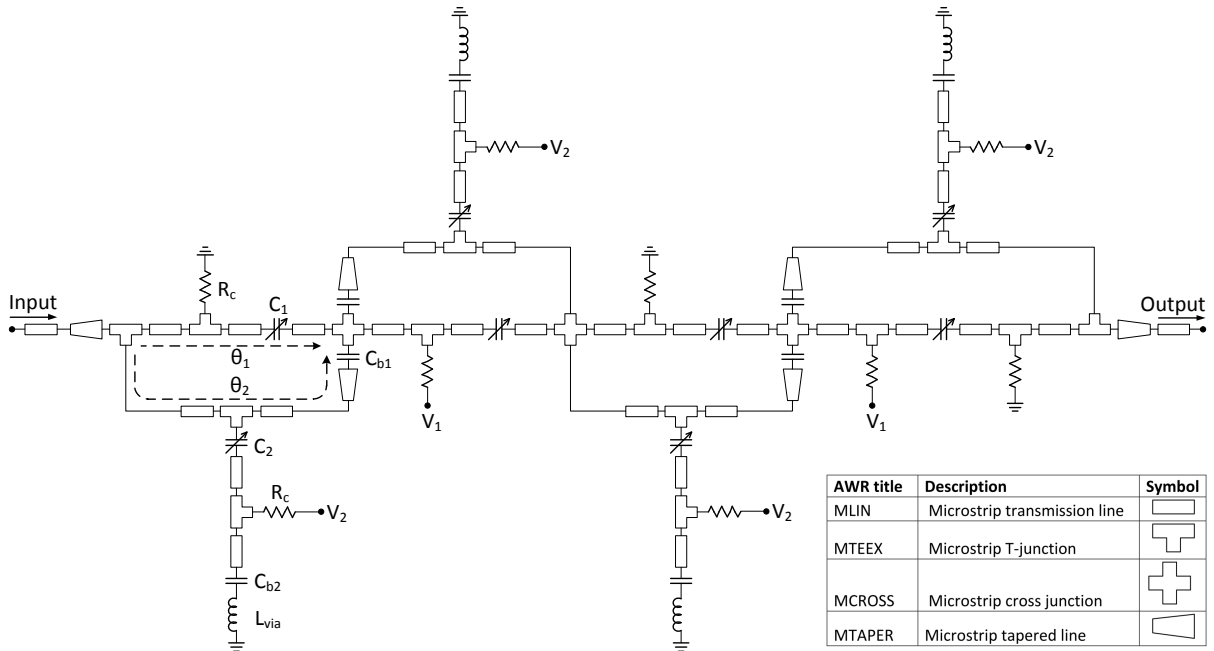


**Figure 5.19:** The complete circuit layout of the first prototype filter with microstrip elements in MWO. The parameters in the first section, closest to the input terminal, are repeated in each of the three sections to the right. The microstrip elements are specified in the table at the bottom right.

The parameters in the first section of the circuit in Fig. 5.19, closest to the input terminal, are repeated in the remaining three sections to the right. The inductor indicated by  $L_{via}$  represents the inductance of the corresponding via. Note that there is an extra RF choke in the last section at the output terminal, in order to ground the signal path at DC.

The microstrip elements with their corresponding symbols are specified in the table at the bottom right of Fig. 5.19. The transmission lines correspond to the lines set out in the simplified TEM-circuit. Note that a short line is added between  $C_2$  and  $C_{b2}$  to realise a physical node for the components. The microstrip junctions are of great importance due to the signal transitions between various characteristic impedance paths. Note that the center line corresponding to the parameter  $\theta_1$ , does not necessarily have the same impedance as the terminals. Therefore short tapered lines are introduced at the terminals for smooth signal transition. Short tapered lines are also used between the longer lines ( $\theta_2$ ) and the DC blocks  $C_{b1}$ , due to the significant change in their physical widths.

In order to obtain a complete microstrip circuit as shown in Fig. 5.19, the simple TEM-circuit without the biasing network is transformed in various steps given below. Note that

in each step new elements are added to the circuit and optimised for the required filter characteristics.

1. Start with the TEM-circuit (refer to Fig. 5.12b) and convert the TEM-lines to microstrip lines on the RO4003C substrate (with characteristics given in Table 5.6). The initial dimensions are calculated with the TXLine calculator of MWO and given in Table 5.9.
2. Introduce the varactor losses ( $R_{s1} = 0.7\Omega$  and  $R_{s2} = 1\Omega$ ) along with the ideal DC blocks  $C_{b1} = C_{b2} = 20$  pF.
3. Introduce the small tapered line between the second path and  $C_{b1}$ . The width of the capacitor is  $w_{b1} = 0.8$  mm.
4. Introduce the node line between  $C_2$  and  $C_{b2}$  along with the via inductance  $L_{via}$ . The via diameter is chosen as 0.5 mm. For a substrate thickness of 0.508 mm, the inductance of the via is calculated as 0.11 nH with equations given in [44] for round wire inductors.
5. Introduce all the T-junctions along with the RF chokes ( $R_c = 100k\Omega$ ).
6. Introduce the cross junctions.
7. Introduce both feeds consisting of a taper and a normal transmission line.
8. Include the s-parameters for  $C_{b1}$  and  $C_{b2}$ .
9. Include the complete model for  $C_2$  (BBY52-02W). This consist of the package parasitics shown in Fig. 3.8, the series resistance ( $R_{s1}$ ) and the actual chip capacitance.
10. Include the complete model for  $C_1$  (BB198). This consist of the same package parasitics as  $C_2$ , the series resistance ( $R_{s2}$ ) and the actual chip capacitance.

**Table 5.9:** The corresponding microstrip dimensions of the parameters of the 4 section TEM-circuit given in Table 5.7. The terminal impedance of  $Z_A = 50\Omega$  has a line width  $w_A = 1.14$  mm. Note that these are calculated for the RO4003C substrate.

Description	Path 1	Path 2
Line length	$l_1 = 31.5$ mm	$l_2 = 77.8$ mm
Line width	$w_1 = 1.33$ mm	$w_2 = 0.14$ mm
Design capacitance	$C_1 = 10$ pF	$C_2 = 2$ pF

Due to losses from the various components, substrate and copper, no passband ripple exists with the insertion loss being 0.77 dB. Therefore a new measure for the BW is required, namely the variation in the insertion loss denoted by  $\Delta L_A$ . According to the filter

specifications this must be smaller than 1 dB. For this design it is chosen as  $\Delta L_A = 0.7$  dB, which is the smallest it may be in order to have optimal BW tuning within the realisable parameter boundaries (i.e.  $w_2 > 0.1$  mm).

The optimised circuit is implemented in a microstrip structure, with layout shown in Fig. 5.20, and a full wave EM simulation including all the component models is done in Sonnet. Note that the DC voltage terminals are grounded with vias in this simulation, in order to decrease the number of mesh cells leading to faster computation. The dimensions of the mesh cells in Sonnet are chosen as  $0.05 \times 0.05$  mm<sup>2</sup> for high accuracy and therefore the structure dimensions are multiples of 0.05 mm. The final dimensions of the structure are given in Table. 5.10.

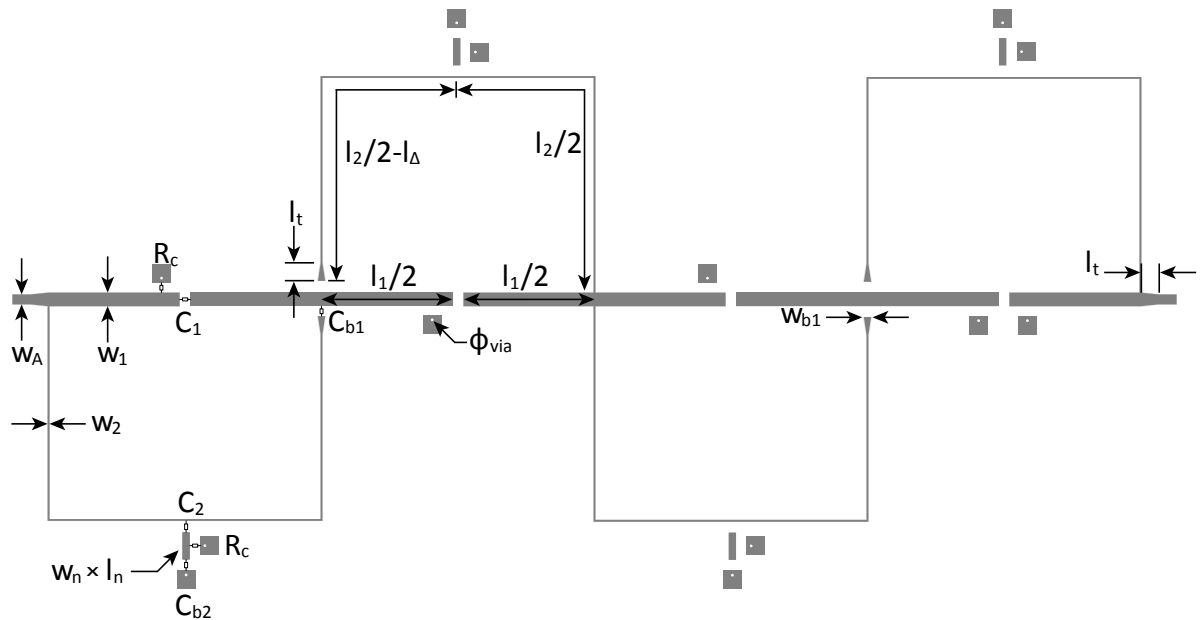


**Figure 5.20:** The layout of the 4 section microstrip structure with all the dimension parameters.

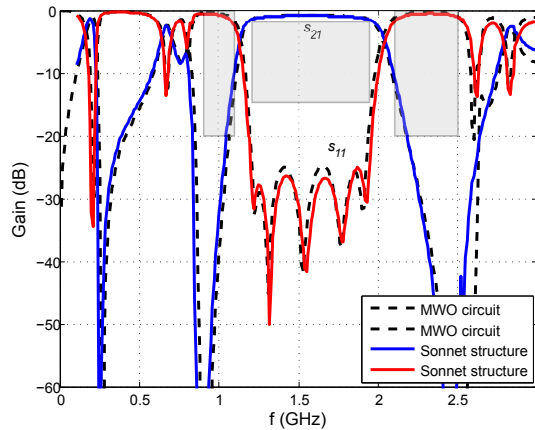
Note that the length of the line ( $l_2/2 - l_\Delta$ ) where  $C_{b1}$  is mounted on, is smaller than  $l_2/2$ . This is due to the influence of the DC block. The compensation parameter  $l_\Delta$  is the only dimension that is different in the microstrip structure, to that of the corresponding MWO circuit model that is 2 mm. The design capacitance values are also slightly changed in order to obtain the correct filter response. The new values at the centred response are  $C_1 = 11$  pF and  $C_2 = 1.92$  pF.

The results of both the microstrip circuit and EM simulation are given in Fig. 5.21. The filter responses have very good agreement. Therefore this optimisation approach, i.e. first optimising a circuit and then implementing the obtained values in a physical structure, proves to be the best implementation approach for these type of filter networks.

The insertion loss of the simulation is 0.83 dB and the return loss 25 dB. Very good

**Table 5.10:** Dimensions of the microstrip structure in Fig. 5.20 as obtained with the full wave EM simulation in Sonnet.

Parameter	Description	Value (mm)
$l_1$	Length of path 1	29
$l_2$	Length of path 2	78
$l_\Delta$	Compensation length	1.5
$l_t$	Length of tapered line	2
$l_n$	Length of node	3
$w_1$	Width of path 1	1.5
$w_2$	Width of path 2	0.2
$w_{b1}$	Width of $C_{b1}$ package	0.8
$w_n$	Width of node	0.8
$w_A$	Width of feed	1.1
$\phi_{via}$	Diameter of via	0.5

**Figure 5.21:** The centred filter responses of the 4 section microstrip model in MWO and EM simulation in Sonnet.

tunability is achieved with this filter as shown in Fig. 5.22. Here  $\Delta BW = 17.5\%$  is achieved while maintaining  $f_0 = 1.53$  GHz and  $\Delta f_0 = 5\%$  for a fixed  $FBW = 49\%$ .

#### 5.4.6 Fabricated filter

The filter is fabricated with a laser machine and very high accuracy is achieved. The vias are made with through-hole plating. A picture of the fabricated filter with the complete biasing network is shown in Fig. 5.23. Two potentiometers are used to tune the two types of varactor diodes separately, with a DC supply of 15V. Decoupling capacitors of 100 nF each are used for the DC lines. Note that the two wires extending across the centre conductor are bonding wires at DC.

The measurements of the tuned responses are given in Fig. 5.24. It is found that the passband is lower in frequency and therefore the tuning is done at lower frequencies in order to illustrate the filter working. The tuning is determined as  $\Delta BW = 24.1\%$  while

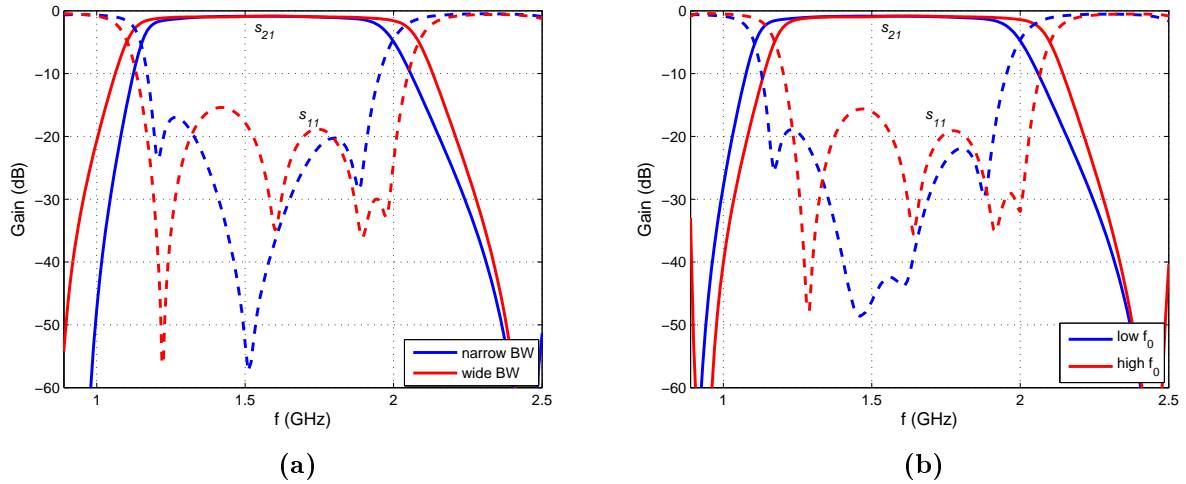


**Figure 5.22:** The results of the EM simulation of the 4 section filter for (a) BW tuning and (b)  $f_0$  tuning.

maintaining  $f_0 = 1.445$  GHz and  $\Delta f_0 = 6.1\%$  for a fixed  $FBW = 49\%$ . Despite the 85 MHz frequency shift, the tuning is better in BW and  $f_0$ , although the return loss is much poorer (with a minimum of 10 dB) than in the simulated results.

The aim of the tunability in this filter, is to fine-tune the response after fabrication in order to obtain the centred response. This is illustrated in Fig. 5.25 where the fabrication's response is fine-tuned and plotted against the designed response. Here the FBW is correct, however, due to the limited capacitor range of the BB198 varactor ( $C_1$ ), the  $f_0$  is 1.49 GHz. The return loss is also too small at 11.2 dB.

In order to determine the cause of the frequency shift a few additional measurements are done. The first is the determination of the permittivity of the RO4003C substrate. This is done with a test board consisting of a  $90^\circ$  open-circuit stub. From the measurements it is determined that the permittivity is in fact 3.38. The physical dimensions of the fabricated filter are measured with a microscope, but no significant deviations are found. Therefore the frequency shift must be due to tolerances in the components.

The components with the most influence on the passband is the varactor diodes. This is demonstrated in Fig. 5.26 where the filter responses are plotted for 100% deviation in the values of both the varactors' series inductances, i.e.  $0.7 \pm 0.7$  nH. Note that these results are obtained with the microstrip circuit in MWO.

Following these graphs, as well as the measured results of the fabrication and the compensated parasitic simulations with the MWO circuit, the best explanation for the frequency shift is that the parasitic inductances of the BB198 varactor ( $C_1$ ) is not modelled correctly. This could also be due to the inductance caused by the soldering on the pins of the varactor.

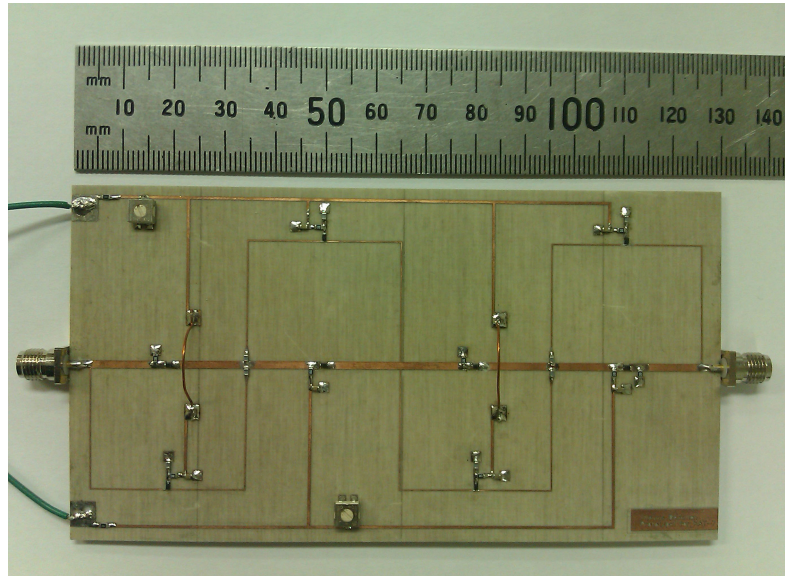


**Figure 5.23:** A picture of the fabricated first prototype filter.

## 5.5 Second prototype: 6 cascaded filtering-sections

In this section the second prototype filter is designed. The aim of this filter, in contrast to the first prototype, is to achieve the required selectivity with the attenuation slopes, while maintaining reasonable tunability.<sup>6</sup> The prototype consists of 6 cascaded filtering-sections and the design process is similar to that of the first prototype.

### 5.5.1 Design of prototype circuit

The second prototype filter must achieve the required 20 dB suppression at both 1.1 and 2.1 GHz. The best way to achieve this high selectivity with the attenuation slopes, is to increase the number of cascaded filtering-sections as shown in Subsection 5.4.1.

Increasing the sections deteriorates the return loss in the passband which leads to poor tunability. In other words when tuning the passband, especially for wide BW as shown before, the return loss decreases due to a terminal mismatch in the passband. For a considerable tuning range, the 4 cascaded sections is tuned on the limit of  $L_R \geq 15$  dB (refer to Table 5.8). Thus for more cascaded sections this tuning range cannot be achieved for the specifications.

Due to the trade-off between the return loss and selectivity, with the aim of this filter being to achieve high selectivity, it is decided to lower the limit of the return loss to  $L_R \geq 10$  dB in order to have measurable attributes in the design process.

Considering a 5 section network it is found that the required selectivity is only achieved for a lowered capacitance value of  $C_2$ . However, in Fig. 5.27 it is shown that although the selectivity is achieved, the out-of-band spurious passbands do not adhere to the spec-

<sup>6</sup>The term *reasonable* is used due to trade-offs between the tunability and the selectivity.

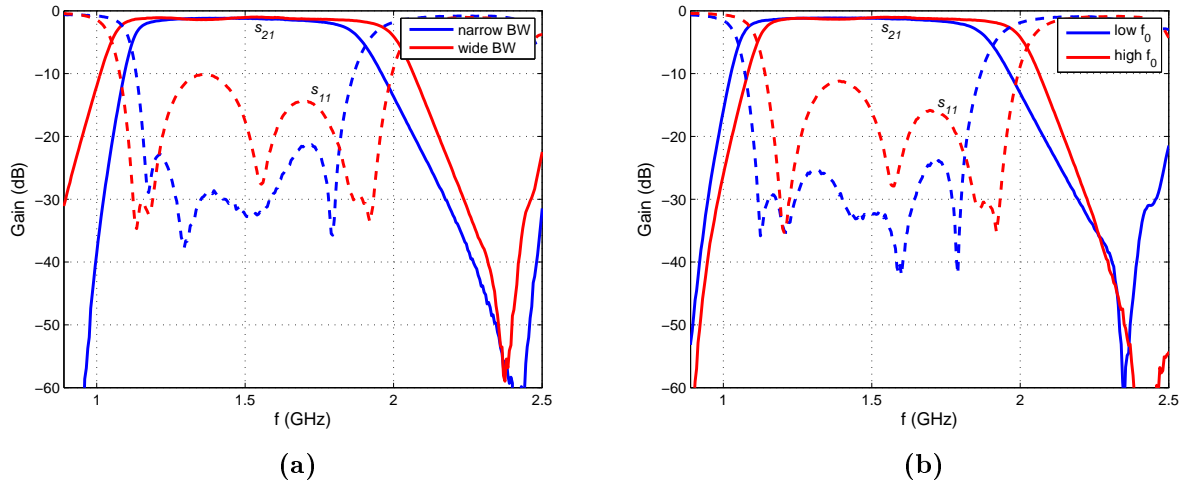


**Figure 5.24:** The measurements of the 4 section fabricated filter for (a) BW tuning and (b)  $f_0$  tuning.

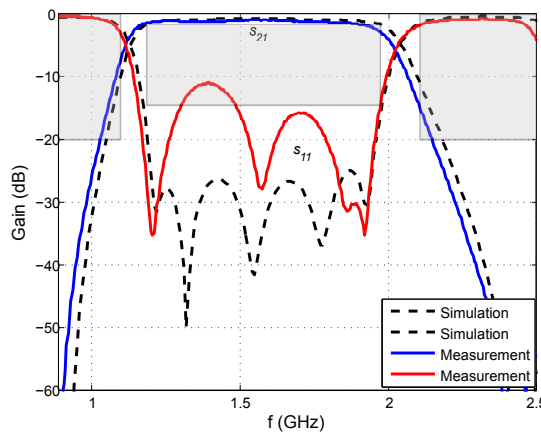


**Figure 5.25:** The passband of the 4 section fabrication that is tuned closest to the specifications for the centred response, plotted against the passband of the simulation. Due to a shift in frequency the fabrication’s return loss deteriorates significantly.

ifications. From the design graphs of the 4 section network in Fig. 5.14 it is clear that there exists a trade-off between the slope selectivity and spurious response suppression.

The 6 section network, however, does meet the required selectivity and spurious response suppression as seen in Fig. 5.27. Although the return loss is lower than in the case of the 5 sections network, it is possible with  $L_R \geq 10$  dB to achieve the same tuning range as obtained with the first prototype filter. Therefore, the filter network consisting of 6 cascaded sections is chosen for the second prototype filter design.

The design graphs for the 6 section prototype circuit are given in Fig. 5.28. The data is obtained in similar manner as the 4 section network using MWO.<sup>7</sup> Here the lower limit for the capacitance range of  $C_1$  is chosen as 5 pF because beyond this, the lower spurious

<sup>7</sup>Bear in mind that the prototype circuit is only the simple TEM-circuit shown in Fig. 5.12a and doesn’t take into account any parasitic affects.



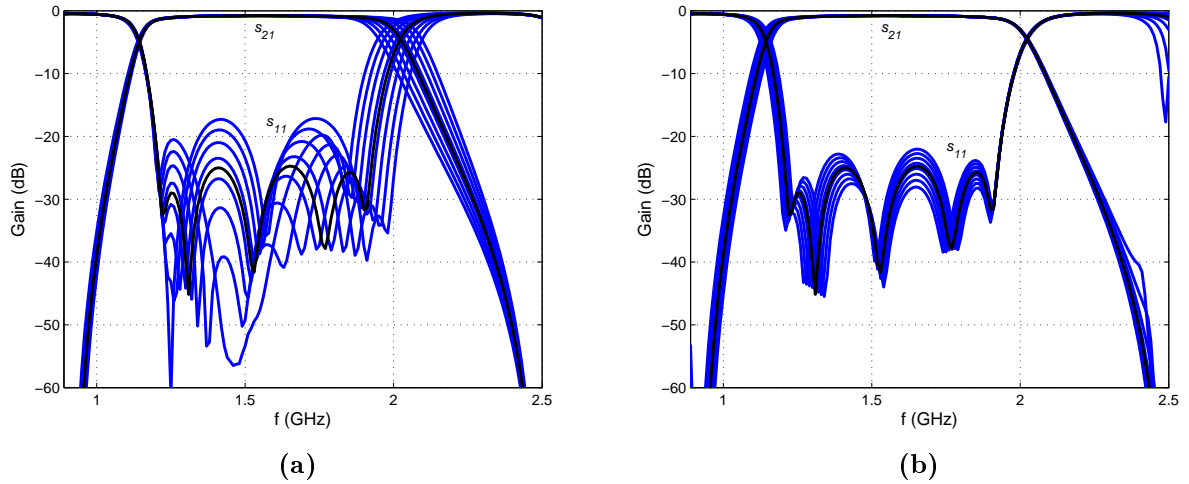


**Figure 5.26:** The filter responses of the first prototype for a 100% deviation in the value of the series inductance ( $0.7 \pm 0.7$  nH) of the varactor (a)  $C_1$  and (b)  $C_2$ , respectively. These results are obtained with the microstrip circuit in MWO.

passband is too close to the designed passband when the response is tuned for wide BW. The 20 pF instance is only given to illustrate the affect on these characteristics, because optimal tuning cannot be achieved for higher values than 10 pF. The lower limit for  $C_2$  is chosen as 2 pF because of the position of the lower spurious passband, while the upper 10 pF limit is chosen to avoid poor selectivity.

From Fig. 5.28a and Fig. 5.28b it is clear that the selectivity at both 1.1 and 2.1 GHz are met for these capacitance ranges. Fig. 5.28c shows the frequency where the lower spurious passband starts for  $|s_{21}| \geq -20$  dB. Therefore the frequency samples are taken at  $|s_{21}| = -20$  dB. The lower spurious passband may not be closer to the designed passband, specified by  $f \leq 0.89$  GHz. The same concept applies to the upper spurious passband but for  $f \geq 2.5$  GHz, as shown in Fig. 5.28d. Therefore in order to keep within these specifications it is required that  $C_2 \geq 3.5$  pF for  $C_1 \leq 10$  pF. Note that for  $C_1 = 5$  pF and  $C_2 = 5$  pF the spurious passbands closest to  $f_0$  are suppressed by more than 20 dB, hence the sudden change in these graphs.

Fig. 5.28e shows the impedance of the longer line ( $Z_2$ ) in the filtering-sections. This is much lower for the 6 section network than in the 4 section network. Note that the same substrate is used for this design with characteristics given in Table 5.6.

It is clear from these graphs that most of the specifications indicated with the gray regions are met. Therefore the focus is turned to the tunability of the response. In order to obtain optimal tunability, i.e. for symmetrical BW and  $f_0$  tuning around the centred specifications, the capacitance range  $5 \leq C_1 \leq 10$  pF is required. For these values it is clear from the design graphs that  $3.5 \leq C_2 \leq 10$  pF is required.

By adding inductances to the capacitors, to model the actual varactor's parasitics,

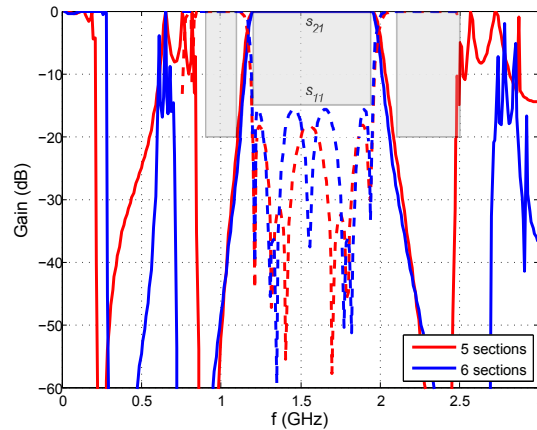


**Figure 5.27:** The filter responses of the networks consisting of 5 and 6 cascaded sections. These results are obtained with the simplified TEM-circuit in MWO shown in Fig. 5.12a. The gray regions indicate the areas not adhering to the filter specifications. Note that  $s_{11}$  (dashed line) is only plotted at the passband frequencies.

it is found that resonance occurs on the upper attenuation slope. This is caused by  $C_2$  and its corresponding series inductance. Therefore to increase the resonant frequency, the value for  $C_2$  must be chosen as small as possible. It is decided to work with  $C_2 = 5$  pF in order to safely clear the spurious passband requirements. The value for  $C_1$  is chosen in the middle of its range as  $C_1 = 7$  pF.

The optimised parameter values for the prototype circuit is given in Table 5.11 with the corresponding filter response shown in Fig. 5.29. From these results it is clearly seen that all the KAT-7 specifications for the centred response are met with this prototype circuit. Note also that the spurious passbands closest to  $f_0$  are suppressed by more than 10 dB.

The filter response is tuned to the four different tune-all states as shown in Fig. 5.30. The tuning results are summarised in Table 5.12. Note that the tuning is here limited by  $L_R \geq 10$  dB. The tunability of the prototype circuit is determined as  $\Delta BW = 16.1\%$  while maintaining  $f_0 = 1.53$  GHz and  $\Delta f_0 = 6\%$  for a fixed  $FBW = 49\%$ . The results are similar to that obtained with the 4 section prototype, although in this case the return loss specification is lowered.

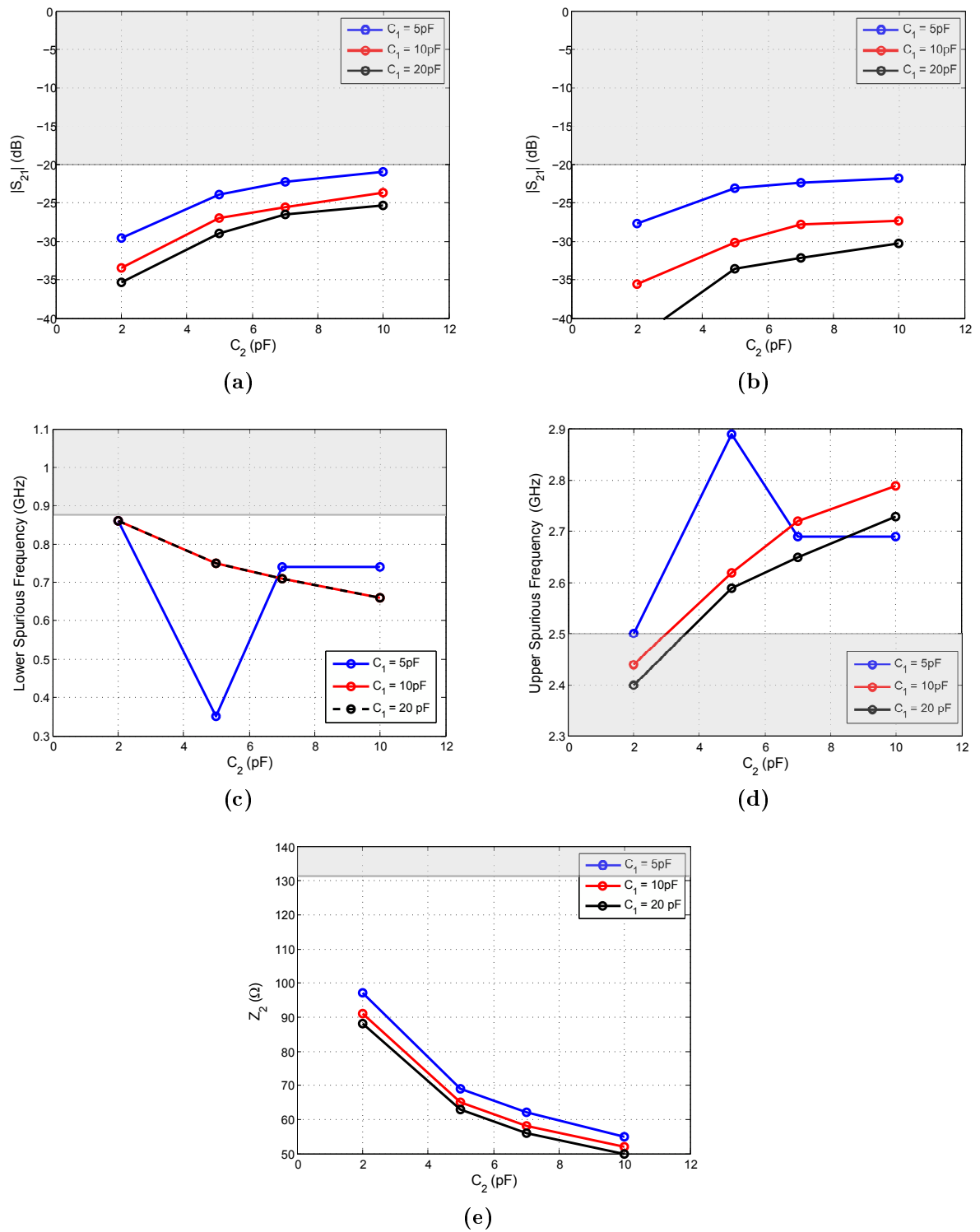


**Figure 5.28:** The design graphs of different capacitor values for a filter network consisting of 6 cascaded sections. The TEM-network is optimised in each case for the correct passband specifications. The gray regions indicate the areas not adhering to the filter specifications.

**Table 5.11:** The optimised parameter values of the 6 section prototype circuit with filter response shown in Fig. 5.29. The terminal impedance is  $Z_A = 50\Omega$ .

Path 1	Path 2
$\theta_1 = 99.2^\circ$	$\theta_2 = 207^\circ$
$Z_1 = 42.1\Omega$	$Z_2 = 66.7\Omega$
$C_1 = 7 \text{ pF}$	$C_2 = 5 \text{ pF}$

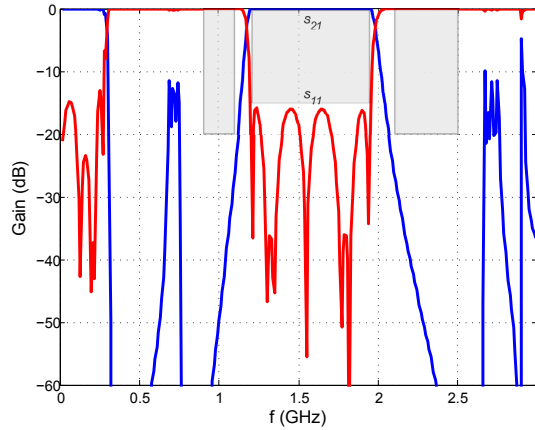


**Figure 5.29:** The filter response of the optimised 6 section prototype circuit in MWO. The parameter values are given in Table 5.11.

## 5.5.2 Components for filter network

It is clear from the tuning range in Table 5.12 that the capacitor range of  $C_1$  is from 3.84 to 18 pF and for  $C_2$  it is from 4.25 to 5.85 pF. In similar manner to the first prototype (refer to Fig. 5.18), it is found that the second prototype must have a series resistance ratio of  $R_{s1}/R_{s2} \approx 1.75$ , for the corresponding varactors, in order to obtain a flat passband. The resistances should be as small as possible due to the increased number of varactors required for this prototype, consequently increasing the insertion loss.

The SMV1235-079LF varactor diode from Skyworks is chosen to satisfy the conditions for  $C_1$ . It has a capacitor range from 2.38 to 18.22 pF with an equivalent series resistance of  $0.6\Omega$ . The 079LF package is similar to that of the varactors used in the previous design.

For a flat passband the equivalent series resistance of  $C_2$  should be  $0.34\Omega$ . Therefore the SMV1413-079LF also from Skyworks is chosen. It has a capacitor range from 1.77 to 9.24 pF with an equivalent series resistance of  $0.35\Omega$ . The complete Spice models for both of these varactors with the package parasitics are given in the datasheets provided by Skyworks.

This prototype filter has filtering-sections in multiples of two and therefore the biasing layout proposed in Subsection 5.4.3 is used for the design. All the parameters in Fig. 5.17b remain the same here as well as the corresponding components. I.e. a 20 pF capacitor for the DC blocks ( $C_{b1}$  and  $C_{b2}$ ) and a 100 k $\Omega$  resistor for the RF chokes ( $R_c$ ).

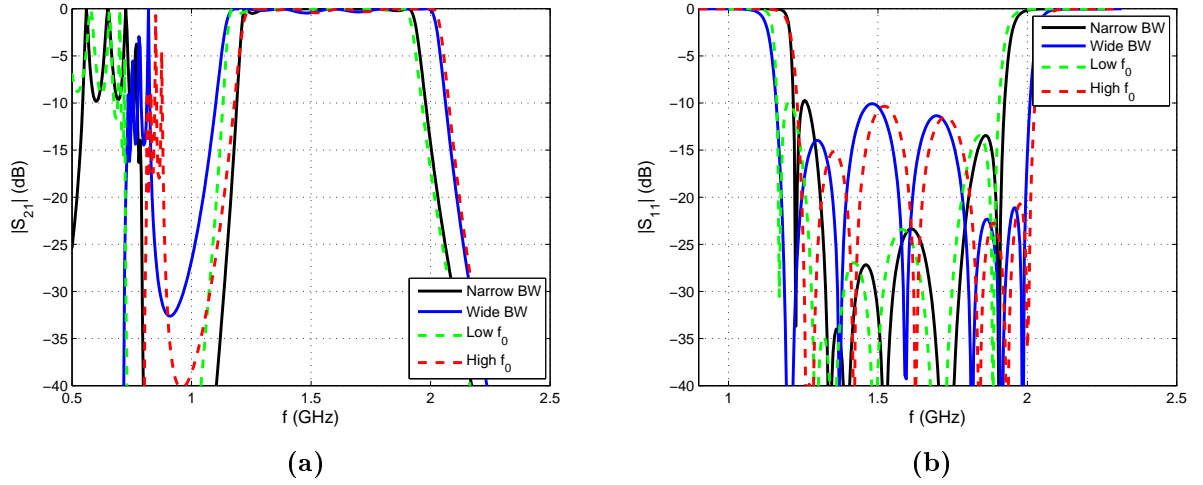


**Figure 5.30:** The (a) transmission coefficient and (b) reflection coefficient for different tuned passband states, summarised in Table 5.12.

**Table 5.12:** The tune-all results of the 6 section prototype for the design values given in Table 5.11.

Description	$C_1$ (pF)	$C_2$ (pF)	FBW (%)	$f_0$ (GHz)	$L_R$ (dB)
Narrow BW	12	4.42	45.3	1.53	9.8
Wide BW	4.34	5.85	54	1.53	10
Low $f_0$	18	5.71	49	1.487	10
High $f_0$	3.84	4.25	49	1.582	10.3

### 5.5.3 Implementation of filter network

The same microstrip circuit used in the optimisation phase of the first prototype (Fig. 5.19), is used for this design. The layout remains the same, but with a slight difference in the node between  $C_2$ ,  $C_{b2}$  and  $R_c$ .

The higher capacitance value for  $C_2$ , along with the parasitic inductances, causes a resonance close to the upper cut-off frequency of the passband. In order to increase this resonant frequency, the path between  $C_2$  and  $C_{b2}$  must be shortened. Therefore a new node is defined for the microstrip filter as shown in Fig. 5.31. The varactor  $C_2$  is mounted at port 1,  $C_{b2}$  at port 2 and  $R_c$  at port 3, with the strip widths corresponding to the package width as  $w_{C2}$ ,  $w_{b2}$  and  $w_c$  respectively.

This microstrip layout of the node is simulated with Sonnet and the results are integrated in the microstrip circuit in MWO. The circuit is optimised with the same steps given in Subsection 5.4.5. The optimised parameter values are then implemented in the microstrip structure shown in Fig. 5.32. Note that this layout illustration only shows the first 3 sections of the filter. The remaining 3 sections are symmetrical to the first 3.

The final values for the dimensions of the microstrip structure are given in Table 5.13. The main difference between these dimensions and that of the microstrip circuit is the

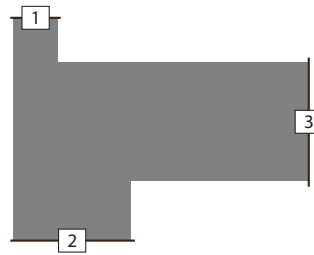


**Figure 5.31:** The microstrip node between  $C_2$  (at 1),  $C_{b2}$  (at 2) and  $R_c$  (at 3).

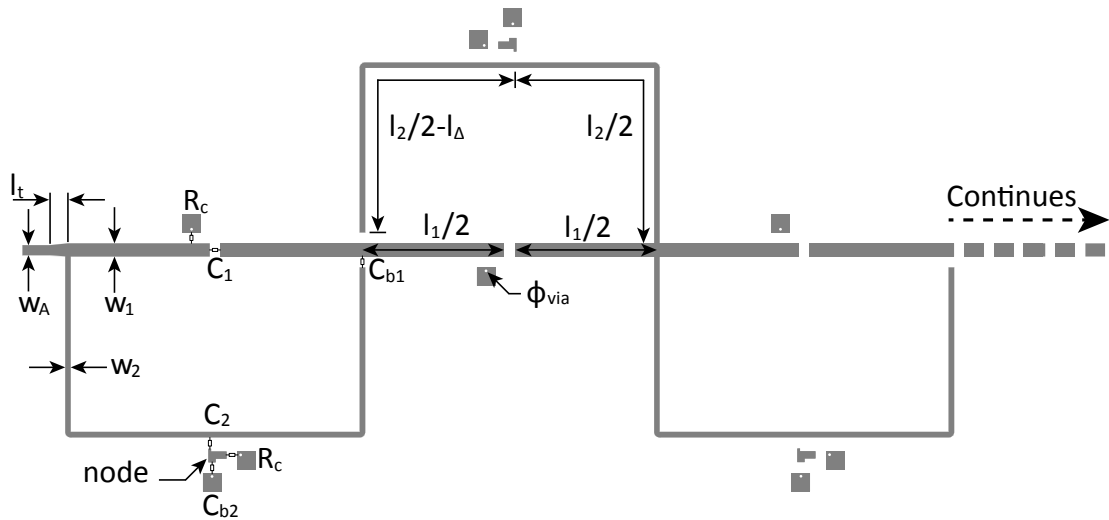


**Figure 5.32:** The layout of the 6 section microstrip structure with all the dimension parameters. Note that only the first 3 sections of the filter are shown here. The remaining 3 sections are symmetrical to the first 3. The polygon indicated as “node” is shown more clearly in Fig. 5.31.

length of path 2 ( $l_2$ ) and the compensation length ( $l_\Delta$ ). In the microstrip circuit these are  $l_2 = 68.8$  mm and  $l_\Delta = 0.3$  mm.

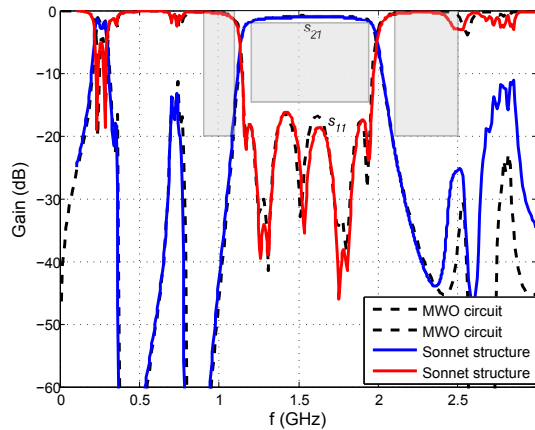
The corresponding centred responses of the microstrip circuit and microstrip structure are shown in Fig. 5.33. Good correlation is again found between the two responses, although the peaks at 2.5 and 2.8 GHz have much higher gain in the Sonnet simulation.

The initial suspicion for this effect is the  $TM_{110}$  mode that may propagate at 2.79 GHz because of the large cavity, i.e. the enclosed box of the board in the Sonnet environment. However, when dividing this simulation up into subcircuits with smaller boxes and joining it together using a netlist, in order to exclude the propagation of such a mode, it is found that there is no major difference in the response. Therefore this mode is not the cause of the higher gain. This leaves a margin for improvement to the microstrip circuit.

Nevertheless, these peaks are still suppressed below 10 dB and adheres to the upper rejection specifications. Note that the peak at 2.5 GHz is the result of the resonance of  $C_2$  and the parasitic inductances. The insertion loss of the simulation is 0.94 dB and the

**Table 5.13:** Dimensions of the microstrip structure in Fig. 5.32 as obtained with the full wave EM simulation in Sonnet.

Parameter	Description	Value (mm)
$l_1$	Length of path 1	31.2
$l_2$	Length of path 2	70.4
$l_\Delta$	Compensation length	0
$l_t$	Length of tapered line	2
$w_1$	Width of path 1	1.45
$w_2$	Width of path 2	0.6
$w_{b2}$	Width of $C_{b2}$ package	0.8
$w_{C2}$	Width of $C_2$ package	0.3
$w_c$	Width of $R_c$ package	0.8
$w_A$	Width of feed	1.1
$\phi_{via}$	Diameter of via	0.5

**Figure 5.33:** The centred filter responses of the 6 section microstrip model in MWO and EM simulation in Sonnet.

return loss 16.2 dB. It has to be mentioned that because of the increase in losses, the BW is designed for  $\Delta L_A = 0.9$  dB.

It is found that  $|s_{21}| = -16$  dB at 1.1 GHz on the lower attenuation slope. This does not satisfy the -20 dB specification. The reason is that there are more losses in the biasing network of  $C_2$ , resulting in poorer roll-off and compensating on the selectivity.

The tunability of the simulated structure is shown in Fig. 5.34 and determined as  $\Delta BW = 18.8\%$  while maintaining  $f_0 = 1.53$  GHz and  $\Delta f_0 = 8.5\%$  for a fixed  $FBW = 49\%$ . The return loss is higher than 10 dB in all instances. These results are much better than that obtained with the prototype circuit.

#### 5.5.4 Fabricated filter

The filter is fabricated with a laser machine and the vias are made with through-hole plating. A picture of the fabricated filter with the complete biasing network is shown in

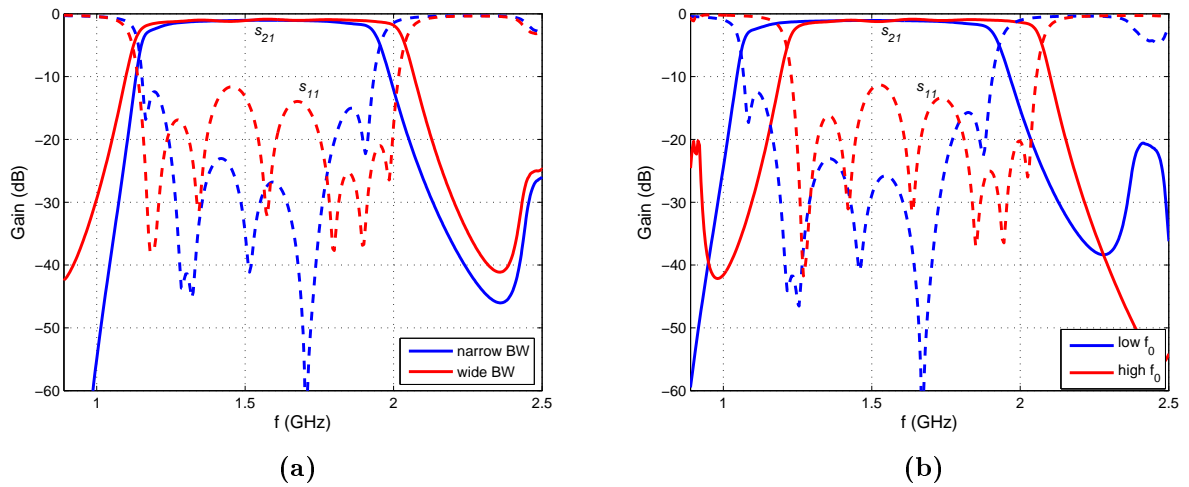


**Figure 5.34:** The results of the EM simulation of the 6 section filter for (a) BW tuning and (b)  $f_0$  tuning.

Fig. 5.35. Note that the three wires extending across the centre conductor are bonding wires at DC.

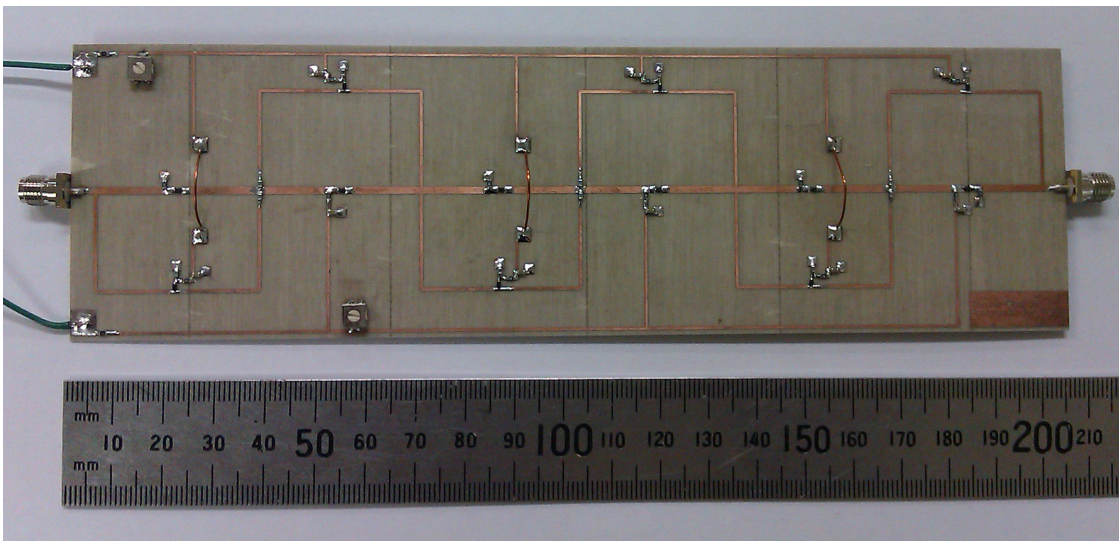


**Figure 5.35:** A picture of the fabricated second prototype filter.

Two potentiometers are used to tune the voltages of the two types of varactors separately, with a DC supply of 15V. The tuning results are shown in Fig. 5.36. It is found that the passband is shifted lower in frequency and therefore the tuning is also done at lower frequencies in order to illustrate the filter working. The tuning is determined as  $\Delta BW = 19.8\%$  while maintaining  $f_0 = 1.465$  GHz and  $\Delta f_0 = 8.5\%$  for a fixed  $FBW = 49\%$ .

The aim of the tunability in this filter, is again to fine-tune the response after fabrication in order to obtain the centred response. This is illustrated in Fig. 5.37a where the



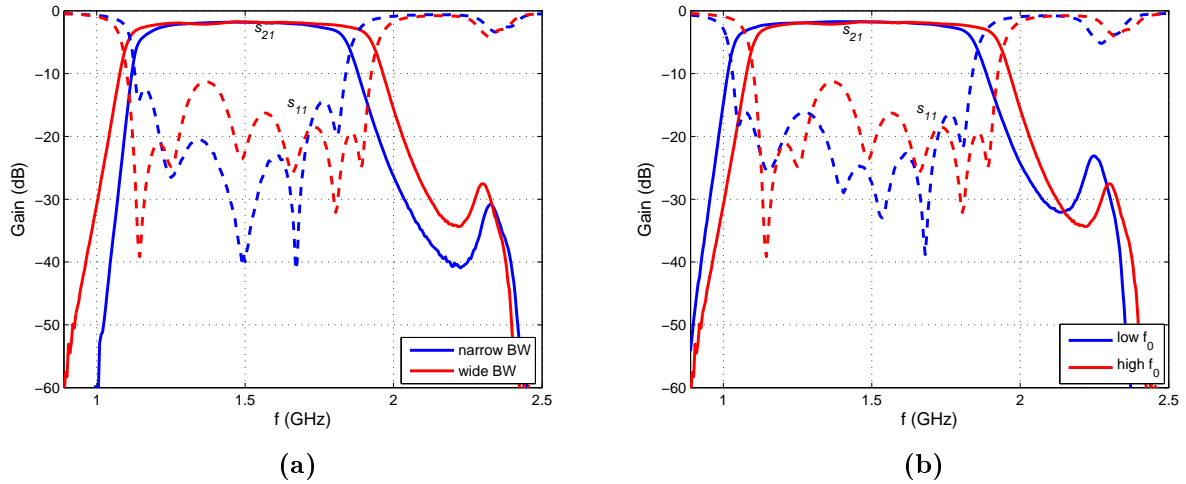


**Figure 5.36:** The measurements of the fabricated 6 section filter for (a) BW tuning and (b)  $f_0$  tuning.

fabrication’s response is fine-tuned and plotted against the designed response. Both the BW and  $f_0$  is correct, however, the return loss is quite low at 6.4 dB.

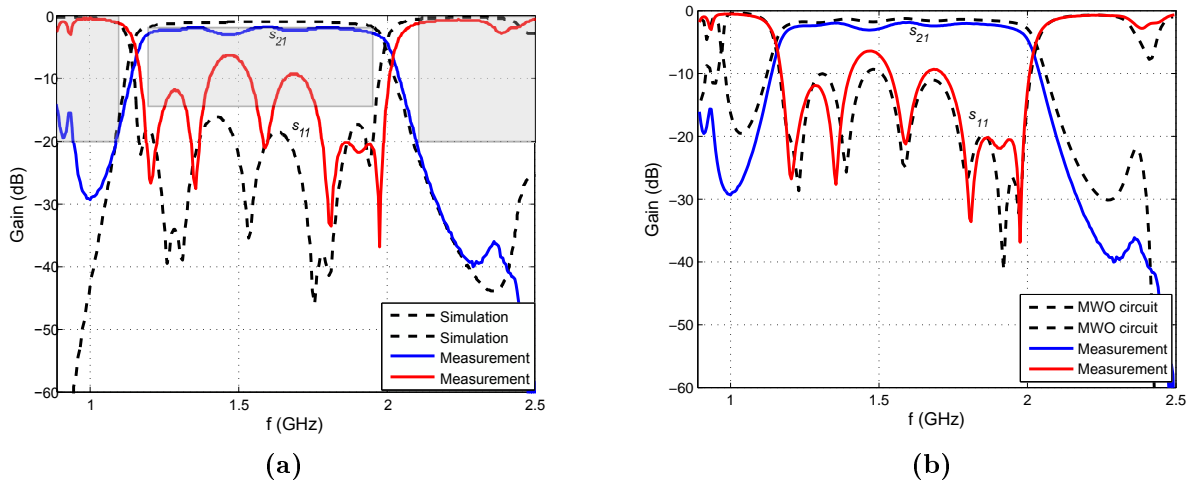


**Figure 5.37:** The passband of the 6 section fabrication that is fine-tuned to the specifications for the centred response, plotted against (a) the designed passband of the simulation and (b) the adapted microstrip circuit in MWO. Due to a shift in frequency the fabrication’s return loss deteriorates significantly.

From the measured results, along with the circuit modelling in MWO, it seems that the 65 MHz frequency shift is again due to varactor parasitics. However, in this fabrication it is both varactors that do not correspond correctly to the Spice models, opposed to the first prototype filter. In Fig. 5.38 this affect is illustrated with a 100% deviation in the series inductance of the corresponding varactor, i.e.  $0.7 \pm 0.7$  nH. Note in Fig. 5.38b how the resonance of  $C_2$ , on the upper side of the passband, shifts in frequency as the

inductance is changed.

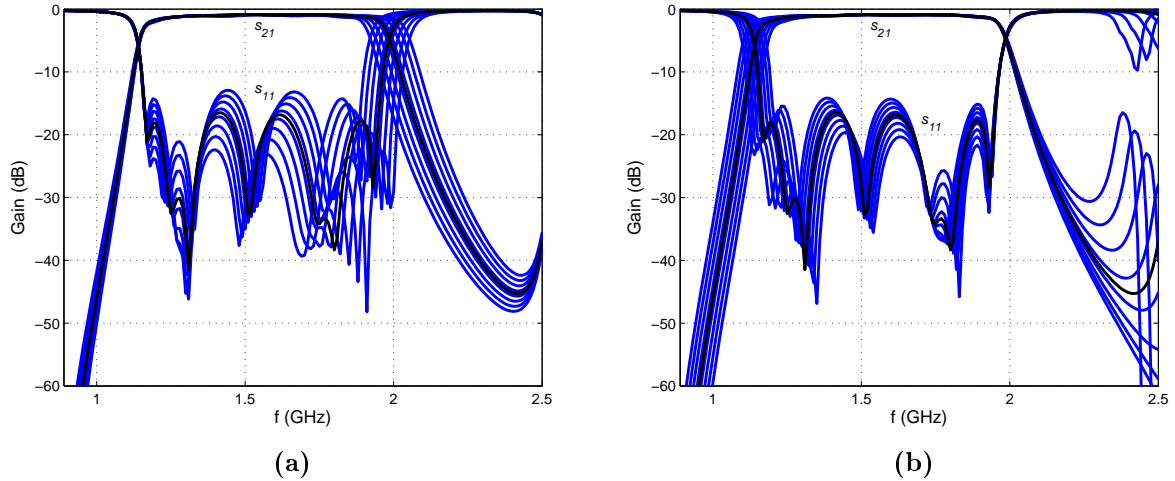


**Figure 5.38:** The filter responses of the second prototype for a 100% deviation in the value of the series inductance ( $0.7 \pm 0.7$  nH) of the varactor (a)  $C_1$  and (b)  $C_2$ , respectively. These results are obtained with the microstrip circuit in MWO.

To illustrate this more clearly, the parasitic affects along with the added losses of the fabrication are implemented into the microstrip circuit in MWO. First the voltages of  $C_1$  and  $C_2$  are set to 12.5V and 5.5V respectively, according to the fabrication's state. Then the dissipation factor of the substrate is increased from 0.0027 to 0.01, in order to emulate the extra losses possibly caused by the DC blocks and other unknown affects. Following this the series inductances of both varactors are tuned to obtain the same BW and  $f_0$  as the results of the fabrication.

The results of the adapted microstrip circuit is plotted in Fig. 5.37b against that of the fine-tuned response of the fabrication. It is found that both the series inductances of  $C_1$  and  $C_2$  should be changed in the varactor models from 0.7 nH to 1.8 nH. Note that this might also be due to soldering on the pins of the components.

## 5.6 Compare prototype filters

The first and second prototypes, consisting of 4 and 6 cascaded filtering-sections respectively, have been designed and fabricated. The results of both filters are summarised in Table 5.14. These are specifically only the EM simulated results because too many deviations exist in the measured results, in order for the filters to be compared with each other.

The insertion loss in both filters are quite low, given their high order responses. As mentioned before, the advantage of transversal sections is the fact that there are no coupled-lines that introduce radiation losses. The return loss is also satisfying in both

**Table 5.14:** The characteristics of both the simulated prototype filters, consisting of 4 and 6 cascaded sections respectively.

Characteristic	First prototype	Second prototype	Required
Minimum $L_A$ in passband	0.83 dB	0.94 dB	$\leq 3.0$ dB
Minimum $L_R$ in passband	25 dB	16.2 dB	$\geq 15.0$ dB
$ s_{21} $ at 1.1 GHz	-9.7 dB	-16 dB	$\leq -20$ dB
$ s_{21} $ at 2.1 GHz	-10.6 dB	-21.8 dB	$\leq -20$ dB
Lower spurious response	0.83 GHz	0.76 GHz	$\leq 0.89$ GHz
Upper spurious response	2.64 GHz	2.67 GHz	$\geq 2.5$ GHz
$\Delta L_A$	0.7 dB	0.9 dB	$\leq 1.0$ dB
$\Delta BW$	17.5%	18.8%	$> 0$
$\Delta f_0$	5.0%	8.5%	$> 0$
Worst $L_R$ across tuning range	15.4 dB	11.3 dB	$\geq 15$ dB
Physical size of board	$0.54\lambda_g \times 1.07\lambda_g$	$0.47\lambda_g \times 1.69\lambda_g$	None

filters for a centred passband.

The major trade-off between these two filters are the selectivity and the return loss. It is clear that the second prototype partially meets the selectivity requirements of  $|s_{21}| < -20$  dB at 1.1 and 2.1 GHz. However, due to high component losses in the biasing network of  $C_2$ , the roll-off is increased on the lower attenuation slope, causing poor selectivity. Therefore, to compensate for this either the DC blocks need higher Q or  $C_1$  need lower Q in order to obtain a flat passband.

The  $\Delta L_A$  is chosen higher for the second prototype because of the higher insertion loss leading to poor roll-off. In both filters the required  $\Delta L_A < 1$  dB are met.

The second prototype does not have high enough return loss so that  $L_R \geq 15$  dB is maintained while tuning the passband. In this regard the first prototype meets the specifications, although not in selectivity.

The tunability of the filters are generally very good, given that these are in fact wideband filters. The BW and  $f_0$  tunability is higher in the second prototype, however, this is partially a result of the lowered return loss specification for this design, i.e.  $L_R \geq 10$  dB.

The physical dimensions are smaller in the first prototype due to the number of filtering-sections. This is not specified for the filters and therefore is only for interest sake.

## 5.7 Conclusion

In this chapter new tune-all wideband filters were proposed with regard to the KAT-7 specifications. Tunability of perturbation effects were exploited in transversal-sections, in order to realise such filters.

The significance of this type of filter is that it has a wideband response that is tunable in both BW and  $f_0$ . Given the amount of varactor diodes used, the filter does not exhibit very high insertion loss and a flat passband is achieved. Due to the transmission zeros around the passband, high selectivity is obtained.

This type of filter also has the potential for fixed passband wideband filters. To illustrate this, a 6 section filter is designed with the varactors replaced by lumped capacitors. The filter is fabricated and shown in Fig. 5.39. A very good filter response is obtained as shown in Fig. 5.40, which meets all the specifications of the centred response. Note that the measured and simulated results have very good agreement and it is evident that much less effort is required for the design of a fixed passband filter. The wide out-of-band suppression is achieved by strategically choosing the capacitances as  $C_1 = 5$  pF and  $C_2 = 5$  pF, with the help of the design graphs in Fig. 5.28c and d.

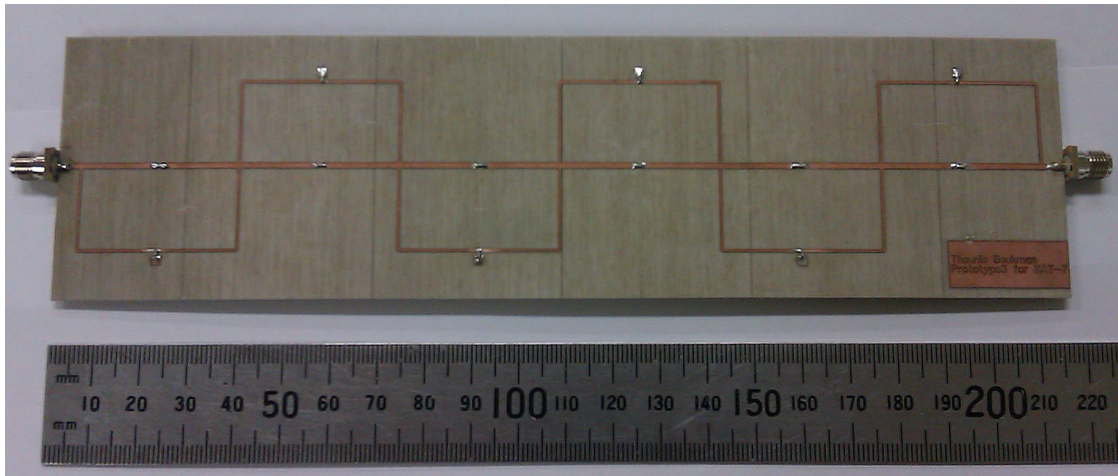


**Figure 5.39:** A picture of the fabricated fixed passband filter consisting of 6 cascaded sections.

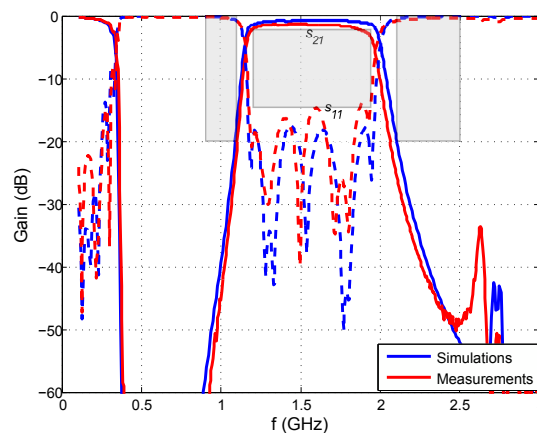


**Figure 5.40:** The simulated and measured results of the fixed passband filter consisting of 6 cascaded sections.

For the tunable filters a trade-off is found between the selectivity of the attenuation

slopes and its tunability. Hence, the purpose of the first prototype was to obtain good tunability, while the second was to obtain high selectivity. Very good results were obtained with both these filters, although spurious passbands are found towards DC.

Spurious responses are an inherent result of transversal-sections. Therefore it is proposed that wider BW filters are cascaded with the network, in order to suppress these responses. A good candidate for such a type of filter is the one proposed in [4], with the layout and filter response given in Fig. 4.8.

A disadvantage of these filters is that they are very large in physical size. Therefore it is recommended that the lines are meandered in order to reduce the size of the layout. The 4 section prototype has a very high impedance line that has a narrow width of 0.2 mm on this substrate. Therefore high accuracy is required for this fabrication and may result in a costly process.

The filters are also quite sensitive to component tolerances and care must be taken in the modelling thereof. A good practise is to measure and characterise the varactors before implementing it in such a design.

Both of the designed prototypes exhibit very good results, although all the specifications are not entirely met. The prototype consisting of 6 cascaded sections would be ideal for KAT-7, given that the specification  $L_R \geq 15$  dB across the tuning range is lowered to  $L_R \geq 10$  dB.

# Chapter 6

## Conclusion

### 6.1 Conclusion of reviewed literature

This thesis presented numerous syntheses for tunable and wideband microstrip filters. It was shown that the coupled resonator approach is the most desirable synthesis for tunable filters. This synthesis is based on narrowband approximations, although wideband applications are possible. However, for microstrip realisation this is limited to narrowband filters if BW tuning is implemented using detuned resonators.

A common approach for wideband application is the exact synthesis [3], but unfortunately this is not appropriate for the implementation of tuning elements. The proposed wideband filters that are based on signal-interference techniques, found in literature, also do not give the capability for tuning.

Therefore, following the reviewed literature it is concluded that no suitable wideband filter synthesis for microstrip realisation, with tunability in both  $f_0$  and BW, exists. However, much potential was found with filters based on perturbed ring-resonator configurations.

### 6.2 Achievement of initial goals

Following the conclusion of the reviewed literature, perturbation with tuning elements in transversal-sections was investigated. It was found that the ring-resonator (same as the transversal-section with  $\theta_1 = 90^\circ$  and  $\theta_2 = 270^\circ$ ) is the most desirable filtering-section for the required BW and out-of-band rejection.

A new filtering-section (shown in Fig. 5.7a) with tune-all characteristics was developed and characterised. Multiples of this filtering-section was cascaded to form complete prototype filters for the KAT-7 specifications. Two filters were designed and fabricated, due to a trade-off found between the tunability and selectivity of the filter response.

In Table 6.1 the characteristics of these filters are summarised and compared with

the specifications given in Table 1.1. Note that the specifications that are not met are indicated in red.

**Table 6.1:** The characteristics of the simulated and measured results of both prototype filters, consisting respectively of 4 and 6 cascaded sections. Note that the red numbers indicate the specifications not met by the corresponding filter.

Specification	4 Cascaded Sections		6 Cascaded Sections	
	Simulation	Fabrication	Simulation	Fabrication
$\Delta f_0 > 0$ (%)	5	6.1	8.5	8.5
$\Delta BW > 0$ (%)	17.5	24.1	18.8	19.8
$f_0 = 1.53$ (GHz)	1.53	1.49	1.53	1.53
FBW = 0.49 (%)	49	49	49	49
$\Delta L_A \leq 1$ (dB)	0.7	0.7	0.9	0.9
$L_A \leq 3$ (dB)	0.83	1.02	0.94	1.86
$L_R \geq 15$ (dB)	25	11.2	16.2	6.4
$ s_{21}  \leq -20$ dB $f = 0.89 - 1.1$ (GHz)	0.83 - 1.05	0.83 - 1.03	0.75 - 1.09	0.94 - 1.09
$ s_{21}  \leq -20$ dB $f = 2.1 - 2.5$ (GHz)	2.18 - 2.64	2.15 - 2.55	2.09 - 2.68	2.10 - 3.33

The first filter consists of 4 cascaded filtering-sections. With this filter the aim is to maintain  $L_R \geq 15$  dB across a reasonable tuning range, hence at the cost of poor selectivity of the attenuations slopes. The second filter consists of 6 cascaded filtering-sections. Oppose to the former, the aim with this filter is to obtain high selectivity, though at the expense of the return loss. For the indicated tuning range of this filter  $L_R \not\geq 15$  dB. Therefore, with an increase in the number of cascaded sections, the selectivity increase while the return loss decrease.

The end goal of the tunability in these wideband filters for KAT-7, is to be able to fine-tune the passband of the fabricated device to the centred specifications. However, all the specifications were not entirely achieved with the fine-tuned fabrications as indicated in Table 6.1.

The main reason for the drastic deviation in both fabrication responses, is the values of the parasitic components that are not modelled accurately enough. The soldering on the pins of the components could also account for this effect.

Nevertheless, the second fabricated filter is fine-tuned to the correct  $f_0$  and BW, but with poor return loss. The first filter is limited by the capacitance range of the series varactor and therefore the fabrication could not fine-tune the required  $f_0$ . It is concluded, therefore, that these filters have great tuning abilities, given the fact that it has wide BW.

A complete step-by-step procedure was presented for the design of such a type of filter. An advantage of this design procedure is that full wave simulations are minimal, due to the complete circuit models of the microstrip structures used for optimisation.

### 6.3 Recommendations for future work

Future development of this work could include:

- Measurements and characterisations of the DC blocks and varactor diodes should take place prior to their implementation in the design.
- Incorporate tunable matching networks at the terminals of the filter network. This will improve the tunability of the filter consisting of 6 cascaded sections, because the return loss can be maintained above 15 dB across the tuning range. With such a filter all the KAT-7 specifications should be achievable. However, the disadvantage is that both the return loss and insertion loss will most probably deteriorate.
- To suppress the spurious passbands, a wider BW filter can be cascaded with the original filter network. This is illustrated in Fig. 6.1, where the filter consisting of 6 cascaded sections are cascaded with a coupled-line transversal-section proposed in [4]. The results of the TEM-circuit in MWO yields more than 20 dB out-of-band suppression from DC up to 3.72 GHz. The disadvantage of this approach, as before, is that both the return loss and insertion loss will deteriorate in a microstrip implementation with losses.
- As proposed in [42], cascade filtering-sections with different characteristics in such a way that the spurious responses are suppressed. The disadvantage, however, is that the varactor diodes of different sections will have to be biased separately.

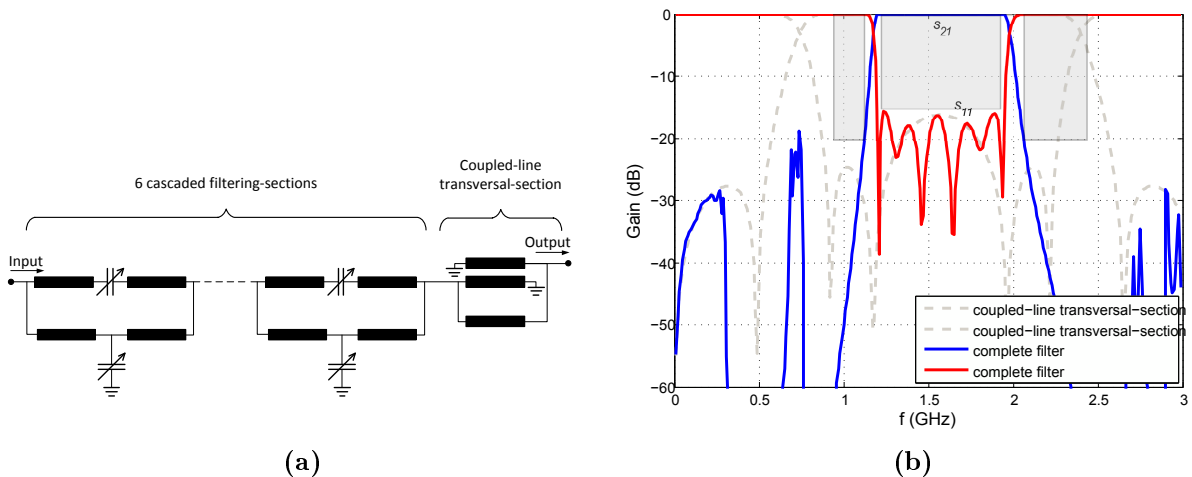


**Figure 6.1:** (a) The 6 section TEM-circuit, with filter response shown in Fig. 5.29, in cascade with the coupled-line transversal-section in Fig. 4.8a. (b) The response of the complete filter network against the response of the coupled-line transversal-section indicated by the dashed lines.



# Bibliography

- [1] M. Lazarus, “The great spectrum famine,” *Spectrum, IEEE*, vol. 47, no. 10, pp. 26–31, October 2010.
- [2] M. Sanchez-Renedo, R. Gomez-Garcia, J. Alonso, and C. Briso-Rodriguez, “Tunable combline filter with continuous control of center frequency and bandwidth,” *Microwave Theory and Techniques, IEEE Transactions on*, vol. 53, no. 1, pp. 191–199, January 2005.
- [3] R. Wenzel, “Synthesis of combline and capacitively loaded interdigital bandpass filters of arbitrary bandwidth,” *Microwave Theory and Techniques, IEEE Transactions on*, vol. 19, no. 8, pp. 678–686, August 1971.
- [4] M. Sanchez-Soriano, E. Bronchalo, and G. Torregrosa-Penalva, “Compact uwb bandpass filter based on signal interference techniques,” *Microwave and Wireless Components Letters, IEEE*, vol. 19, no. 11, pp. 692–694, November 2009.
- [5] S. Sun, L. Zhu, and H.-H. Tan, “A compact wideband bandpass filter using transversal resonator and asymmetrical interdigital coupled lines,” *Microwave and Wireless Components Letters, IEEE*, vol. 18, no. 3, pp. 173–175, March 2008.
- [6] L.-H. Hsieh and K. Chang, “Compact, low insertion-loss, sharp-rejection, and wideband microstrip bandpass filters,” *Microwave Theory and Techniques, IEEE Transactions on*, vol. 51, no. 4, pp. 1241–1246, April 2003.
- [7] K.-S. Chin, L.-Y. Lin, and J.-T. Kuo, “New formulas for synthesizing microstrip bandpass filters with relatively wide bandwidths,” *Microwave and Wireless Components Letters, IEEE*, vol. 14, no. 5, pp. 231–233, May 2004.
- [8] D. M. Pozar, *Microwave engineering*, 3rd ed., B. Zobrist, Ed. John Wiley & Sons, Inc., 2005.
- [9] G. Matthaei, L. Young, and E. Jones, *Microwave filters, impedance-matching networks, and coupling structures*. Artech House, Inc., 1980.

- [10] J.-S. Hong, *Microstrip Filters for RF/Microwave Applications*, 2nd ed., P. K. Chang, Ed. John Wiley & Sons, Inc., 2011.
- [11] A. I. Zverev, *Handbook of Filter Synthesis*. New York: Wiley, 1967.
- [12] A. Atia, A. Williams, and R. Newcomb, "Narrow-band multiple-coupled cavity synthesis," *Circuits and Systems, IEEE Transactions on*, vol. 21, no. 5, pp. 649 – 655, September 1974.
- [13] R. Cameron, "General coupling matrix synthesis methods for chebyshev filtering functions," *Microwave Theory and Techniques, IEEE Transactions on*, vol. 47, no. 4, pp. 433 –442, April 1999.
- [14] S. Gevorgian, "Agile microwave devices," *Microwave Magazine, IEEE*, vol. 10, no. 5, pp. 93 –98, August 2009.
- [15] P. Wong and I. Hunter, "Electronically tunable filters," *Microwave Magazine, IEEE*, vol. 10, no. 6, pp. 46 –54, October 2009.
- [16] I. Hunter and J. Rhodes, "Electronically tunable microwave bandpass filters," *Microwave Theory and Techniques, IEEE Transactions on*, vol. 30, no. 9, pp. 1354 –1360, September 1982.
- [17] G. Torregrosa-Penalva, G. Lopez-Risueno, and J. Alonso, "A simple method to design wide-band electronically tunable combline filters," *Microwave Theory and Techniques, IEEE Transactions on*, vol. 50, no. 1, pp. 172 –177, January 2002.
- [18] B.-W. Kim and S.-W. Yun, "Varactor-tuned combline bandpass filter using step-impedance microstrip lines," *Microwave Theory and Techniques, IEEE Transactions on*, vol. 52, no. 4, pp. 1279 – 1283, April 2004.
- [19] A. Brown and G. Rebeiz, "A varactor-tuned rf filter," *Microwave Theory and Techniques, IEEE Transactions on*, vol. 48, no. 7, pp. 1157 –1160, July 2000.
- [20] M. Sanchez-Renedo, R. Gomez-Garcia, J. Alonso, and C. Rodriguez, "A new electronically tunable combline filter with simultaneous continuous control of central frequency and bandwidth," in *Microwave Symposium Digest, 2004 IEEE MTT-S International*, vol. 3, June 2004, pp. 1291 – 1294 Vol.3.
- [21] M.-S. Chung, I.-S. Kim, and S.-W. Yun, "Varactor-tuned hairpin bandpass filter with an attenuation pole," in *Microwave Conference Proceedings, 2005. APMC 2005. Asia-Pacific Conference Proceedings*, vol. 4, December 2005, p. 4.

- [22] E. Pistono, M. Robert, L. Duvillaret, J.-M. Duchamp, A. Vilcot, and P. Ferrari, "Compact fixed and tune-all bandpass filters based on coupled slow-wave resonators," *Microwave Theory and Techniques, IEEE Transactions on*, vol. 54, no. 6, pp. 2790–2799, June 2006.
- [23] D. Packiaraj, V. Reddy, G. D'Mello, and A. Kalghatgi, "Electronically switchable suspended substrate stripline filters," in *RF and Microwave Conference, 2004. RFM 2004. Proceedings*, October 2004, pp. 64–66.
- [24] J.-S. Hong, "Reconfigurable planar filters," *Microwave Magazine, IEEE*, vol. 10, no. 6, pp. 73–83, October 2009.
- [25] G. Rebeiz, K. Entesari, I. Reines, S.-j. Park, M. El-tanani, A. Grichener, and A. Brown, "Tuning in to rf mems," *Microwave Magazine, IEEE*, vol. 10, no. 6, pp. 55–72, October 2009.
- [26] I. Hunter and P. W. Wong, "Electronically reconfigurable microwave bandpass filter," *IEEE Transactions on Microwave Theory and Techniques*, vol. 57, no. 12, pp. 3070–3079, December 2009.
- [27] A. Miller and J.-S. Hong, "Wideband bandpass filter with reconfigurable bandwidth," *Microwave and Wireless Components Letters, IEEE*, vol. 20, no. 1, pp. 28–30, January 2010.
- [28] J. Boho andrquez, N. Peñ anda, A. Vaisman, C. Shafai, D. Chrusch, C. Quendo, E. Rius, C. Person, G. Tanne and, and E. Fourn, "Implementation of ground plane membranes to realize a bandwidth and frequency tunable filter," in *Antenna Technology and Applied Electromagnetics the American Electromagnetics Conference (ANTEM-AMEREM), 2010 14th International Symposium on*, July 2010, pp. 1–4.
- [29] B. Carey-Smith, P. Warr, M. Beach, and T. Nesimoglu, "Wide tuning-range planar filters using lumped-distributed coupled resonators," *Microwave Theory and Techniques, IEEE Transactions on*, vol. 53, no. 2, pp. 777–785, February 2005.
- [30] S. Cohn, "Dissipation loss in multiple-coupled-resonator filters," *Proceedings of the IRE*, vol. 47, no. 8, pp. 1342–1348, August 1959.
- [31] I. Hunter, "Filter design with lossy circuit elements," in *Advances in Passive Microwave Components (Digest No.: 1997/154), IEE Colloquium on*, May 1997, pp. 1/1–1/6.
- [32] B. Senior, I. Hunter, and J. Rhodes, "Synthesis of lossy filters," in *Microwave Conference, 2002. 32nd European*, September 2002, pp. 1–4.

- [33] I. Vendik, O. Vendik, V. Pleskachev, A. Svishchev, and R. Wordenweber, "Design of tunable ferroelectric filters with a constant fractional band width," in *Microwave Symposium Digest, 2001 IEEE MTT-S International*, vol. 3, 2001, pp. 1461 –1464 vol.3.
- [34] S. Chandler, I. Hunter, and J. Gardiner, "Active varactor tunable bandpass filter," *Microwave and Guided Wave Letters, IEEE*, vol. 3, no. 3, pp. 70 –71, March 1993.
- [35] C.-Y. Chang and T. Itoh, "Microwave active filters based on coupled negative resistance method," *Microwave Theory and Techniques, IEEE Transactions on*, vol. 38, no. 12, pp. 1879 –1884, December 1990.
- [36] I. Awai and Y. Zhang, "Coupling coefficient of resonators - an intuitive way of its understanding," *Electronics and Communications in Japan (Part II: Electronics)*, vol. 90, no. 9, pp. 11–18, 2007.
- [37] G. Matthaei, "Interdigital band-pass filters," *Microwave Theory and Techniques, IRE Transactions on*, vol. 10, no. 6, pp. 479 –491, November 1962.
- [38] K.-S. Chin, Y.-C. Chiou, and J.-T. Kuo, "New synthesis of parallel-coupled line bandpass filters with chebyshev responses," *Microwave Theory and Techniques, IEEE Transactions on*, vol. 56, no. 7, pp. 1516 –1523, July 2008.
- [39] P. Richards, "Resistor-transmission-line circuits," *Proceedings of the IRE*, vol. 36, no. 2, pp. 217 – 220, February 1948.
- [40] R. Wenzel, "Exact design of tem microwave networks using quarter-wave lines," *Microwave Theory and Techniques, IEEE Transactions on*, vol. 12, no. 1, pp. 94 – 111, January 1964.
- [41] H. Orchard and G. Temes, "Filter design using transformed variables," *Circuit Theory, IEEE Transactions on*, vol. 15, no. 4, pp. 385 – 408, December 1968.
- [42] R. Gomez-Garcia and J. Alonso, "Design of sharp-rejection and low-loss wide-band planar filters using signal-interference techniques," *Microwave and Wireless Components Letters, IEEE*, vol. 15, no. 8, pp. 530 – 532, August 2005.
- [43] K. Chang and L.-H. Hsieh, *Microwave Ring Circuits and Related Structures*, 2nd ed. Wiley-Interscience, 2004.
- [44] B. C. Wadell, *Transmission Line Design Handbook*. Artech House, Inc., 1991.

# Appendix A

## Derivation of Coupling Coefficient

The coupling coefficient is formulated as

$$M = \frac{L_m}{\sqrt{L_1 L_2}} \quad (\text{A.1})$$

so that for maximum coupling  $M = 1$  and for no coupling  $M = 0$ .

For synchronously tuned resonators, the resonance frequency is

$$\omega_0^2 = \frac{1}{L_1 C_1} = \frac{1}{L_2 C_2}. \quad (\text{A.2})$$

The coupling coefficient of two coupled resonators, with circuit model given in Fig. 3.1, can be determined from the natural frequencies of the circuit by considering the nodal equations

$$\begin{aligned} \begin{bmatrix} 0 \\ 0 \end{bmatrix} &= \begin{bmatrix} sL_1 + \frac{1}{sC_1} & -sL_m \\ -sL_m & sL_2 + \frac{1}{sC_2} \end{bmatrix} \cdot \begin{bmatrix} I_1 \\ I_2 \end{bmatrix} \\ &= [Z] \cdot [I]. \end{aligned} \quad (\text{A.3})$$

The only non-trivial solution for this system is found when the determinant of the  $Z$ -matrix is zero,

$$|[Z]| = 0 \quad (\text{A.4})$$

$$\left( sL_1 + \frac{1}{sC_1} \right) \left( sL_2 + \frac{1}{sC_2} \right) - (-sL_m)^2 = 0 \quad (\text{A.5})$$

$$s^2 L_1 L_2 + \frac{1}{s^2 C_1 C_2} + \frac{L_1}{C_2} + \frac{L_2}{C_1} - s^2 L_m^2 = 0. \quad (\text{A.6})$$

Multiplying (A.6) with  $\frac{s^2}{L_1 L_2}$  yields

$$s^4 \left( 1 - \frac{L_m^2}{L_1 L_2} \right) + s^2 \left( \frac{1}{L_1 C_1} + \frac{1}{L_2 C_2} \right) + \frac{1}{L_1 L_2 C_1 C_2} = 0. \quad (\text{A.7})$$

Substituting (A.1) and (A.2) into (A.7)

$$s^4 (1 - M^2) + s^2 (2\omega_0^2) + \omega_0^4 = 0. \quad (\text{A.8})$$

Replacing the Laplace parameter  $s = j\omega$  so that

$$\omega^4 (1 - M^2) - \omega^2 (2\omega_0^2) + \omega_0^4 = 0. \quad (\text{A.9})$$

Now by solving  $\omega^2$  in the quadratic equation leads to

$$\begin{aligned} \omega^2 &= \frac{2\omega_0^2 \pm \sqrt{4\omega_0^4 - 4\omega_0^4(1 - M^2)}}{2(1 - M^2)} \\ &= \frac{\omega_0^2(1 \pm M)}{(1 - M^2)}. \end{aligned}$$

For  $\omega_2^2 > \omega_1^2$  we obtain the two natural frequencies of the network

$$\omega_1^2 = \frac{\omega_0^2(1 - M)}{(1 - M^2)} \quad (\text{A.10})$$

and

$$\omega_2^2 = \frac{\omega_0^2(1 + M)}{(1 - M^2)}. \quad (\text{A.11})$$

Dividing  $\omega_2^2$  by  $\omega_1^2$  gives

$$\frac{\omega_2^2}{\omega_1^2} = \frac{1 + M}{1 - M}, \quad (\text{A.12})$$

which leads to the coupling coefficient in terms of the natural frequencies of the coupling resonator circuit

$$M = \frac{\omega_2^2 - \omega_1^2}{\omega_2^2 + \omega_1^2}. \quad (\text{A.13})$$

Note that the coupling coefficient is not influenced by the values of  $L_1$ ,  $L_2$ ,  $C_1$  or  $C_2$ , and can therefore always be calculated with the natural frequencies as long as the resonators are synchronously tuned.